

EXPLORING AND MAPPING CONFINED AND SENSOR-CHALLENGED
ENVIRONMENTS WITH PROPRIOCEPTION OF AN ARTICULATED MOBILE
ROBOT

by

Jacob Everist

A Dissertation Presented to the
FACULTY OF THE GRADUATE SCHOOL
UNIVERSITY OF SOUTHERN CALIFORNIA
In Partial Fulfillment of the
Requirements for the Degree
DOCTOR OF PHILOSOPHY
(COMPUTER SCIENCE)

March 2014

Copyright 2014

Jacob Everist

Dedication

to family

Table of Contents

Dedication	ii
List of Figures	vi
List of Tables	viii
List of Algorithms	1
1 Introduction	2
1.1 Challenges	2
1.1.1 Limitations of Exteroceptive Sensors	2
1.1.2 Tracking Position	3
1.1.3 Proprioceptive Sensors	3
1.1.4 Void Space and Features	4
1.1.5 Map Representation	4
1.1.6 Data Association	5
1.2 Related Work	5
1.3 Approach	7
1.4 Experimental System	9
2 Sensing Space	14
2.1 Proprioceptive Sensing	14
2.2 Pose Map	14
2.3 Problem	15
2.4 Behavior	16
2.5 Proprioceptive Sensor Data	19
2.5.1 Data Capture	20
2.5.2 Data Processing	25
2.6 Failures	34
2.6.1 Error Prevention	34
2.6.2 Error Mitigation	37
3 Control and Locomotion	41
3.1 Control Methodology	41
3.2 Behaviors	41

3.3	Problem	41
3.4	Anchoring	46
3.5	Curves	51
3.6	Behaviors	51
3.7	Smooth Motion	53
3.8	Behavior Merging	54
3.9	Compliant Motion	58
3.10	Stability Assurance	60
3.11	Adaptive Step	62
3.11.1	Front-Extend	63
3.11.2	Front-Anchor	65
3.11.3	Back-Extend	69
3.11.4	Back-Anchor	70
3.12	Analysis	71
3.12.1	Case: Snake as a Curve	72
3.12.2	Case: Snake with Width	75
3.12.3	Case: Snake with Segments	75
3.13	Experimental Results	77
4	Defining Position	78
4.1	Defining Pose and Direction	78
4.2	Motion Models	78
4.3	Problem	78
4.4	Immobilizing the Anchors	79
4.5	Tracking Motion	82
4.5.1	Pose and Coordinate Frames	82
4.5.2	Reference Poses	87
4.6	Robot-Centered Coordinate Frame	90
4.6.1	Gross Posture Approximation Curve (GPAC)	91
4.6.2	Generation of GPAC Local Frame	94
4.6.3	Geometric Transform between Poses	95
4.7	Results	96
5	Environmental Landmarks	99
5.1	Finding Landmarks	99
5.2	Corner Examples and Results	100
5.3	Wall Detection	100
5.4	Pipe Shape, Macro Features	101
5.5	Macro Feature Extraction	101
5.6	Different Macro Features	101
6	Pose-Based Mapping	103
6.1	Inter-Pose Correction	103
6.2	Paired Pose Correction	104
6.3	Constraint Mapping	105

6.4	Aggregate Pose Constraint Mapping	106
7	Mapping with Junctions	110
7.1	Map Algorithm	110
7.2	Junctions	111
7.3	Shoot Map Representation	114
7.4	Generating Shoots	116
7.5	Adding Poses to Shoots	116
7.6	Detecting Branch	120
7.7	Localizing On Shoot Map	120
7.8	Finding the Best Fitted Location	122
7.8.1	Choosing Shoot Splices	122
7.8.2	Selecting Initial Poses for ICP	123
7.8.3	ICP Algorithm	124
7.8.4	Collate, Sort, Filter	125
7.9	Curve Segment Algorithms	126
8	Probabilistic Mapping	131
8.1	Space of Possibilities	131
8.2	Pose Particle Filter	133
8.2.1	Particle Filter Implementation	134
8.3	Pose + Branch Location Particles	135
8.4	Branch Decision	137

List of Figures

1.1	Example environment.	10
1.2	Definitions of snake and pipe parameters.	11
2.1	TODO: Remove the obstacle map. Free space map from PokeWalls behavior.	16
2.2	PokeWalls behavior assembly.	17
2.3	Snapshot of $\bar{\phi}_t$ in local coordinates.	24
2.4	Single forward sweep.	25
2.5	Forward and backward sweep.	26
2.6	Free space data before and after convex hull.	27
2.7	Free space data of curved posture before and after convex hull.	28
2.8	Alpha Shape example from \cite{cgal:d-as2-12b}	29
2.9	Alpha Shape changing radius from \cite{cgal:d-as2-12b}	30
2.10	Alpha hull of free space data.	31
2.11	Process of generating medial axis.	32
2.12	Process of generating medial axis.	33
2.13	Largest set of contiguous reference poses.	36
2.14	Separation of Sweep Maps.	37
2.15	Local map rotational error.	38
2.16	Gross Posture Approximation Curve of sample posture.	39
3.1	Biological Concertina Gait of a Snake in a Confined Space. Image taken from \cite{Gans:1980p775}	42
3.2	Improperly tuned concertina posture using equation Equation 3.1.	43
3.3	One sine period curve	45
3.4	Anchor with not enough segments	47
3.5	Anchor Points	48
3.6	Anchor with amplitude larger than pipe width.	49
3.7	Separation of functionality	52
3.8	Smooth motion from interpolation of posture.	54
3.9	Discontinuity in behaviors results in clash of functionality.	56
3.10	Splice joint and connecting segments.	57
3.11	Convergence merge.	58
3.12	Compliance merge.	59
3.13	Adaptive Step Concertina Gait	62
3.14	Front-Extend behavior assembly	64

3.15	Front-Anchor behavior assembly	66
3.16	Posture that creates a 3-point anchor.	68
3.17	Back-Extend behavior assembly.	69
3.18	Back-Anchor behavior assembly	70
3.19	Parameterization of 3-point stable anchor in a smooth pipe.	72
3.20	3-point stable anchor with $w = 0$, $l = 0$, and $n = \infty$	73
3.21	Plot of snake arc length L for various values of W and P	74
3.22	Plot of snake length L while $P = 1$, for various values of W and w	76
3.23	Intersecting circles along the line of the curve. Demonstration of curve fitting algorithm.	77
4.1	Pose of rigid body with respect to global frame.	83
4.2	Pose of A and B with respect to global frame.	84
4.3	Local coordinate frames attached to segments and described by reference poses.	89
4.4	Robot Posture, Gross Posture Approximation Curve (GPAC), and Local Frame Origin	92
4.5	Estimated Trajectory of Robot through Variable-Width Pipe	97
4.6	Estimated Trajectory of Robot through Fixed-Width Pipe with Junctions	98

List of Tables

List of Algorithms

1	PID Controller	12
2	Point-in-Polygon Test	23
3	Anchor Fitting	50
4	Reference Pose Creation and Deactivation	88
5	<i>computeRefPose(i)</i> : Kinematics for Computing Reference Pose	90

Chapter 1

Introduction

In this dissertation, we develop an algorithmic approach for robotically mapping confined environments using internal sensors only. Some challenging environments such as underground caves and pipes are impossible to explore and map with external sensors. Such environments often cause external sensors to fail because they are too confined, too hostile for the sensors, or incompatible to the fluid medium. These environments are also impossible for humans to explore for similar reasons. Robotic solutions are possible, but such environments often cause available external sensors to fail. A robotic solution that can explore and map without external sensors would allow access to previously inaccessible environments.

For example, an approach that is invariant to ambient fluid (air, water, muddy water, etc.) would significantly impact cave exploration and underground science by the access to still deeper and smaller cave arteries regardless of whether they are submerged in water. Search and rescue operations would have additional tools for locating survivors in complicated debris piles or collapsed mines. Utility service workers would be able to map and inspect pipe networks without having to excavate or evacuate the pipes.

1.1 Challenges

1.1.1 Limitations of Exteroceptive Sensors

Exteroceptive sensors are sensors that are affixed externally and designed to sense information about the robot's environment. They're biological equivalents include such things as vision, hearing, touch, taste and smell. The robot equivalents include touch, cameras, sonar, and laser range-finders.

Currently we cannot effectively explore and map these environments with exteroceptive sensors. Current state-of-the-art mapping methods depend on exteroceptive sensors such as vision, range, or touch sensors that are sensitive to the ambient properties of the environment. Sonar and laser-range finders are sensitive to the ambient fluid properties for which they are calibrated. They are also often ineffective due to occlusions, distortions, reflections, and time-of-flight issues. Changing visibility, lighting conditions and ambient fluid opacity impact the usefulness of vision sensors. Hazardous environments may also damage fragile external touch sensors.

1.1.2 Tracking Position

In addition to the challenges of sensing the environment, we also have the challenge of tracking the robot's position in the confined environment. Due to the enclosed nature of the environment, global positioning information is often unavailable. Therefore, any mapping method will need an accurate motion estimation approach for the robot. Wheeled dead-reckoning may be very difficult or impossible if the environment is highly unstructured or otherwise untenable to a wheeled locomotion approach. Even a well designed motion estimation approach will be susceptible to accumulation of errors and will require localization techniques that will reduce and bound the positional error of the robot.

1.1.3 Proprioceptive Sensors

Given these restrictions, developing an approach that will work on all the most challenging conditions forces us to rely on a strictly proprioceptive approach for collecting environmental information and building the map. Such proprioceptive sensors include accelerometers, gyros, INS (inertial navigation systems), and joint angle sensors. Examples of biological proprioception includes sense of hunger, fatigue, shortness of breath, pain, sense of hot, sense of cold, perceived configuration of the body, and numerous others.

Exteroceptive mapping approaches directly sense large sweeps of the environment at a distance and allow us to make multiple observations of environmental features from multiple poses, integrating this into a map. With a proprioceptive approach, the information is by definition internal to the robot's body and local to the robot's position. Any inferred information about the environment is limited to the immediate vicinity of the robot's pose. The challenge is to explore the environment and construct a map with fundamentally less information.

1.1.4 Void Space and Features

Limited information about the immediate vicinity of an articulated robot can be obtained by sweeping the robot's body to cover all of the void space that is reachable. By taking posture snapshots while the robot is sweeping and plotting them into an image, we can create a rudimentary void space image of the local environment. The challenge then becomes how to utilize this particular type of data in a robotic mapping approach.

In the exteroceptive approach (external sensors), one would use the ability to sense landmark features at a distance and identify and merge their position across several views. However, in a proprioceptive approach, all sensed information is local. Not only will the opportunities for spotting landmark features between consecutive views be limited, but we must also define what exactly we will use as landmark features. In exteroceptive mapping, the boundaries of the environment are sensed and landmark features are extracted that represent corners, curves, structures, and visual characteristics. With proprioceptive sensors, we present the different kinds of features that can be extracted and used from void space information.

1.1.5 Map Representation

How is a map built and how is it represented? How can it be used and how accurate can it be? The map is built to void space data taken from proprioception. The map must

be sufficiently accurate to navigate the environment to a given destination. What kinds of environmental characteristics can it capture and what are its limitations?

1.1.6 Data Association

In the event of visiting the same place twice, we wish to detect the sameness of the location and correct the map to make it consistent. This is often called the loop-closing or data association problem. In the case of exteroceptive mapping, this is often achieved by finding a correspondence between sets of landmark features that are similar and then merging the two places in the map. In the proprioceptive case, the availability of landmark features is scarce. The current best-practice methods for solving the data association problem depend on an abundance of landmark features with which multiple combinations of associations are attempted until an optimal correspondence is found. In our approach, with only a few landmarks to use, performing data association in this way becomes ineffective at best, destructive at worst. We determine a different approach to data association using void space information.

1.2 Related Work

The mapping of confined spaces is a recurring theme in the research literature. Work has been done to navigate and map underground abandoned mines [Thrun04] with large wheeled robots traveling through the constructed corridors. Although the environment is large enough and clear enough to make use of vision and range sensors, its location underground makes the use of GPS technologies problematic. This work can be applied to confined environments where exteroceptive sensors are still applicable.

Robotic pipe inspection has been studied for a long time [Fukuda89], but usually requires that the pipe be evacuated. The robotic solutions are often tailored for a specific pipe size and pipe structure with accompanying sensors that are selected for the

task. Often the solutions are manually remote-controlled with a light and camera for navigation.

Other work has focused on the exploration of flooded subterranean environments such as sinkholes [Gary08] and beneath sea-ice or glaciers. This involves the use of a submersible robot and underwater sonar for sensing.

Other work has approach the problem of identifying features in the absence of external sensors. This work comes from the literature on robotic grasping and is described as contact detection. That is, the identification and reconstruction of object contacts from the joint sensors of the grasping end effector. Various methods to this approach are described in [Kaneko], [Gruppen], [Haidacher], [Mimura].

Our earlier paper [Everist09] established the basic concept of mapping using void space information with a rudimentary motion estimation technique. This early work attempted to merge the information from contact detection with the new void space concept. We did not yet have an approach for localization, feature extraction, and data association.

Another researcher [Mazzini11] tackled the problem of mapping a confined and opaque environment of a pipe junction in an oil well bore hole deep underground where high temperature, high pressure, and mud make external sensors infeasible. Mazzini’s approach focuses on mapping one local area of the underground oil well. They use physical probing with a robotic finger to reconstruct the walls of the pipe. The robot remains anchored and immobile so there are no need for motion estimation. Our dissertation differs from this work in that we use void space information instead of contact or obstacle information, our robot is mobile instead of anchored to one location, and that we are exploring and constructing a complete map instead of one local environment of interest.

1.3 Approach

To address these challenges, our approach is to develop algorithmic methods for utilizing proprioceptive joint angle information on an articulated mobile robot to enable exploration and mapping of a confined environment. From a series of complete posture information sets, we build up void space information into a posture image and integrate it into a whole map. We hypothesize that with the posture images taken at multiple robot poses in the environment, we can integrate them into a map; we believe this approach will serve as effective alternative for mapping confined environments when exteroceptive sensors have failed or are unavailable.

Our claim here is that the type of robot used and its method of locomotion are not important so long as the robot is articulated and with many joints. The more joint sensors the robot has, the better capable the robot is of mapping.

In this design we use a simulator that enables us to rapidly develop and test different algorithmic techniques without becoming overly worried about the hardware and locomotive aspects of the robot. We use a simplified flat pipe-like environment with a snake robot that is capable of anchoring to the sides of the walls and pushing and pulling itself through the pipe on a near frictionless floor.

We do not simulate any sensor-inhibiting fluid in the environment or sensor-failure scenarios, nor do we use any type of external sensor, be it touch sensors, vision sensors, or range sensors such as laser range-finders and sonar. Additionally, no global positioning system is used since it is not practical to expect GPS to function underground. The only sensors we permit ourselves to use are joint sensors.

For capturing the posture images, we examine a number of difficulties and pitfalls to capturing this information. Notably, the prevalence of slip of the robot can corrupt the posture image because the robot loses its stable frame of reference to the environment. We develop a number of techniques for safely capturing the void space information,

reducing the likelihood of slip, detecting slip, and mitigating the damage if slip should occur.

We examine several possibilities for extracting landmark features from the posture images. We try several traditional forms of features such as corners and edges, but in the end we develop our own macro-feature which is the overall shape of the local environment captured by the posture image and reduced to the form of a medial axis.

When the robot is moving through the environment, we must also have techniques for estimating the motion between the poses at which we capture the posture images. We show a highly accurate but very slow method [Sec Motion 1] for our particular snake robot morphology, and compare it to a coarse but fast motion estimation method [Sec Motion 2]. We discover that the coarse method is sufficient so long as we rely on the macro-features of the posture images to constrain the possibilities.

Given these basics, we then delve into the heart of the matter: the actual integration of poses, motion estimates, and posture images into a coherent map. We develop and experiment with a few techniques using the constraints from the macro-features in a variety of ways [Sec Constrain 1]. We finally settle on an aggregate pose constraint method where the whole set of past poses is used to generate a feature that constrains the next pose [Sec Constrain 2].

We show how our mapping approach works in a variety of different environments for example, a single path pipe where there are no branches in the environment. The environment only contains a single path that includes a different variety of turns and angles. We then complicate matters by adding in different types of junctions such as T-junctions, Y-junctions, and X-junctions. We do not yet consider environments that have loops in them.

The adding of junctions adds significant complications and requires us to have a better understanding of the structure of our map. We establish a new type of mapping structure called a shoot map. A shoot is a section of the environment that is a single path. The shoot has an origin and a termination point which indicates either the boundary

of the environment or more space yet to be explored. New shoots are created when a junction is detected, where the new shoot’s origin is at the location of the parent shoot where the junction was detected. That representation allows us to deal with the restrictions on the type of information we can acquire and the often incompleteness of the posture image capture with respect to the actual local environment.

Finally, given the fundamental mapping structures and methods we have developed, we cast them into a probabilistic framework. This allows us to keep track of different map possibilities, discarding improbable ones, and selecting the most probable. Our mapping approach has certain ambiguities in the type of environmental information we can acquire. The probabilistic framework keeps track of these ambiguities until they can be resolved when more information is acquired.

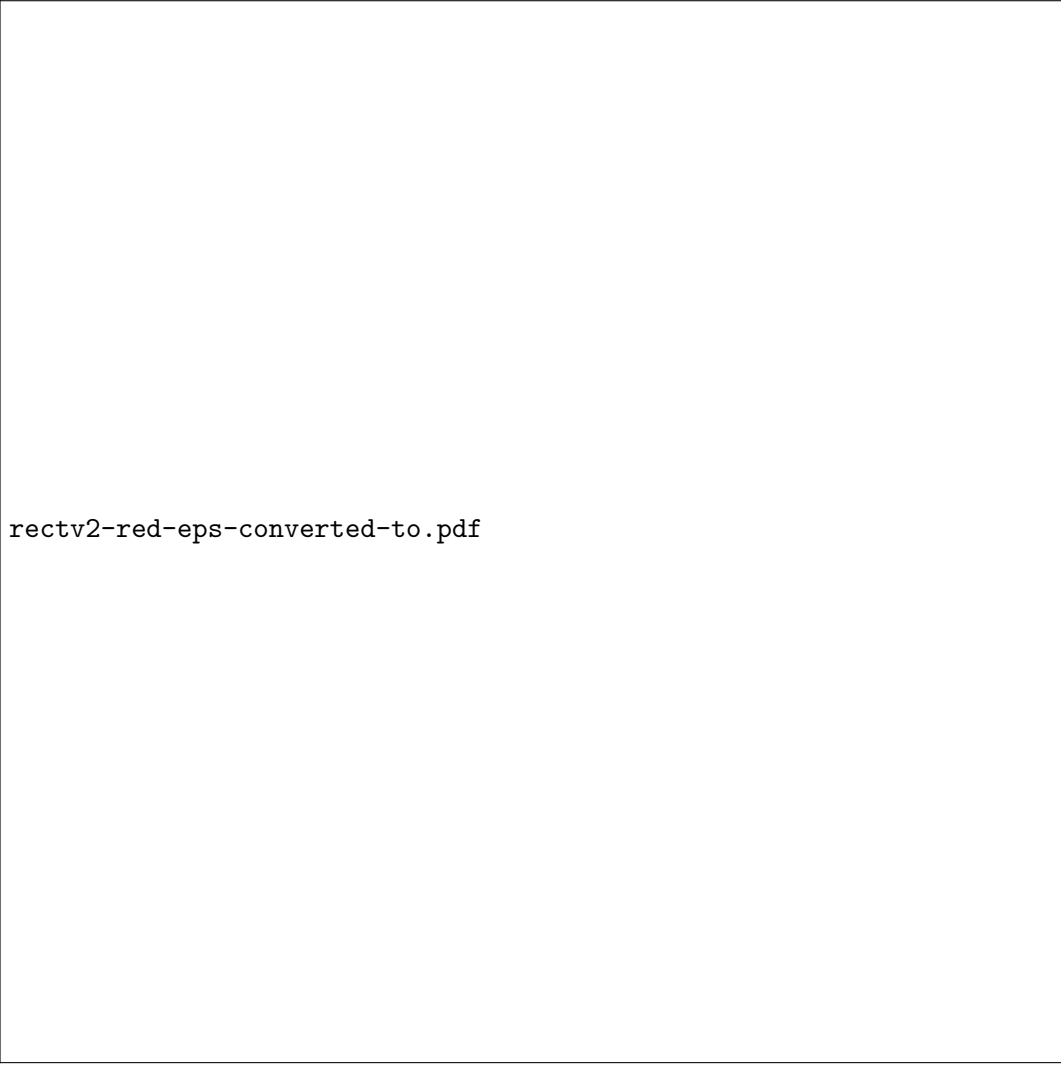
1.4 Experimental System

Robot setup, joints and geometry, environmental parameters, simulation.

We explicitly chose to develop our approach in a simulation environment in order to rapidly develop a theoretical framework to the problem of mapping without external sensing. In future work, we will apply these techniques to physical robots.

We choose to use the Bullet physics engine (version 2.77) because it is free, open source, mature, and actively developed. Though it is primarily designed for games and animation, it is acceptable to our robotics application. Our primary requisites are simulation stability and accurate modeling of friction and contact forces. True friction and contact modeling are not available to us without specially designed simulation software at a monetary and performance speed cost. Our choice of Bullet gives us believable results so long as we do not demand too much and try to simulate challenging situations (e.g. high speed, high mass, 1000s of contact points).

We focus our attention on environments such as the one depicted in Figure 1.1. We build a flat plane and place a number of vertical walls to create a pipe-like maze



rectv2-red-eps-converted-to.pdf

Figure 1.1: Example environment.

environment. All environments we study are flat and have no vertical components. This means we need only focus on building 2D maps to represent the environment. From here on in this paper, we refer to such environments as pipes even though they may not correspond to the even and regular structures of physical utility pipes.

A snake robot is placed in the pipe environment as shown in Figure 1.1. The snake robot consists of regular rectangular segments connected by actuated hinge joints. Each of the joint axes is parallel and coming out of the ground plane. This means the snake

has no means to lift its body off the ground because all of its joints rotate in the plane of the ground. It is only capable of pushing against the walls and sliding along the ground. We choose a reduced capability snake robot because we wish to focus on the mapping problem instead of the more general serpentine control problem.

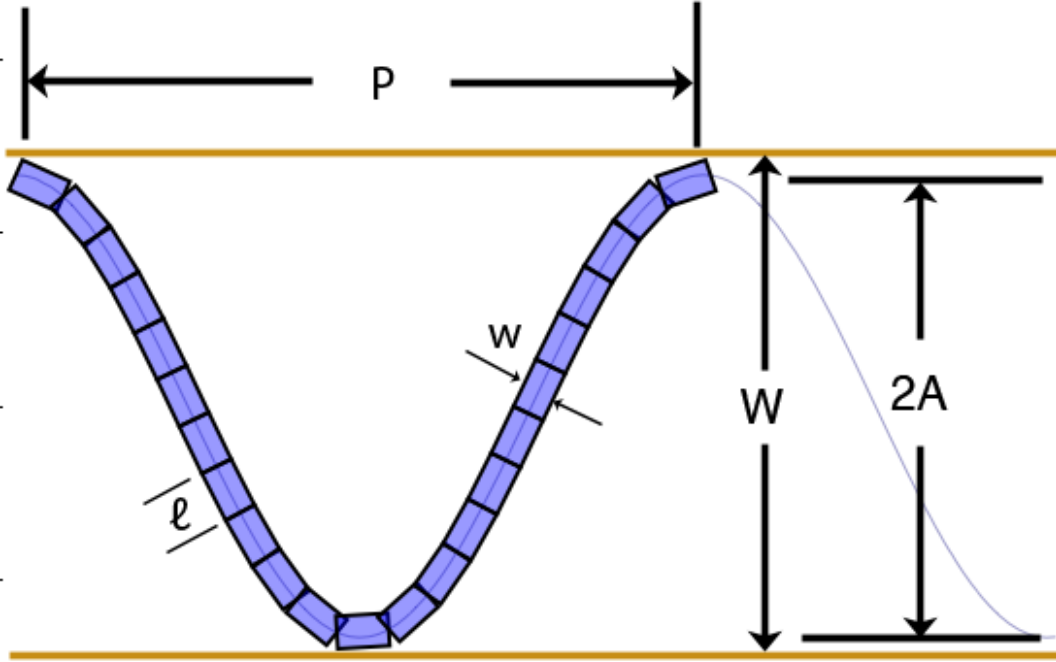


Figure 1.2: Definitions of snake and pipe parameters.

We can parameterize the snake and the pipe environment. For the snake robot, l is the snake segment length, w is the segment width, N is the number of segments connected by $N - 1$ joints, and m is the maximum torque capable by each of the joint motors.

[?]

For the environment, we can begin by defining the pipe width W . For a pipe with parallel and constant walls, this is a straightforward definition as seen in Figure 1.2. For non-regular features, we define the pipe width at a given point on one wall to be the distance to the closest point on the opposing wall. This correctly captures the fact that

a robot that is wider than the smallest pipe width W will be unable to travel through that smallest width and will create a non-traversable pinch point. Conversely, a pipe width W that is larger than the reach of a robot will become a void space that the robot will have difficulty completely sensing without the aid of external sensors. For both the minimum and maximum pipe widths of a given environment, we define W_{min} and W_{max} respectively where $W_{min} \leq W_i \leq W_{max}$ where W_i is the pipe width at some point on wall p_i of the pipe environment.

Each joint on the robot is actuated by a motor and PID controller. It can actuate the joint anywhere from ± 160 degrees. It uses the built-in motor capabilities of Bullet that allows us to set the joint angular velocity at run-time. Therefore, all outputs of the PID controller set velocity commands to the joint and the physics engine does its best to satisfy those as velocity constraints.

Algorithm 1 PID Controller

```

 $\epsilon \leftarrow (\alpha - \phi)$ 
if  $|\epsilon| > \text{tol}$  then
     $\epsilon_{sum} \leftarrow \epsilon_{sum} + \delta t \times \epsilon$ 
     $\delta\epsilon \leftarrow \epsilon - \epsilon_{last}$ 
     $\epsilon_{last} \leftarrow \epsilon$ 
     $\hat{v} \leftarrow P \times \epsilon + I \times \epsilon_{sum} + D \times \delta\epsilon / \delta t$ 
    if  $\hat{v} > v_{max}$  then
         $\hat{v} \leftarrow v_{max}$ 
    end if
    if  $\hat{v} < -v_{max}$  then
         $\hat{v} \leftarrow -v_{max}$ 
    end if
end if

```

The structure of the PID controller is shown in Algorithm 1. Line 1 defines the error as the difference between the target and the actual joint angle. Line 2 prevents the controller from executing if the error falls below an acceptable threshold. This prevents the motor from attempting to perform minor corrections to an already near-correct angle in order to avert oscillations or error-producing compensations. Line 3 is the summation term for error over time while line 4 and 5 is the instantaneous error change from the

previous controller iteration. The actual PID control law is shown on line 6 where P is the proportional term coefficient, I is the integration term coefficient, and D is the derivative term coefficient. The result outputs a command velocity for the Bullet engine. Finally, lines 7–10 limit this velocity to a maximum.

Each of the joints gives angle position information to simulate a shaft encoder or potentiometer. For this study, we do not simulate calibration error, sensor noise, resolution error, or gear backlash. Calibration error has been studied elsewhere /cite and there exists correction mechanisms for it. In the case of sensor noise, the noise on potentiometers is small enough not to affect our algorithms. Gear backlash was encountered and studied in /cite Mazzini. The primary error of concern is resolution error caused by the discretization process of a shaft encoder or an A/D converter. This problem has been studied /cite. Given a sensitive enough A/D converter (really?), this problem can be eliminated. In this study, we assume correct and noise-free joint sensors.

A joint provides an API to the controlling program with 2 read-write parameters and 1 read-only parameter. The read-write parameters are the target joint angle α_i and the maximum torque m_i , with the actual angle ϕ_i being the read-only parameter. α_i is the angle in radians that we desire the joint to rotate to. ϕ_i is the actual angle of the joint that reflects the current physical configuration of the robot. m_i is the maximum permitted torque that we wish to limit the individual motors to. The maximum torque can be lowered to make the joints more compliant to the environment.

Chapter 2

Sensing Space

2.1 Proprioceptive Sensing

- Sweep the space. Limited using the geometry of the robot.
- Posture Images $I_1:t$
- More here

Integrate (Posture vector ϕ_t, t) = posture image

Breaking up the posture image into forward sweep and backward sweep. The transition between backward anchoring and forward anchoring causes the reference frame to slip and the posture image to be distorted. We show that is better to have two separate images that do not disrupt the anchored reference frames.

In the event, we have local correction that sanitizes the data. If there should be a sudden breach of the arm outside of the containing polygon of the posture image, we classify this as a slip and adjust the local coordinate system to keep the instantaneous posture within the boundaries of the polygon.

Should the data be too hopelessly corrupted from a bow tie effect in the posture image, we can reject the overall data and take the instantaneous shot of the current posture as the only data. This gives a sparse snapshot of the environment and leaves the exploratory data out, but it will capture the gross shape of the local environments.

2.2 Pose Map

Actions and posture images are raw input.

Images $I_{1:t}$

Actions: $U_{1:t}$

Find poses $P_{1:t}$ to solve mapping problem

Combine the elements to get a naive map. Simple motion estimation and plotting of poses and posture images to a grid map. No capability for correction.

2.3 Problem

Now that we are able to travel through the environment and estimate our motion, the next order of business is to be able to sense the environment. With no exteroceptive sensors, this is quite a challenging problem. Somehow, we must use our proprioceptive joint sensors to build some information about the environment.

We use a common sense assumption that the robot's body can never intersect with an obstacle. We call this the Obstacle-Exclusion Assumption. If we take the corollary of this assumption, we conclude that all space that intersects with the robot's body must be free space. If we record the robot's body posture over time, we can use this to build a map of the local environment's free space.

We need 3 key ingredients to build an accurate map of the free space in the local environment: 1) known geometry of the robot's rigid body linkages, 2) accurate joint sensors for computing kinematics, and 3) an accurate reference pose to the global frame. If all of these things are available, we can build a local map such as shown in Figure 2.1.

The map is achieved by rigidly anchoring to the environment and maintaining a set of stable reference poses. One side of the snake's body is used to sweep the free space, making multiple snapshots of the robot's posture over time and plotting them into a map. We discuss each aspect of our approach and show the results for a variety of environmental configurations.

The key point here is that sensing cannot be accomplished without action. Action by itself runs the risk of disturbing the environment or causing errors in the reference pose.

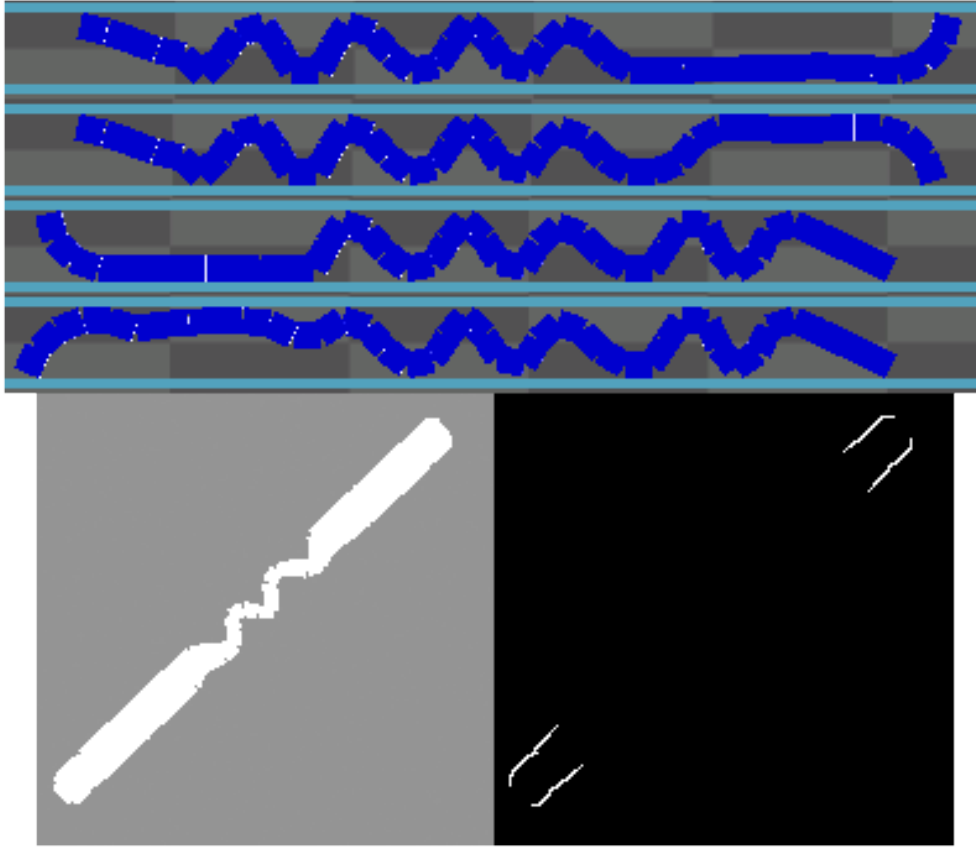


Figure 2.1: TODO: Remove the obstacle map. Free space map from PokeWalls behavior.

Though sensing cannot be accomplished without action, action runs the risk of modifying the result. Special care must be taken that the risk of modifying the environment is minimized. Here, we include the robot's body in our definition of the environment so that anchor slippage is a form of environment modification.

2.4 Behavior

In order to capture as much information about the environment as we can, we need to sweep the robot's body around as much as possible while trying to cover as much space as possible without losing our reference pose to the global frame. Therefore, we have

devised a behavior assemblage that separates responsibility for anchoring on one half of the snake and for probing the environment with the other. This assemblage is shown in Figure 2.2. The resulting behavior is shown in Figure 2.1.

The resultant behavior sweeps the front end of the snake back and forth, impacting both sides of the pipe. The front is gradually extended to increase the probe reach down the pipe. Once the extension has reached the maximum, the behavior is terminated after returning the snake back to its original fully anchored Rest-State posture.

At regular intervals during the sweeping behavior at the end of each Transition termination, the posture is recorded for later processing. The end result is an ordered list of posture vectors representing each snapshot of the robot during the behavior. These postures are then processed into a map.

We describe each behavior in the assemblage.

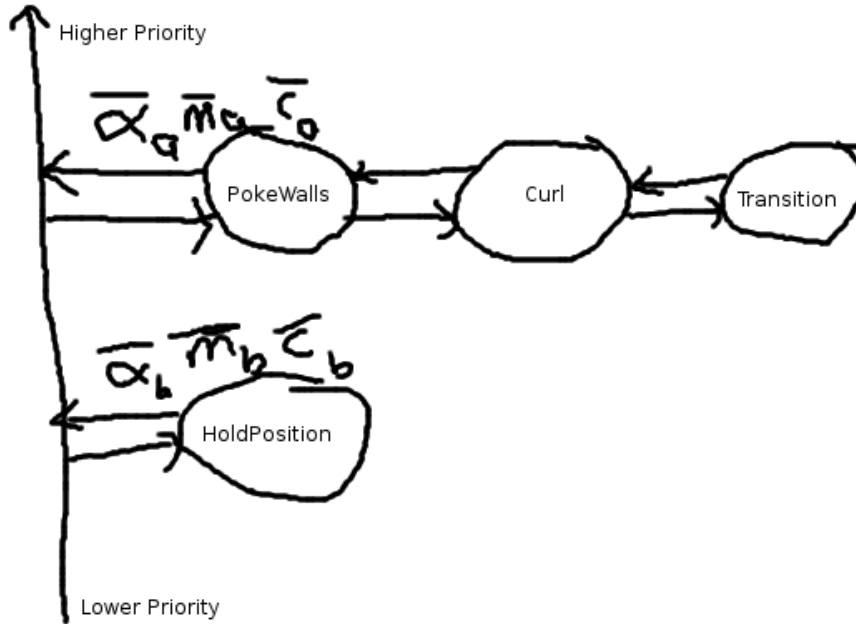


Figure 2.2: PokeWalls behavior assembly.

Curl: The sweeping behavior is performed by setting a series of consecutive joints all to a 30 degree angle, resulting in a curling motion. In a confined environment,

the result of the commanded joints usually results in the snake impacting the walls of the environment. By steadily increasing the number of joints to perform this sweeping motion, the reach of the snake is gradually increased and more space is swepted out.

The Curl sub-behavior is responsible for commanding these joint angles given the specified joint range by the parent. It is also responsible for executing a simple contact detection heuristic in the course of the curling behavior. We describe both here.

Given the top joint j_t specified by the parent, the Curl behavior gives commands to the joints $(j_0 \dots j_t)$, setting $\alpha_i = 0$. All α are set to the following sequence of angles: $(0, 25, 30, 0, -25, -30, 0)$. Between each movement command we use the Transition sub-behavior to manage the motion as a linear interpolation between postures. We also wait for the tip of the snake’s position to become stable for executing another movement transition. At the end of the movement sequence and once the tip has become stable, the Curl behavior then terminates and waits to be reset by the parent.

For the contact detection heuristic, once the joints have been set to $\alpha = 25$, the tip of the snake’s position p_a is computed kinematically. The joints are then set to $\alpha = 30$ and the tip’s position p_b is again computed kinematically. The Cartesian distance between p_a and p_b is computed. If the value is negligible, we assume that the tip of the snake has made contact with the walls. Otherwise, we do not assume contact has been made. The repeat this for the negative angle commands on the other side of the pipe.

The way the sweeping behavior is performed is by setting the commanded position of all the joints from the tip of the snake down to a top joint simultaneously from 0 to 30 degrees. This results in a “curling” behavior which gives the subbehavior its name. The joints are set at angles of 0, 25, 30, 0, -25, -30, 0.

PokeWalls: The PokeWalls behavior is responsible for specifying the range of joints that perform the Curl operation, instantiating and configuring the Curl behavior. The PokeWalls behavior is configured with the sweeping direction on the snake, starts the Curl behavior with the joint range specified by $j_t = 6$. It then passes through the outputs of the Curl behavior.

At the termination of the Curl behavior, PokeWalls increments j_t by 2 and restarts the Curl behavior with the new parameters. If $j_t = 10$, we then begin decrementing j_t by 2 until we go back to $j_t = 6$. Once the Curl has been executed for the second for $j_t = 6$, we terminate the PokeWalls behavior.

The PokeWalls behavior is also responsible for setting the maximum torque for each of the curling joints to be compliant. This ensures that the posture of the snake complies to the environment and gives us as much information as possible about the structure of the free space. If we do not have compliant joints, the curling behavior can result in disruption of the anchors and loss of our reference poses.

Transition: This is the same behavior as described in Chapter 2. It takes an initial and final posture and outputs a series of postures that provides a smooth transition between the two using interpolation. Its parent behavior is Curl which instantiates it and resets it whenever it needs to perform a new move.

HoldPosition: This is the same behavior as described in Chapter 2. It is initialized with the complete posture of the snake at the beginning of the behavior. This posture is usually the result of the Rest-State stage of the Adaptive Step locomotion process. It continually outputs the anchored posture. Its output is subsumed by the output from the PokeWalls behavior in a precedence merge. It is 2nd in the behavior ordering as shown in Figure 2.2.

2.5 Proprioceptive Sensor Data

Now that we’ve specified the actions we perform to sense the environment by way of the PokeWalls and Curl behavior, we now need to show how we capture sensor data and process it for consumption for our later mapping algorithms.

2.5.1 Data Capture

Once the posture of the snake has stabilized and the anchor points give us good reference poses to the global frame, our objective is take the posture vector, $\bar{\phi}_t$ at time t , and convert it to a 2D spatial representation of free space, M_p at the current pose p . We separate the tasks of spatial representation and positioning the data in the global frame. To do this, we create a local map centered on the robot’s body on which the spatial data is plotted while the robot remains in one position.

The local map is an occupancy grid representation where each cell of the grid has two states: *unknown* or *free*. If the body of the robot is present on a cell, this cell is marked *free*. Otherwise, it is *unknown*. It is unknown instead of *occupied* because our approach does not have any means to specifically observe obstacles beyond contact detection heuristics. The heuristics are not accurate enough to plot their positions into the occupancy grid, so we leave the cells unknown for now.

The size of a cell is chosen for the desired accuracy we require. Smaller cell sizes require more computational time, but larger cell sizes will result in blocky maps. We choose our cell dimensions $s_p \times s_p$ to be

$$s_p = \frac{l}{3} = 0.05, \text{ or one third the length of a snake segment.}$$

Given that we now have our cell dimensions, we can compute the dimensions of our local map to be

$s_M = l * N + 4$, where l is the segment length and N is the number of segments. s_M is the maximum length from the origin at the center of our local coordinate system. We want the dimensions to be larger than the worse case scenario of the snake’s posture. We also include an extra padding of 4 to ensure that the snake never reaches the boundary of the grid.

The number of cells or pixels in our local map will be $n_p \times n_p$ where

$n_p = \left\lceil \frac{2s_M}{s_p} + 1 \right\rceil$. This equation ensures that n_p is an odd integer. The +1 factor adds an extra cell whose center will act as the origin of our local coordinate system.

Now that we have the dimensions of the grid space and its relation to Cartesian space, we need to know how to convert points from one space to the other. To convert a grid index (i_x, i_y) to Cartesian space point (p_x, p_y) centered within the cell, we compute the following:

$$p_x = \left(i_x - \left\lfloor \frac{n_p}{2} \right\rfloor \right) \frac{s_p}{2} \quad (2.1)$$

$$p_y = \left(i_y - \left\lfloor \frac{n_p}{2} \right\rfloor \right) \frac{s_p}{2} \quad (2.2)$$

Conversely, to find the index of a cell (i_x, i_y) that contains a Cartesian point (p_x, p_y) , we compute the following:

$$i_x = \left\lfloor \frac{p_x}{s_p} \right\rfloor + \left\lfloor \frac{n_p}{2} \right\rfloor \quad (2.3)$$

$$i_y = \left\lfloor \frac{p_y}{s_p} \right\rfloor + \left\lfloor \frac{n_p}{2} \right\rfloor \quad (2.4)$$

Now that we have the tools for mapping positions in physical space to our grid space occupancy map, we need data to plot into the map. Using kinematics, we compute the geometry of the posture of the snake. We can represent this by a 4-sided rectangle for each segment of the snake. We set the origin of our coordinate system on segment 19 and joint 19 which is the midway point for $N = 40$. We define this to be:

$$O_t = (x_{19}, y_{19}, \theta_{19}) = (0, 0, 0) \quad (2.5)$$

where O_t is the pose of P_{19} in the local frame at time t . This may change which is explained in section 2.6.2.

To compute the segment 19 rectangle, starting from the origin for $k = 19$, $x_k = 0$, $y_k = 0$, and $\theta_k = 0$, we compute the following:

$$\begin{aligned}
x_{k+1} &= x_k + l \cos(\theta_k) \\
y_{k+1} &= y_k + l \sin(\theta_k) \\
\theta_{k+1} &= \theta_k - \phi_{k+1} \\
p_1 &= \left(x_{k+1} - \frac{w \sin(\theta_k)}{2}, y_{k+1} + \frac{w \cos(\theta_k)}{2} \right) \\
p_2 &= \left(x_{k+1} + \frac{w \sin(\theta_k)}{2}, y_{k+1} - \frac{w \cos(\theta_k)}{2} \right) \\
p_3 &= \left(x_{k+1} - l \cos(\theta_k) + \frac{w \sin(\theta_k)}{2}, y_{k+1} - l \sin(\theta_k) - \frac{w \cos(\theta_k)}{2} \right) \\
p_4 &= \left(x_{k+1} - l \cos(\theta_k) - \frac{w \sin(\theta_k)}{2}, y_{k+1} - l \sin(\theta_k) + \frac{w \cos(\theta_k)}{2} \right) \\
R_k &= (p_4, p_3, p_2, p_1)
\end{aligned} \tag{2.6}$$

The result is the rectangle polygon R_k , which represents the rectangle of the segment 19. The next reference pose $(x_{k+1}, y_{k+1}, \theta_{k+1})$ is also computed. Here $k + 1 = 20$. To compute the k^{th} rectangle for $k \geq 19$, we need only compute this iteratively until we reach the desired segment.

To perform this backwards, to find segment 18, where $k+1 = 19$ and $(x_{k+1}, y_{k+1}, \theta_{k+1}) = O_t$, we compute the following:

$$\begin{aligned}
\theta_k &= \theta_{k+1} + \phi_k \\
x_k &= x_{k+1} - l \cos(\theta_k) \\
y_k &= y_{k+1} - l \sin(\theta_k) \\
p_1 &= \left(x_{k+1} - \frac{w \sin(\theta_k)}{2}, y_{k+1} + \frac{w \cos(\theta_k)}{2} \right) \\
p_2 &= \left(x_{k+1} + \frac{w \sin(\theta_k)}{2}, y_{k+1} - \frac{w \cos(\theta_k)}{2} \right) \\
p_3 &= \left(x_{k+1} - l \cos(\theta_k) + \frac{w \sin(\theta_k)}{2}, y_{k+1} - l \sin(\theta_k) - \frac{w \cos(\theta_k)}{2} \right) \\
p_4 &= \left(x_{k+1} - l \cos(\theta_k) - \frac{w \sin(\theta_k)}{2}, y_{k+1} - l \sin(\theta_k) + \frac{w \cos(\theta_k)}{2} \right) \\
R_k &= (p_4, p_3, p_2, p_1)
\end{aligned} \tag{2.7}$$

The result is the same polygon as well as the new reference pose for segment 18. To compute the k^{th} segment rectangle for $k < 19$, we need only use this

equation iteratively. Computation of all N rectangles results in the set of rectangles \bar{R}_t for the current posture.

Now that we have a set of rectangles which represent the geometry of the robot in its current posture, we want to plot its occupied space into the local occupancy map. To do this, we need to convert polygons in Cartesian space into sets of grid points. To do this, we use a point-in-polygon test algorithm for each of the pixels in the map.

The simplest approach is as follows. For each pixel, convert it to Cartesian space, test if it's contained in any of the polygons, and if it is, set the pixel to *free*. Otherwise, let the pixel remain in its current state. The pseudocode for the point-in-polygon test for convex polygons derived from \cite{orourke98} is seen in Algorithm 2.

Algorithm 2 Point-in-Polygon Test

```

 $R \leftarrow$  rectangle
 $P \leftarrow$  point
for  $i = 0 \rightarrow 4$  do
     $A_x \leftarrow R[i \bmod 4][0]$ 
     $A_y \leftarrow R[i \bmod 4][1]$ 
     $B_x \leftarrow R[(i + 1) \bmod 4][0]$ 
     $B_y \leftarrow R[(i + 1) \bmod 4][1]$ 
     $C_x \leftarrow P[0]$ 
     $C_y \leftarrow P[1]$ 
    if  $!((B_x - A_x) * (C_y - A_y) - (C_x - A_x) * (B_y - A_y) \geq 0)$  then
        return False
    end if
end for
return True

```

A single snapshot of the snake posture plotted into the local map is shown in Figure 2.3. The posture $\bar{\phi}_t$ is captured, the rectangles \bar{R}_t representing the body segments are computed from kinematics, each pixel (i_x, i_y) of the map M_p is converted to Cartesian space point (p_x, p_y) and checked by the point-in-polygon algorithm if it is in a rectangle R_k . If it is, $M_p(i_x, i_y)$'s value is set to *free*. This is repeated for each point in each rectangle for a posture snapshot at time t .

While running the PokeWalls behavior, we periodically take snapshots at the conclusion of each Transition step and plot them into the map. A complete sweep with the



Figure 2.3: Snapshot of $\bar{\phi}_t$ in local coordinates.

PokeWalls behavior is shown in Figure 2.4. Furthermore, if we also perform a sweep with the other side of the snake, we can get a map like Figure 2.5.

Notice in Figure 2.5 that there is a gap in the free space data in the center of the body. These segments at the center remain immobilized throughout the sweeping process and never give extra information. This gap in the center is our “blind spot” for this configuration. It is necessary that the center remain immobilized to ensure anchors do not slip so that we maintain correct reference poses to the global frame.

We have no guarantee that there are obstacles at the boundaries of our free space map. We also have no quick way to determine if the boundary of our map is an obstacle or a frontier. While the boundaries at the front and back are usually assumed to lead to more free space, anywhere along the sides could be a missed side passage that the snake failed to discover due to it being too small or being in our blind spot. To combat this situation, we either must perform laborious and time-consuming contact probing of

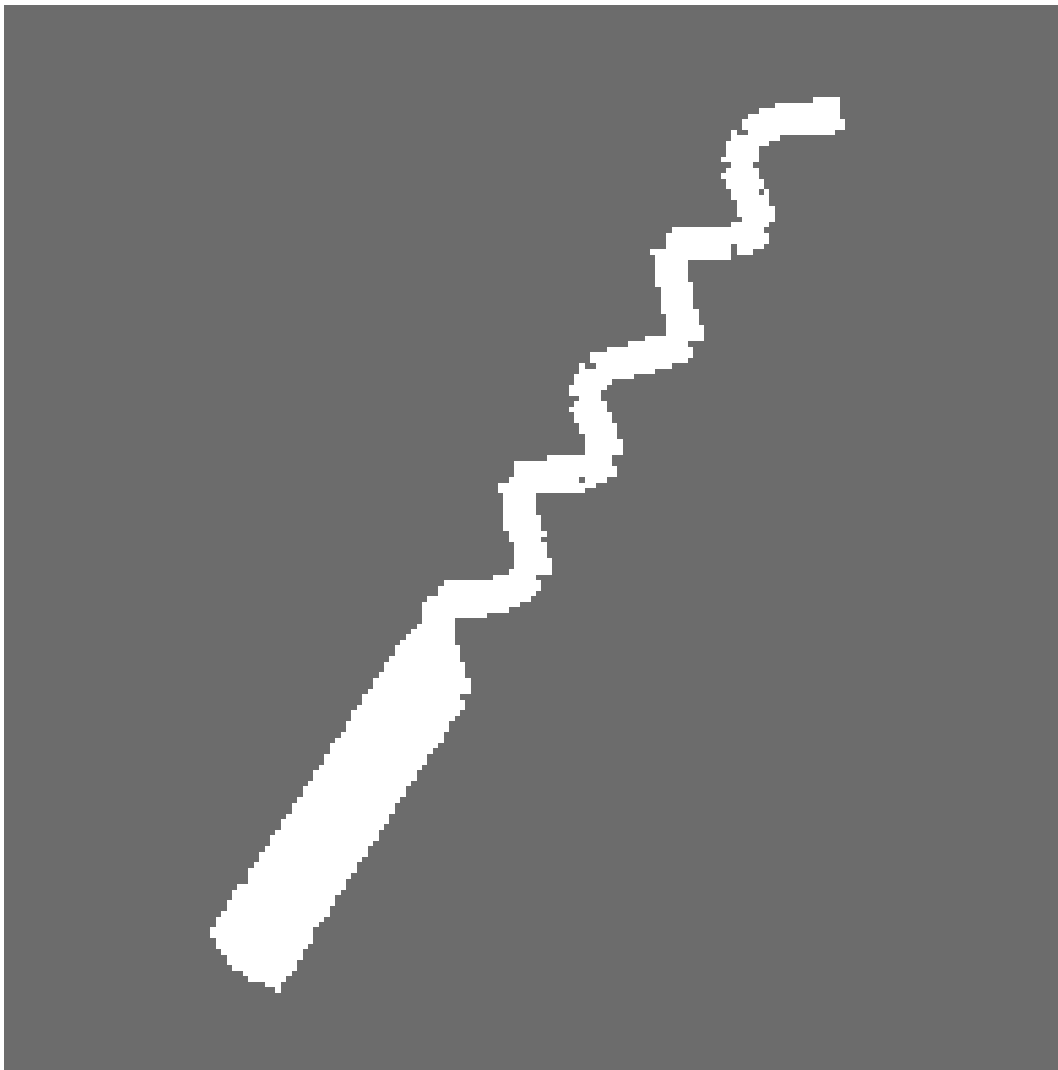


Figure 2.4: Single forward sweep.

every surface, or use quick-and-dirty contact detection heuristics to guide our mapping process.

2.5.2 Data Processing

Once we have the raw sensor data successfully plotted into a local occupancy map, we must convert this data into a form that is useful for our mapping algorithms. Here, we present three different forms of data processing that we use in our approach.

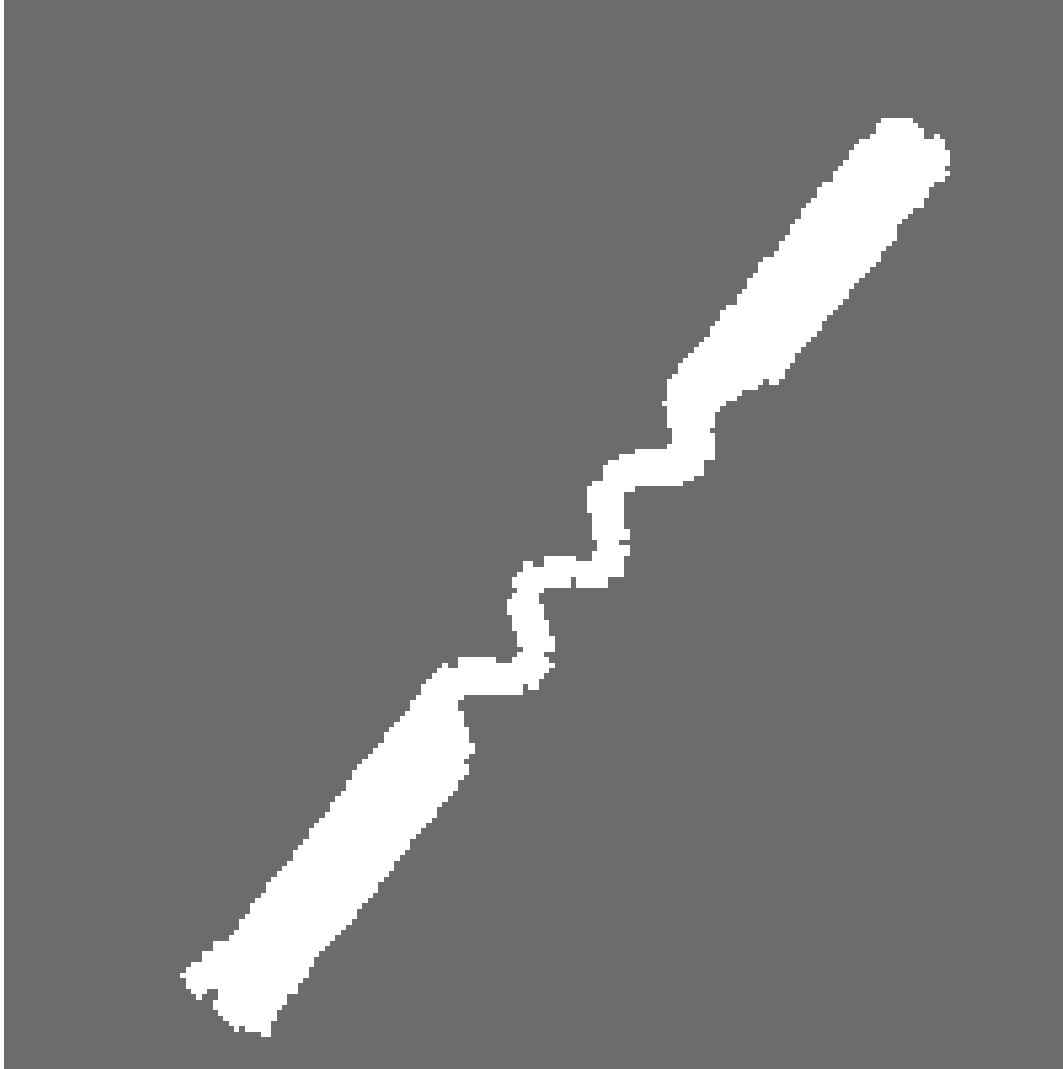


Figure 2.5: Forward and backward sweep.

Convex Hull

One way we process our free space data is by taking its convex hull. In theory, this would create some smooth boundaries and can plausibly represent the true local space under some certain conditions. The definition of the convex hull is, given a set of points P , find the convex polygon H with minimum area that contains all of P .

To create our set of points P , for each pixel (i_x, i_y) of the occupancy map M_p whose state is *free}, convert the pixel to Cartesian space point (p_x, p_y) using Equation Equation 2.1 and add to P . Using any convex hull algorithm, produce the resultant polygon in Cartesian space. For our work, we use the convex hull algorithm available in CGAL \cite{cgal:hs-chep2-12b}.

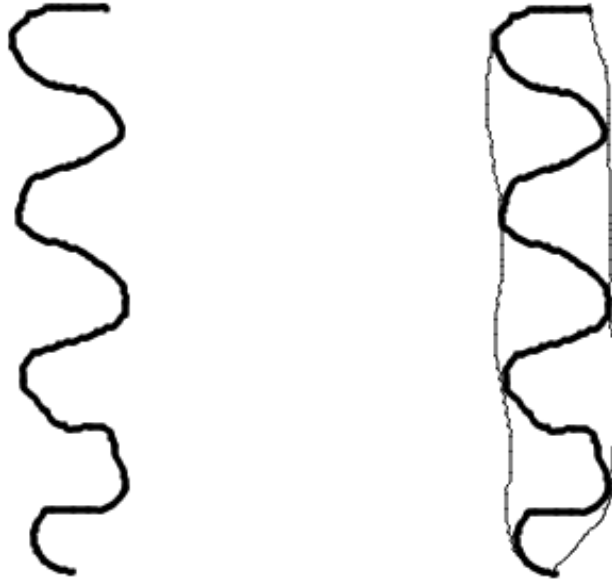


Figure 2.6: Free space data before and after convex hull.

An example of the convex hull operation on our free space data set appears in Figure 2.6. We can see for the case that the snake is in a straight pipe, the convex hull creates a natural representation of the local pipe environment, filling in the blanks of our blind spot. However, if the pipe is curved as in Figure 2.7, the convex property of the

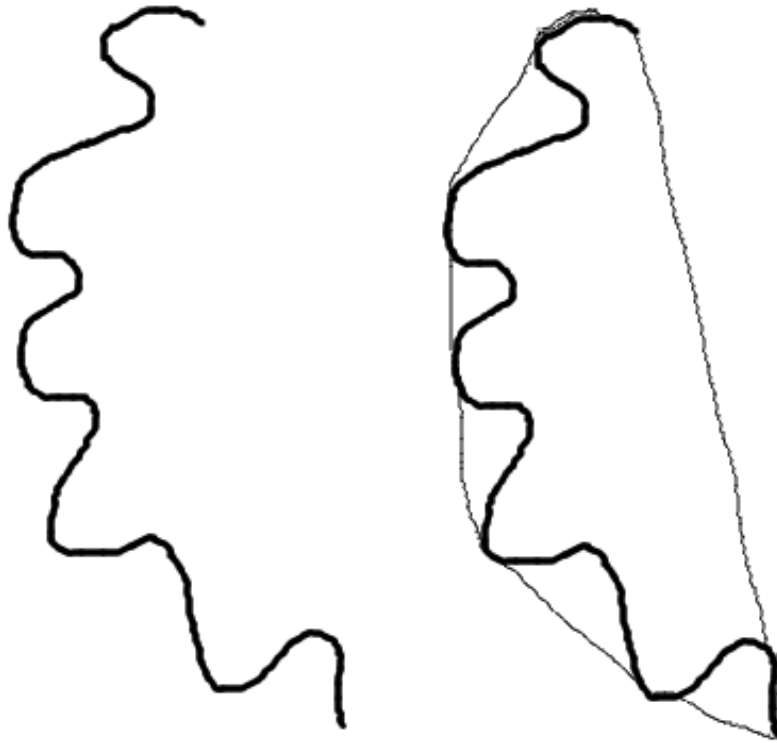


Figure 2.7: Free space data of curved posture before and after convex hull.

polygon necessarily erases any concave properties of the environment. This also removes any sharp features of the environment such as corners. Therefore, any use we may have for the convex hull will be in limited situations.

Alpha Shape

An alternative to the convex hull is the alpha shape \cite{Edelsbrunner:1983p772}. Like the convex hull, it creates a polygon or polygons that contain all the points. Unlike the convex hull, it can construct a containing polygon with concave or even hole features.

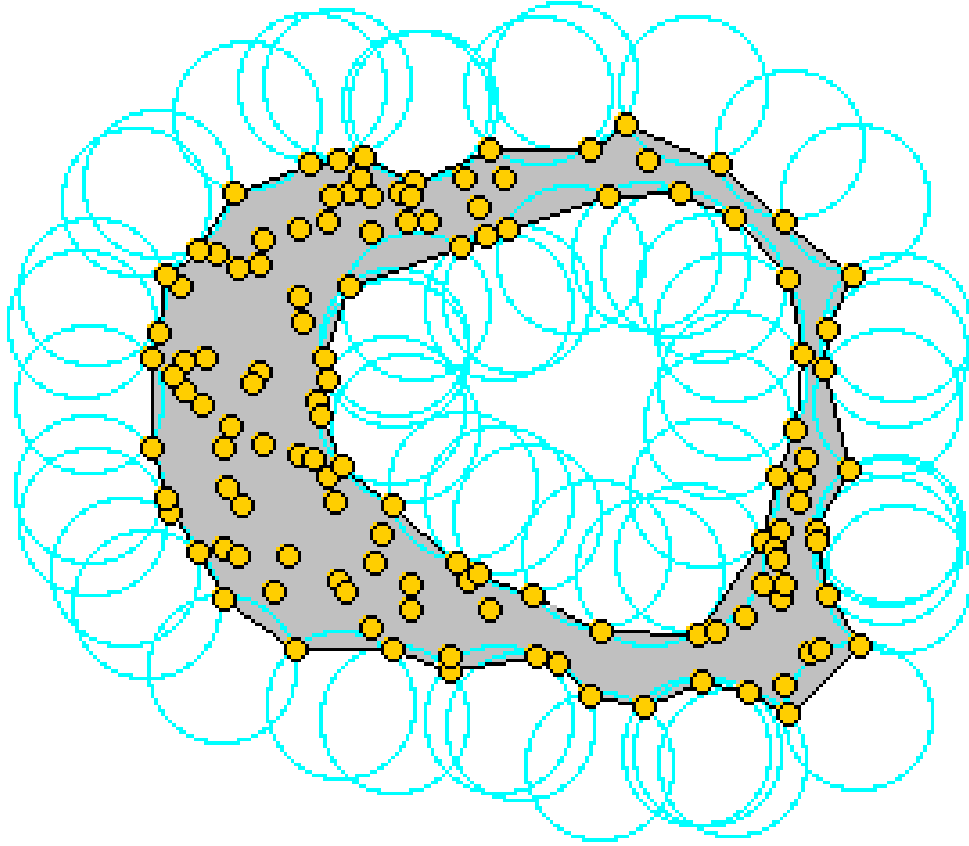


Figure 2.8: Alpha Shape example from \cite[cgal:d-as2-12b]

To construct the alpha shape, first we choose a radius r for a circle C . Next, if a pair of points p_i and p_j can be put on the boundary of C where no other point is on or contained by C , we add an edge between p_i and p_j . The result is seen in Figure 2.8

By changing the radius size, we can tune how much smoothing we want to occur in the resultant polygon, seen in Figure 2.9. If we set the radius to $r = \infty$, the alpha shape reduces to the convex hull. Therefore, this is a kind of “generalized convex hull” algorithm.

The benefit to this approach is that we can now capture the concave features of some of our local maps where the convex hull failed. Where Figure 2.7 shows the convex hull, Figure 2.10 shows its corresponding alpha shape. In both cases, the blind spot it

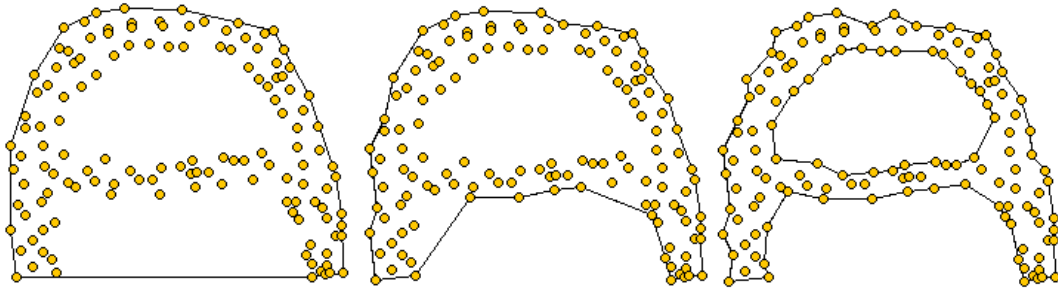


Figure 2.9: Alpha Shape changing radius from \cite{cgal:d-as2-12b)

smoothed over and filled in. This approach still suffers from the loss of sharp salient corner features, but the gross topology of the local environment has been captured.

For clarity, we refer to the alpha shape of our local free space as the *alpha hull* from here on out.

Medial Axis

Although polygons that represent the swept free space are useful, we need something that is more compact that also filters out the smoothing effects of blind spots and sharp features. That is, we want an approach where the negative effects of missing data, erroneous data, and loss of salient features are minimized.

For this purpose, we compute the medial axis, also sometimes known as thinning or skeletonization [cite]. This concept takes a shape and reduces it to a path or series of edges that follow the “spine” of a shape. Approaches range from a strict computational geometry approach such as the Voronoi diagram to image processing approaches of image thinning and skeletonization that erode a pixelized shape until the skeleton is all that remains [cite].

We are interested in extracting the medial axis of the alpha hull generated from our free space map. Since the alpha hull smooths the boundaries of the free space map, generating a medial axis will give us a topological representation of the free space that is resistant to boundary features. Given the free space map in Figure 2.11a, and

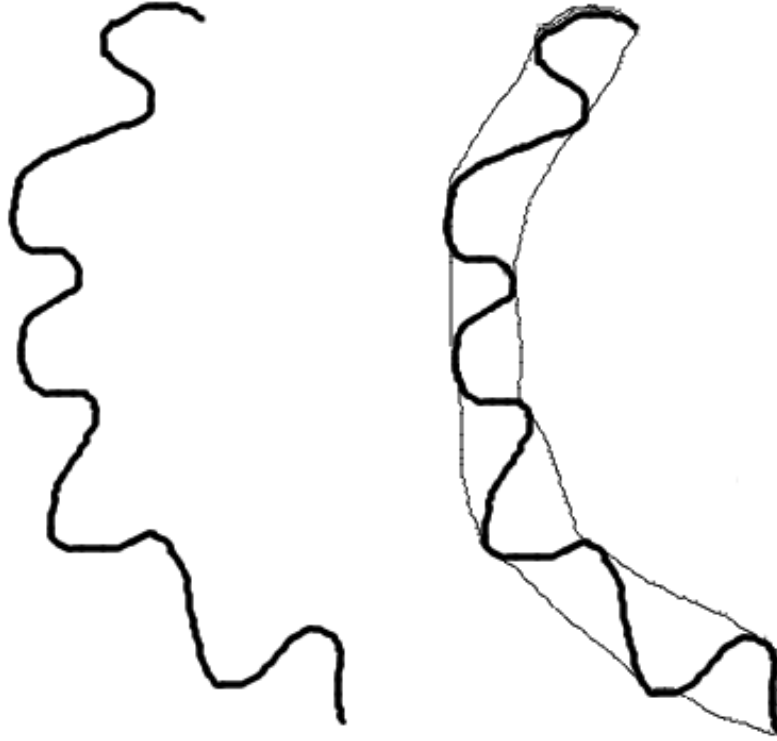


Figure 2.10: Alpha hull of free space data.

its corresponding alpha hull in Figure 2.11b, the alpha hull's conversion back to an image in Figure 2.11c, and its resultant medial axis shown in Figure 2.11d. We use the skeletonization algorithm from [ParkerJR] \footnote{C/OpenCV code written by Jose Iguelmar Miranda, 2010}.

We can see that the medial axis roughly corresponds to the topological representation of the pipe environment. However, it is crooked, pixelated, and does not extend the full length of the data set. We further treat this data to give a more useful representation.

Starting with the result from Figure 2.11d shown in Figure 2.12a, we create a minimum spanning tree (MST) graph where each node is a pixel from the medial axis and

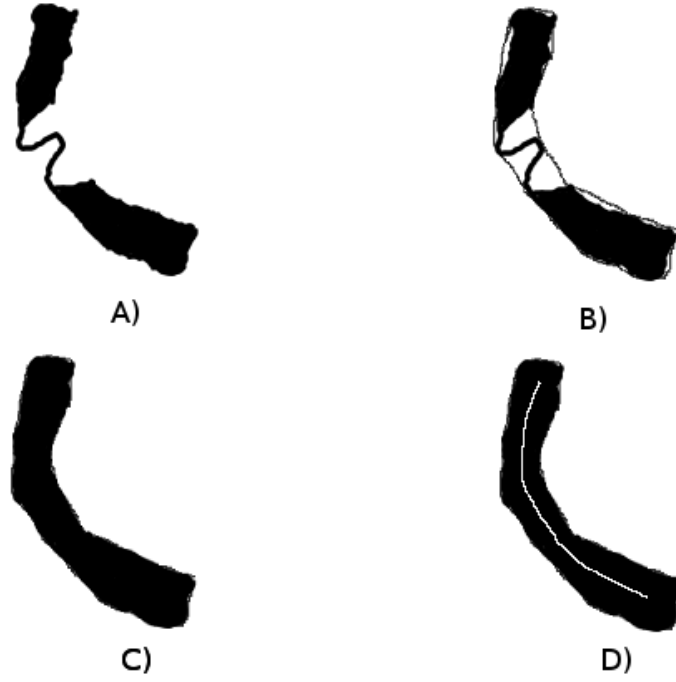


Figure 2.11: Process of generating medial axis.

an edge is added between two nodes if their corresponding pixels are neighbors, shown in Figure 2.12b.

This MST has many leaves due to the artifacts of pixelation. We can simply prune the whole tree by sorting all nodes by degree, and removing the nodes with 1 degree and their corresponding edges. In most cases, this will leave us with a single ordered path of nodes with no branches. In some cases, we will have a branch if the original free space map shows evidence of a junction.

In the case of a single path, our next step is to extend this path to full extent of the original shape. We begin by fitting a B-Spline curve to the ordered path. With an appropriate smoothing parameter, the spline curve will follow the path of the ordered points but will ignore the jagged edges from pixelation. We then uniformly sample points along this curve to convert it back to an ordered set of points. We extend this

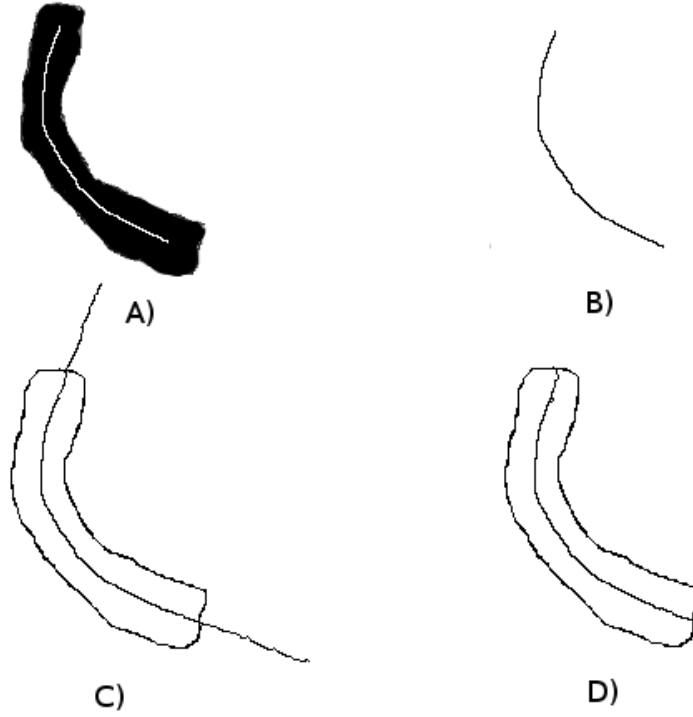


Figure 2.12: Process of generating medial axis.

path in the front and back by extrapolating more points along the direction specified by the curve tip, as in Figure 2.12c. Multiple tangent vectors are sampled along the tip neighborhood and their direction is averaged to get a direction that is immune to spline curving artifacts at the terminals. Finally, the series of points is cut off once the extrapolated points cross the alpha hull boundary, shown in Figure 2.12d.

In the case that we have a branch, we perform this series of operations for the path between each combination of pairs of terminals. For each medial axis of a free space map, there are $n = 2 + B$ end points where B is the number of branches. The number of unique paths of a medial axis is found by $\binom{n}{2}$ since we are using the MST and there is a unique path between each pair of points.

The final form is a compact representation of the topology of the local free space that removes the noise and uncertainty of the boundary and allows us to only represent

the area we can move through. This has a number of uses for our map-making that we describe in the next chapter.

2.6 Failures

Since the possibility of error occurring in our free space maps is very real and has the consequences of making the data near-useless, we want to do all we can to prevent and mitigate any failure conditions. As the primary source of error is anchor slip, we do all we can to focus on this issue while probing the environment. We use a number of techniques for both prevention and detection of error. We describe all of our approaches below.

2.6.1 Error Prevention

We have 6 strategies for preventing anchor slip during the course of probing the environment. These are the following:

1. Prescriptive Stability
2. Local Stability
3. Smooth Motion
4. Averaging Reference Poses
5. Separation of Sweep Maps

The first three we have discussed earlier, with prescriptive stability and local stability in section section 4.4 and smooth motion in section section 3.7. We use prescriptive and local stability to determine which reference poses are available to be activated. Whereas, smooth motion through the use of linearly interpolated steps by using the Transition behavior reduces the chance that our anchors will slip.

The prescriptive stability selection of the PokeWalls behavior requires the robot to only use the anchored portion of the snake body for reference poses. In particular, it is

very conservative, where only the segments at the very back and mechanically isolated from any of the sweeping motions in the front will be used for reference. This reduces the chance that any perturbations from the probing motions will have an effect on any of the active reference poses that we are using.

Averaging Reference Poses

For our fourth strategy, when actually using the reference poses to compute the position of the snake in our local free space map, we want to use as many of the reference poses as possible while filtering out any errors that would occur from possible pathological cases. If just one reference pose is erroneous and we use that reference pose to compute position of the snake in free space, it will severely damage our results. We want to mitigate the possibility of negative effects by taking the average of a set of reference poses when computing a snake’s position.

For instance, if we wanted to compute the origin of our local free space map in global space, we would compute the kinematic position of joint 19 with respect to some active reference pose P_k on joint and segment k . Using equation Equation 4.12 or Equation 4.13, we compute the position of P_{19}^k . For every P_k we use, we compute a new P_{19}^k that is possibly different. We then take the average of all of the computed P_{19}^k poses and take that as our best guess for P_{19} .

How do we select the set of active reference poses from which to compute our estimated snake pose? Of all available active reference poses, our approach is to use the largest set of contiguous poses to compute the average target pose P_{19} . Our assumption is that if we have a series of reference poses from 0 to 15, and 11 and 12 are deactivated, it is highly possible that 13, 14, and 15 are invalid because whatever caused 11 and 12 to be activated will likely have an effect on its neighbors. The larger section from 0 to 9 has less likelihood of being corrupted since more of our sensors indicate stability. Furthermore, if one or two of these reference poses are corrupted, having a larger set reduces the weight of an erroneous value. This example is shown in Figure 2.13.

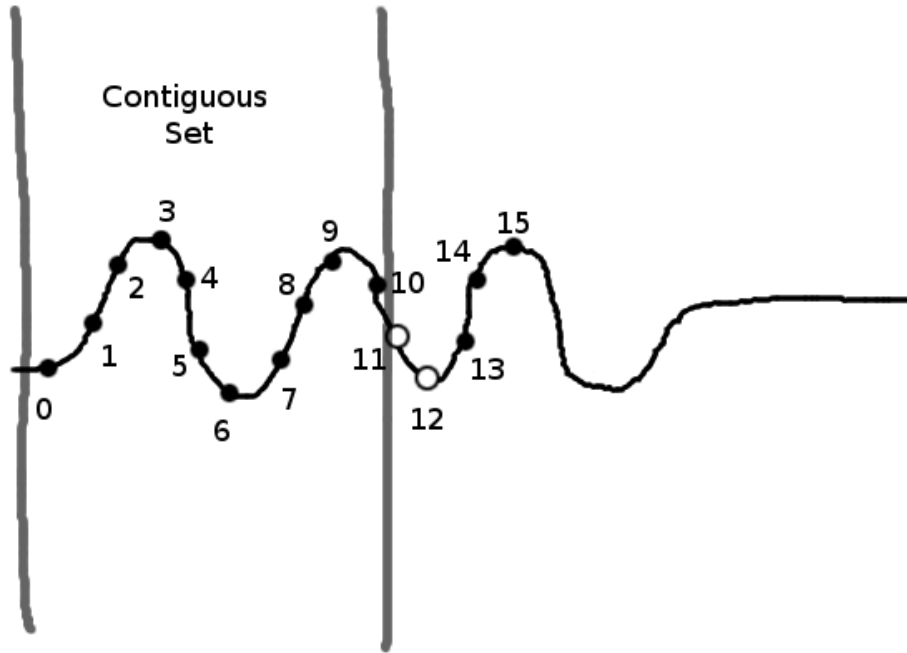


Figure 2.13: Largest set of contiguous reference poses.

Separation of Sweep Maps

Our fifth and final strategy for preventing errors in our sensor maps is to divide the forward sweep phase and backward sweep phase into separate maps. From our experiments, we determined that a consistent source of error occurs when switching the anchoring responsibility from the back half of the snake to the front half. The series of events of retracting the front half of the snake to anchors and extending the back half for sweeping tends to cause some discontinuity between the consensus of the back reference poses and the front reference poses. This will show with a very distinct break in the combined free space map.

To avoid this problem, we instead create two free space maps: one for the front sweep and one for the back sweep. What was previously shown in Figure 2.14a will now become the pair of maps shown in Figure b. Not only does this avoid corrupting the free space data in the map, but it allows us to treat the relationship between the two maps as a separate problem for which there are multiple solutions. Our previous sensor processing

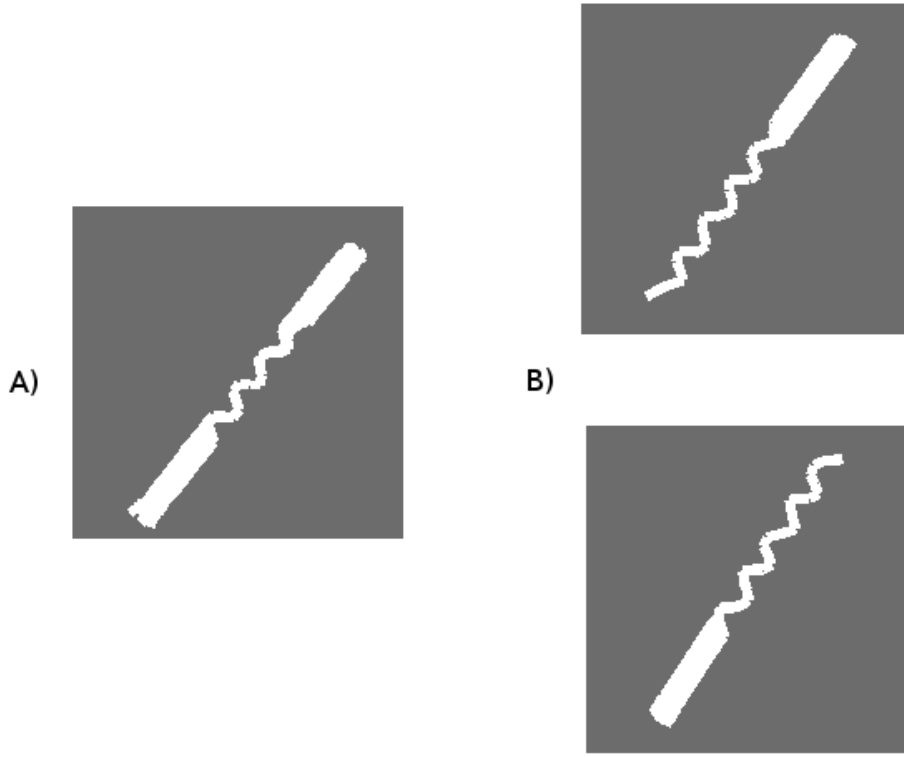


Figure 2.14: Separation of Sweep Maps.

algorithms work just as well because the alpha shape of the half-sweep free space map will result in an alpha hull from which an equivalent medial axis can be extracted.

We discuss our approach to managing the relationship between the two half-sweep local maps in the next chapter.

2.6.2 Error Mitigation

In the case that error is introduced into our local free space map, we are interested in mitigating its negative effects. We have developed two approaches for handling error when it occurs during sensing.

Since we start our mapping process by determining the global pose of the local origin P_{19} , error occurs when P_{19} is no longer in its proper place. Either it moves by translation or more commonly and critically, it experiences rotational error.

Reference Stabilization

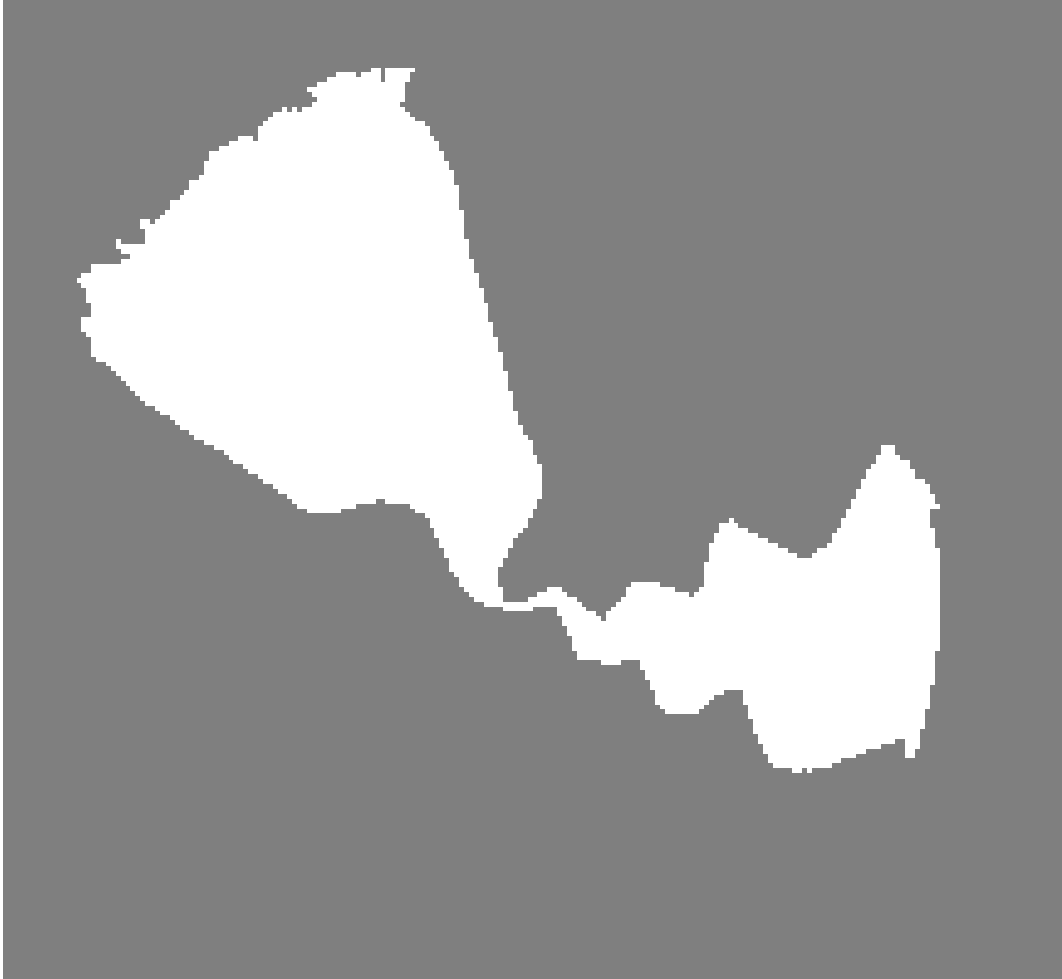


Figure 2.15: Local map rotational error.

A sudden rotation of P_{19} may occur, caused by any of the reasons detailed in Section section 4.4. The consequences of rotational error is that the entire body of the snake will rotate around the origin within the local map. This will result in a map feature shown in Figure 2.15.

We proactively combat this possibility by running a reference stabilization algorithm that continually corrects the local origin O_t for P_{19} in the local map at time t . For $t = 0$, the origin is $(0, 0, 0)$ for inputting into the equations Equation 2.6 and Equation 2.7. However, for each time step, we wish to calculate an O_t that is the most “stable” in case P_{19} becomes destabilized.

To do this, we remark that during the probing phase, the back anchored section of the snake as a whole will remain roughly in the same tight space even if its joints and segments should wobble and slip. Short a large amount of translational slipping down the pipe, taken as a whole, the body should remain in the same place. Therefore, in the local free space map, the back anchored portion should of the snapshot time t should also remain in the same neighborhood of the back anchor snapshot at time $t - 1$.

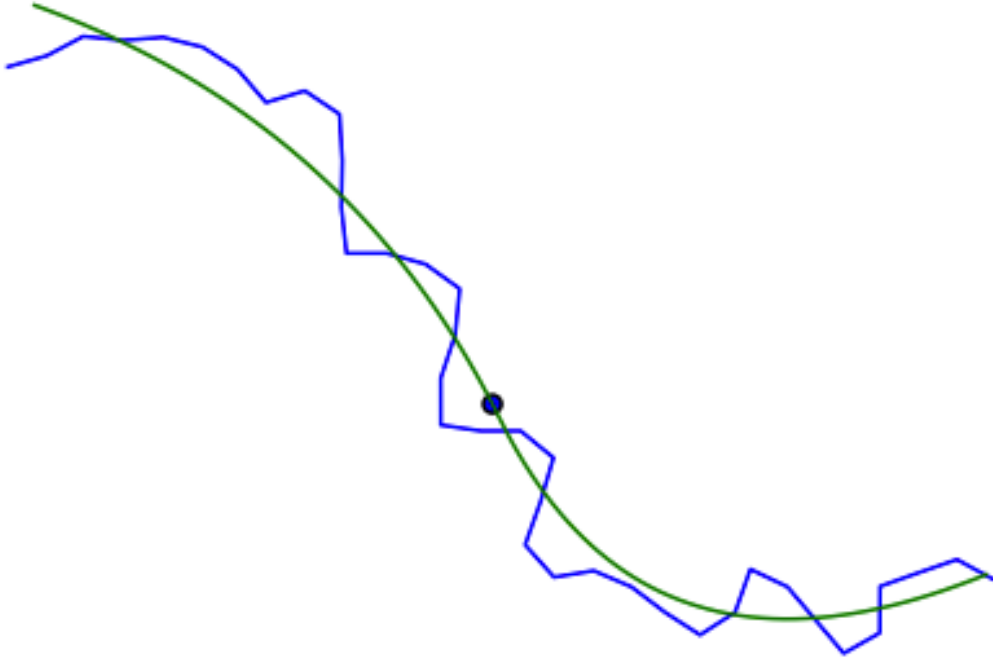


Figure 2.16: Gross Posture Approximation Curve of sample posture.

We enforce this observation by fitting B-spline curve β_t and β_{t+1} along the points that make up the reference poses of the back anchor segments for both the current and

previous snapshots. The B-spline curves are calibrated to smooth out the sinusoidal anchoring posture of the snake body and instead reflect the gross posture of the body in the confined environment as shown in Figure 2.16. We then find a $(\delta x, \delta y, \delta \theta)$ for β_{t+1} such that the two curves are aligned and then we update O_{t+1} to reflect this.

This approach prevents sudden rotational errors from occurring and corrects the snake's estimated pose in the local map while we are capturing sensor data by generating a new O_{t+1} that is consistent with past data. So even if the snake's body is wobbling or slipping, we will likely produce consistent sensor data.

Chapter 3

Control and Locomotion

3.1 Control Methodology

Backbone curve fitting, IK method, segmented behaviors

3.2 Behaviors

Locomotion steps, extensions, path-following, anchoring

3.3 Problem

FIXME: Related work and our contrasted difference. What can we achieve that others cannot. Why is our approach better for this particular case?

In order to successfully control a snake robot and have it move through the environment, we need a solution for locomotion, motion planning, and handling collisions. Since we have no exteroceptive sensors, this makes the problem challenging. The robot is unable to sense what is right in front of it and must move blindly. The snake could move into open space or collide with obstacles.

Part of the challenge is having no external sensors and the other part is general task-oriented control of a hyper-redundant robot. There are many biologically-inspired locomotion strategies that live snakes in nature use to move throughout the environment. The closest biological gait solution to moving in confined environments is the concertina gait shown in Figure 3.1.

This gait is characterized by a concertina motion of alternating extensions and contractions that result in a forward movement. The snake body pushes against both sides

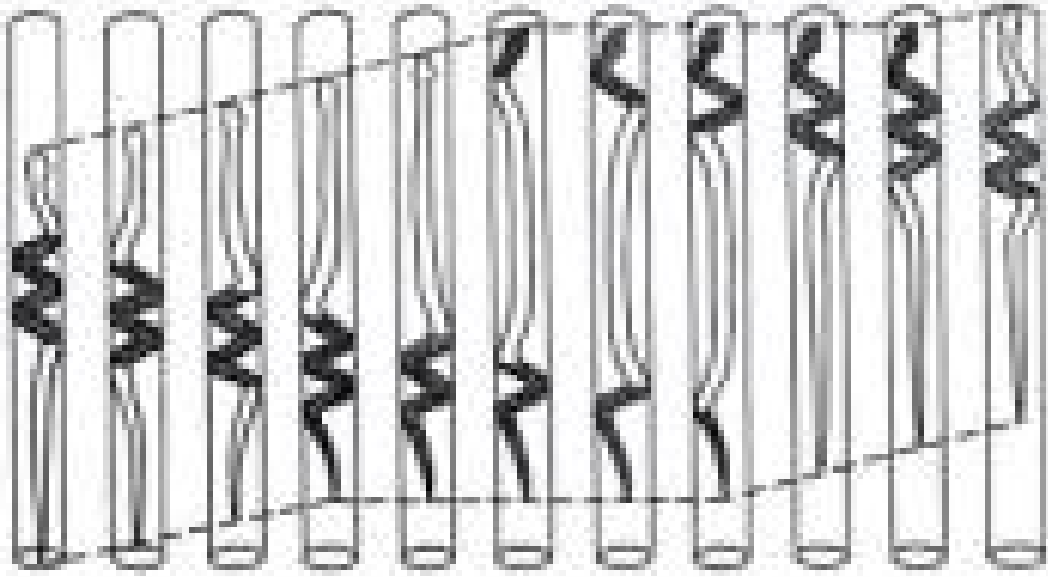


Figure 3.1: Biological Concertina Gait of a Snake in a Confined Space. Image taken from \cite{Gans:1980p775}

of the walls establishing anchors that allow the snake to alternate between pulling and pushing itself forward. Success of locomotion depends on the snake establishing high friction contacts with the environment with which to push and pull.

However, the differences between a real snake and our robot snake make a true implementation impossible. A real snake has the luxury of vision and olfactory sensors to provide early motion planning and a rich tactile sensing surface skin to provide feedback to its control system. Our robot snake has only the benefit of internal proprioceptive joint sensors. If we knew the exact width of the pipe walls, we could prescribe the perfect concertina motion to move through the environment smoothly.

A simple approach to making the fully anchored concertina posture, we could use the following equation:

$$\alpha_i = A * \cos\left(\frac{2\pi i f}{N}\right) \quad (3.1)$$

where α_i is the commanded joint angle for joint i , f is the frequency or the number of sinusoidal cycles per unit segment length, A is the maximum joint command amplitude, and N is the number of segments on the snake. Since there are N segments, there are $N-1$ joints. Therefore, $i \in [0, N-1)$. This equation requires some tuning to give the right results and can result in bad postures such as that shown in Figure 3.2. In order to effect locomotion, a sliding Gaussian mask should be applied to the joint command output to transition parts of the snake between fully anchored to fully straight to reproduce the biological concertina gait.

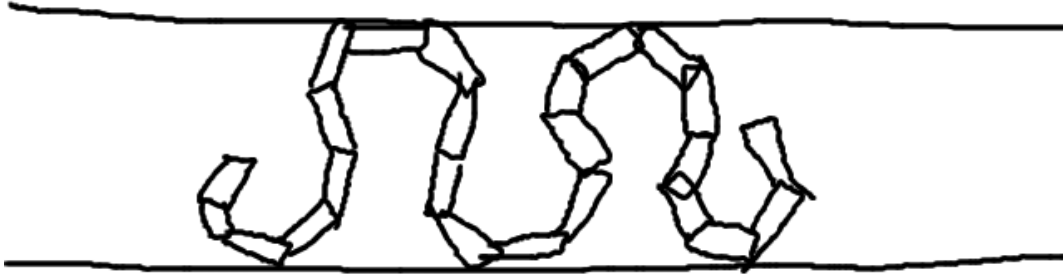


Figure 3.2: Improperly tuned concertina posture using equation Equation 3.1.

The difficulty of this approach is that we need a priori knowledge of the pipe width, the configuration of the snake needs to be tuned by hand for the particular snake morphology, and there is no sensory feedback to this implementation. With no feedback, there is no adaptive behavior possible. We need an approach that will work in environments of unknown and variable pipe width. Our robot needs to be able to adapt its locomotion to the width of the pipe.

Our desire is to be able to prescribe any type of snake posture, for any anchor width and any snake segment length or parameters, and have the snake automatically assume that posture. In order to do this, we need a means of specifying the posture and an inverse kinematics method for achieving that posture.

For both of these requirements, we use the backbone curve-fitting methodology first described by \cite{Chirikijan:1995p774}. This method of control is to produce a parameterized curve that represents the desired posture of the snake over time. Over time the curve changes to reflect desired changes in the snake posture. Snake backbone curve fitting is achieved by finding the joint positions that best fit the snake body onto the curve. This is found either by direct calculation or a search algorithm.

An example of backbone curve fitting can be seen in Figure 3.3. The parameterized curve is shown in light blue in the background. The blue snake body in the foreground is fitted onto the curve using an iterative search algorithm for each consecutive joint.

A typical application would be to specify the posture of the snake using a sinusoidal curve and then applying an inverse kinematics technique to fit the snake to the curve. The problem can be formulated iteratively as follows: for joints $i \in [0, k]$ and joint pose in space $p_i = \langle x_i, y_i, \theta_i \rangle$ are on the curve β with parameter t_i , find the joint angle a_k such that p_{k+1} is on the curve β and $t_k < t_{k+1}$.

For the equation β defined as:

$$y = A \sin(2\pi x) \tag{3.2}$$

the equation is monotonic along the x axis, so satisfying the criteria $t_i < t_{i+1}$ is the same as satisfying $x_i < x_{i+1}$.

If the length a of snake segment is l , we specify a circle equation centered at the joint position (x_i, y_i) with the following:

$$(x - x_i)^2 + (y - y_i)^2 = l \tag{3.3}$$

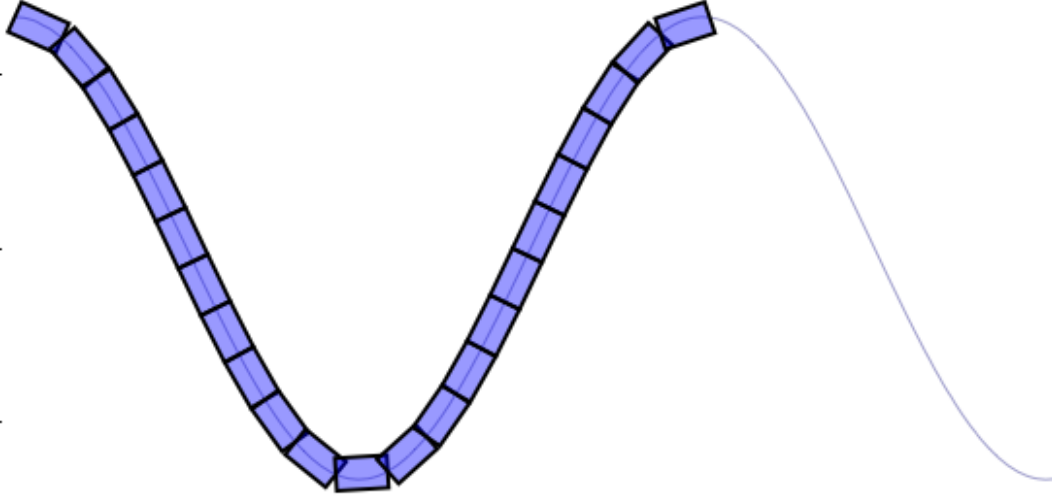


Figure 3.3: One sine period curve

Finding solutions for the simultaneous equations Equation 3.2 and ?? will give us possible solutions to x_{i+1} and y_{i+1} . For these two sets of equations, there are always at least 2 possible solutions. We need only select the solution that satisfies the invariant condition $x_i < x_{i+1}$. There may be more than solution. In which case, we select the x_{i+1} where $(x_{i+1} - x_i)$ is the smallest. This prevents the snake from taking shortcuts across the curve and forces it to fit as closely as feasibly possible to the parameterized curve given the snake robot's dimensions.

The above simultaneous equations do not have closed-form solutions and instead must be solved numerically. This can be computationally expensive using general equation solvers. Instead we propose a more specialized solver for this particular problem.

We choose a series of uniform samples $(q_0 \dots q_k \dots q_M)$ around a circle of radius l centered at (x_i, y_i) such that all points q_k have $x_k \geq x_i$. We are looking for instance of crossover events where the line segment (q_k, q_{k+1}) crosses over the curve β . Given at least one crossover event, we do a finer search between (q_k, q_{k+1}) to find the closest point on the circle to the curve β and accept that as our candidate position for joint point p_{k+1} . As long as we assume that the curve β is monotonic along the x-axis and a point of the curve β can be computed quickly given an x-value, this is a faster method of computing intersections of the circle with the backbone curve than a general numerical solver.

For instance, in Figure 3.23, we show a curve β described by a sine curve and a series of circles intersecting with the curve that indicate candidate locations for placing the subsequent joint on the curve. These are used to determine the appropriate joint angles to fit the snake onto the curve.

Now that we have a means of changing the snake's posture to any desired form given a parameterized, monotonic curve that describes the posture, we now need to form an anchoring approach that will work for arbitrary pipe widths.

3.4 Anchoring

In order to fit the anchor points to a pipe of unknown width, we need some way of sensing the walls. Since we have no exteroceptive sensors, the best way of sensing the width of the walls is by contact. Since we have no direct contact sensor per se, we must detect contact indirectly through the robot's proprioceptive joint sensors.

Using the backbone curve fitting approach, we take one period of a sine curve as the template form we wish the robot to follow. We then modify this sine period's amplitude, at each step refitting the snake robot to the larger amplitude, until the robot make's contact with the walls. This establishes two points of contact with the wall which assist in immobilizing the snake body.

It is clear from Figure 3.3 that as the amplitude of the curve increases, more segments are needed to complete the curve. If the sine curve is rooted at the tip of the snake, this results in the curve translating towards the snake's center of mass. Instead, we root the sine curve on an internal segment, as seen in Figure 3.4, so that the position of the anchor points remain relatively fixed no matter the amplitude and the number of segments required to fit the curve.

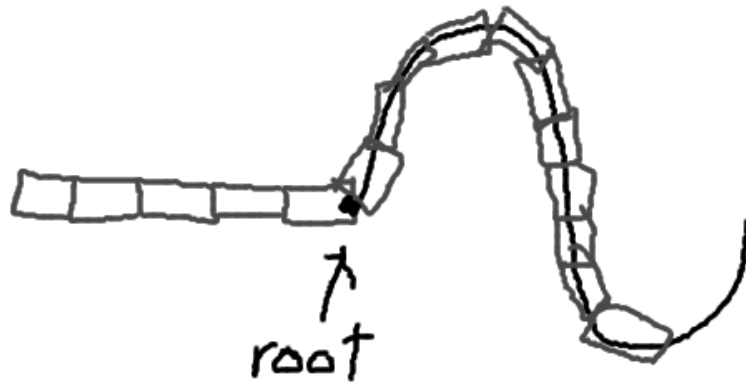


Figure 3.4: Anchor with not enough segments

Two points of contact are not statically stable if we disregard friction. Though friction exists in our simulation and in reality, we do not rely on it to completely immobilize our robot. Our normal forces are often small and the dynamic and transient forces can easily cause a contact slip. Therefore, we need at least 3 contact points to consider an anchor to be statically stable.

One way to achieve this is by adding new sine period sections to create another pair of anchors. The amplitude of the new sine period is separate from the previous anchor's amplitude and is represented by a new curve attached to the previous one. This way the

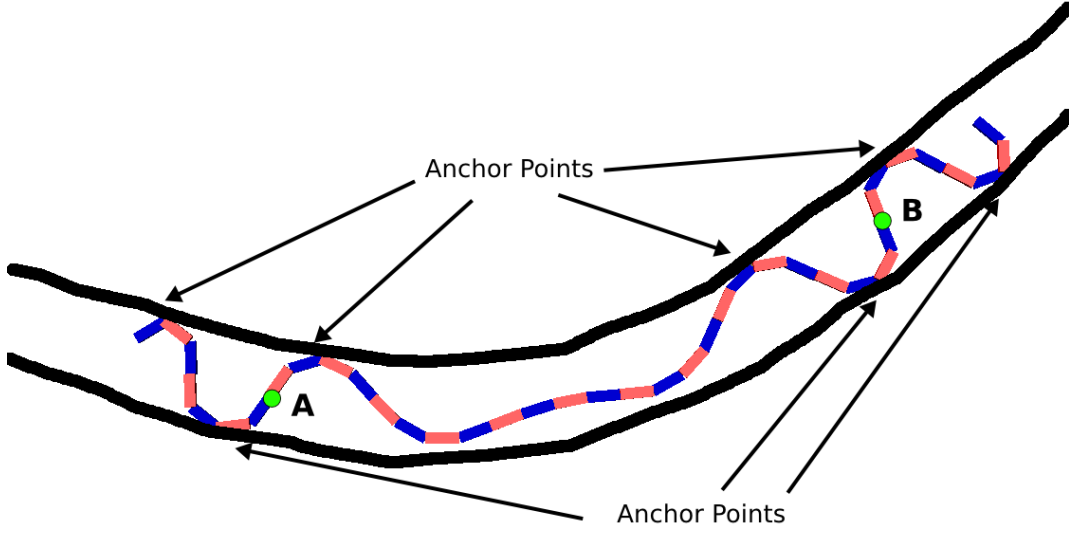


Figure 3.5: Anchor Points

amplitudes remain independent. The equation to describe two sets of sine period curves with independently controlled amplitudes are as follows:

$$y = U(x)U(2\pi - x)A_1 \sin(fx) + U(x - 2\pi)U(4\pi - x)A_2 \sin(fx) \quad (3.4)$$

where f is the frequency and $U(x)$ is a unit step function. Or to generalize for N periods and N pairs of anchor points:

$$y = \sum_{i=0}^{N-1} U(x - i2\pi)U((i+1)2\pi - x)A_i \sin(fx) \quad (3.5)$$

for each anchor curve amplitude A_i .

So now that we have the means to control the amplitude of our anchor points, we need some means of detecting that a contact is made and another to make sure the anchor is secure.

Our approach is to gradually increase the amplitude of an anchor curve until contact with both walls has been made. We will continue to increase the amplitude until we see significant joint error occur when fitting to the curve. If the amplitude became larger

than the width of the pipe, the snake will attempt fitting to a curve that is impossible to fit to and will experience a discrepancy in its joint positions compared to where it desires them to be.

The structure of this error will normally take the form of one or two large discrepancies surrounded by numerous small errors. This reflects that usually one or two joints will seriously buckle against the wall, while the rest of the surrounding joints can reach their commanded position without disturbance. An example of an anchor curve with larger amplitude than the width of the pipe is shown in Figure 3.6.

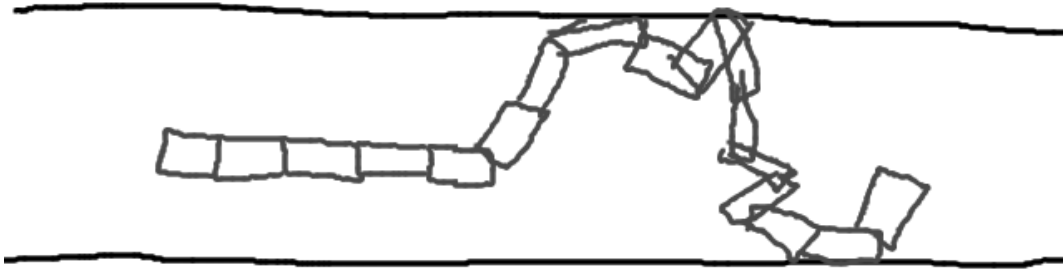


Figure 3.6: Anchor with amplitude larger than pipe width.

The contact is flagged once the maximum error reaches a certain threshold across all the joints of the anchor curve. Of the joints M of the anchor curve and the error e_j , if there exists $e_j > 0.3$ radians, then we flag a contact. It isn't so much that we are detecting a contact but a minimum pushing threshold against the wall. The robot is pushing hard enough to cause joint error over an experimentally determined threshold.

If j_k through j_{k+M} are the joints comprising the fitted anchor curve, the error of one joint is defined by $e_k = |\phi_k - \alpha_k|$. The maximum error is defined by $e_{max} = \max(e_k, e_{k+1} \cdots e_{k+M-1}, e_{k+M})$.

The amplitude is initially changed by large increments to quickly find the walls. Once the threshold has been reached, the current and last amplitude are marked as the max and min amplitudes respectively. We then proceed to perform a finer and finer search on the amplitudes between the max and min boundaries until we reach a snug fit that is just over the error threshold. This is a kind of numerical search(?).

The pseudocode for this algorithm is as follows:

Algorithm 3 Anchor Fitting

```

 $\hat{A} \leftarrow 0$ 
 $A_{min} \leftarrow 0$ 
 $A_{max} \leftarrow \infty$ 
 $\delta A \leftarrow 0.04$ 
while ( $A_{max} - A_{min} \geq 0.001$ ) & ( $\delta A \geq 0.01$ ) do
     $\hat{A} \leftarrow \hat{A} + \delta A$ 
     $e_{flag} \leftarrow \text{setAnchorAmp}(\hat{A})$ 
    if  $\neg e_{flag}$  then
         $A_{min} \leftarrow \hat{A}$ 
    else
         $A_{max} \leftarrow \hat{A}$ 
         $\delta A \leftarrow \delta A / 2$ 
         $\hat{A} \leftarrow A_{min}$ 
         $\text{setAnchorAmp}(\hat{A})$ 
    end if
end while

```

The main objective of this code is to reduce the difference between maxAmp and minAmp as much as possible. minAmp and maxAmp are the closest amplitudes under and over the error threshold respectively. The function setAnchorAmp() sets the amplitude, performs the curve fitting, and reports back any error condition as described earlier. Once this algorithm is complete, we have made a successful anchor with two contact points under compression without the fitted anchor curve being distorted by joint buckling.

3.5 Curves

When we describe curves for use in backbone curve fitting, they must be assigned to a frame of reference and usually have a starting point. Most often, the frame of reference chosen is one of the local segment frames on the snake body. However, sometimes we could choose the global frame if we wanted to navigate or probe something specific in the environment. The local frame curves that we use all start from a specific body segment and sprout from that segment like a plant. We say that this curve is rooted in segment X.

3.6 Behaviors

Our method of control is a behavior-based architecture that is charged with reading and tasking the servo-based motor controllers of each joint. Each behavior may be a primitive low-level behavior or a high-level composite behavior composed of multiple sub-behaviors. Furthermore, a behavior may have complete control of every joint on the snake or the joints may be divided between different but mutually supporting behaviors. This architecture allows us to achieve a hierarchy of behavior design as well a separation of responsibilities in task achievement. For instance, the back half of the robot could be responsible for anchoring, while the front half could be responsible for probing the environment as seen in the example architecture in Figure 3.7.

Each behavior in the behavior-based architecture is time-driven. It is called periodically by a timer interrupt to compute the next commands for the following time-step. This could be variable time or constant time, but to make our behavior design simple, we use 10ms constant time steps in our simulation.

At each time step, the state of the robot is captured and driven to the behaviors. The data includes a vector of joint angles ϕ_i , a vector of commanded angles α_i , and a vector of maximum torques m_i . These values were described in the previous section X. The output of each behavior is a vector of new commanded angles $\hat{\alpha}_i$, a vector of new



Figure 3.7: Separation of functionality

max torques \hat{m}_i , and a vector of control bits c_i . The values of $\hat{\alpha}_i$ can be any radian value within the joint range of motion or it can be NULL. Likewise, the new max torque of \hat{m}_i can be any non-negative max torque threshold or NULL. The NULL outputs indicate that this behavior is not changing the value and if it should reach the servo-controller, it should persist with the previous value.

The bits of the control vector, c_i , are either 1, to indicate that the behavior is modifying joint i , or 0, to indicate that it has been untouched by the behavior since its initial position when the behavior was instantiated. This control vector is to signal the activity to parent behavior that this part of the snake is being moved or controlled. The parent behavior does not need to respect these signals, but they are needed for some cases.

Our behavior-based control architecture follows the rules of control subsumption. That is, parent behaviors may override the outputs of child behaviors. Since we can also run multiple behaviors in parallel on different parts of the snake, sometimes these

behaviors will try to control the same joints. When this happens, the parent behavior is responsible for either prioritizing the child behaviors or adding their own behavior merging approach.

Asymmetric behaviors that run on only one side of the snake such as the front are reversible by nature. That is, their direction can be reversed and run on the back instead. All behaviors with directional or asymmetric properties have this capability..

Finally, parent behaviors can instantiate and destroy child behaviors at will to fulfill their own control objective. All behaviors are the child of some other behavior except the very top root-level behavior which is the main control program loaded into the robot and responsible for controlling every joint. The root behavior is responsible for instantiating and destroying assemblages of behaviors to achieve tasks as specified in its programming. We will discuss some of these behaviors and child behaviors in the following sections.

3.7 Smooth Motion

We desire the motion of our snake robot to be slow and smooth in nature. It does us no benefit for the motion to be sudden and jerky. Moments of high acceleration can have unintended consequences that result in our anchor points slipping. Either collisions with the environment or transient internal dynamics can cause the anchor points to slip.

Our method of ensuring smooth motion is to take the initial and target posture of the joints of the snake, perform linear interpolation between the two poses, and incrementally change the joint angles along this linear path. For instance, if the initial joint angles are $s_0...s_n$ and the target joint angles are $t_0...t_n$, the interpolated path for each joint j is found by $g_{jr} = s_j + (t_j s_j) * (r/100)$ for $r \rightarrow 0, 100$, for 100 interpolated points on the linear path. The resultant motion is a smooth transition from initial to target posture as seen in Figure 3.8.

This is the definition of the HoldTransition behavior. When it is instantiated, it is given an initial pose vector S and target pose T , where some values of t_i in T and s_i in

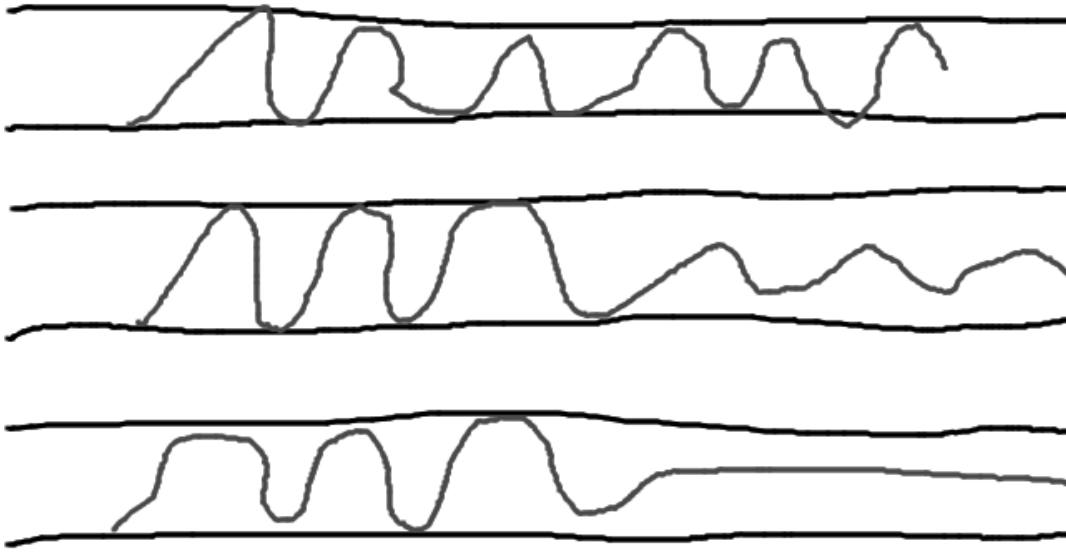


Figure 3.8: Smooth motion from interpolation of posture.

S may have NULL for no command. At each step of the behavior, using the equation $g_{jr} = s_j + (t_j s_j) * (r/100)$, r is incremented to compute the new joint command. If t_j is NULL, then $g_{jr} = s_j$. Once $r = 100$, it returns True on `step()` and on all subsequent steps, $g_j = t_j$.

3.8 Behavior Merging

There are a few methods for merging behaviors that overlap in some way. One way of the previous section is for two behaviors to overlap temporally and using the `HoldTransition` behavior to handle a smooth transition from one configuration to another.

In the event that two behaviors control adjacent sets of joints or overlap their control in some way, a conflict resolution method is needed to not only select the proper command for contested joints, but to prevent either behavior from negatively affecting functionality of the other by modifying any positional assumptions or introducing any unintended forces or torques to the other side.

A common occurrence is that two behaviors may try to control the same set of joints at the same time or otherwise. This is a conflict that requires resolution by the parent behavior. In this section we present three different ways to merge the outputs of different behaviors as means of conflict resolution. They are, in the order presented, the precedence merge, the splice merge, the convergence merge, and the compliance merge respectively.

Given that all child behaviors have an ordering, the default resolution method is to take the first behavior's control output over all others. This is called precedence merging. An ordering is always specified by the parent at the time it instantiates the child behaviors. If the first behavior's output is NULL, then it goes to the next behavior and so on until a non-NULL value is found or the last behavior returns a NULL, in which case the parent also returns a NULL unless the parent otherwise specifies.

Precedence merging can be crude when trying to maintain a stable and immobilized position in the environment. Sudden changes at the behavior-boundary can cause jarring discontinuities on the snake's posture and result in loss of anchoring as seen in Figure 3.9. A more finessed approach would disallow these discontinuities and provide a non-disruptive merging. The first approach that does this is the splice merge.

In the event that two behaviors overlap, we have the option of having a hard boundary between the behaviors centered on a single joint. Except in the rare case that both behaviors want to command the splice joint to the same angle, it is highly likely that the merge will be discontinuous. In order to ensure that positional assumption is maintained for both behaviors, the behaviors must be spliced so that neither behavior disrupts the other.

If the splice joint is j_s , behavior A controls joints j_0 through j_s , behavior B controls joints j_s through j_{N-1} , S_{s-1} is the body segment connected to j_s in behavior A, and S_s is the body segment connected to j_s in behavior B, we have the situation shown in Figure 3.10a. If behavior A commands j_s to α_a to put segment S_s in the position shown in Figure 3.10b and conversely, if behavior B commands j_s to α_b to put segment S_{s-1}



Figure 3.9: Discontinuity in behaviors results in clash of functionality.

in the position shown in Figure 3.10c, the two behaviors can be spliced discontinuously with no disruption to either behavior by setting j_s to $\alpha_s = \alpha_a + \alpha_b$. The result is shown in Figure 3.10d.

This is the behavior splicing approach because it stitches the behaviors together in a clinical way to ensure proper functionality of both. Its primary role is to connect behaviors with discontinuous conflicts on the behavior boundary and whose positions must be maintained for functional purposes. For more fuzzy continuous boundaries, we use the convergence merging approach.

For the two behaviors shown in Figure 3.11a and Figure 3.11b, the resultant convergence merge is shown in Figure 3.11c. For this approach, there is no discrete boundary but one behavior converging to another over several joints. For a given joint j_i somewhere in this convergence zone, and the commanded values for behaviors A and B being α_a and α_b , the converged command value for j_i is computed by:

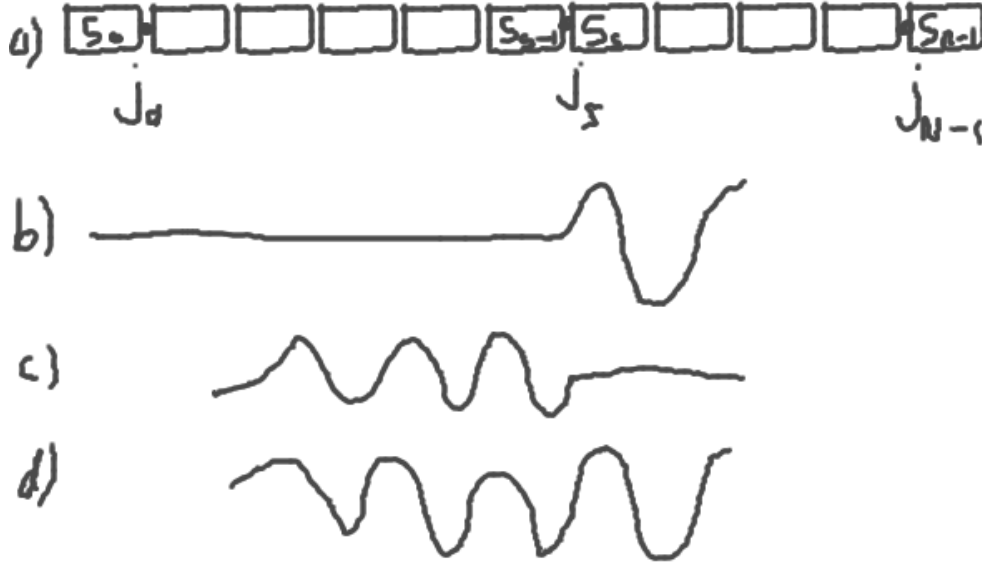


Figure 3.10: Splice joint and connecting segments.

$$\alpha_i = \alpha_a + (\alpha_b \alpha_a) / (1 + \exp(i - c)) \quad (3.6)$$

where c is a calibration parameter that controls the magnitude and location of the convergence along the snake. As $c \rightarrow +\infty$, $\alpha_i \rightarrow \alpha_b$. As $c \rightarrow -\infty$, $\alpha_i \rightarrow \alpha_a$. In practice, $|c| < 20$ is more than sufficient for complete convergence to one behavior or the other. The i parameter in the exponent ensures that the convergence value is different for each of the neighboring joints. This produces the effect shown in Figure 3.11c.

If we modify c , this gives us a control knob on the merge and can be moved up and down. If we move $c \rightarrow +\infty$, behavior B takes complete control of the snake. If we move $c \rightarrow -\infty$, behavior A takes control of the snake. c can be changed over time to create a sliding transition effect with a convergence boundary. In fact, this is the basis for a behavior called HoldSlideTransition.

A fourth and final way for two behaviors to be merged is the compliance merge. This is the case where two behaviors are not adjacent but are far away from each other, but

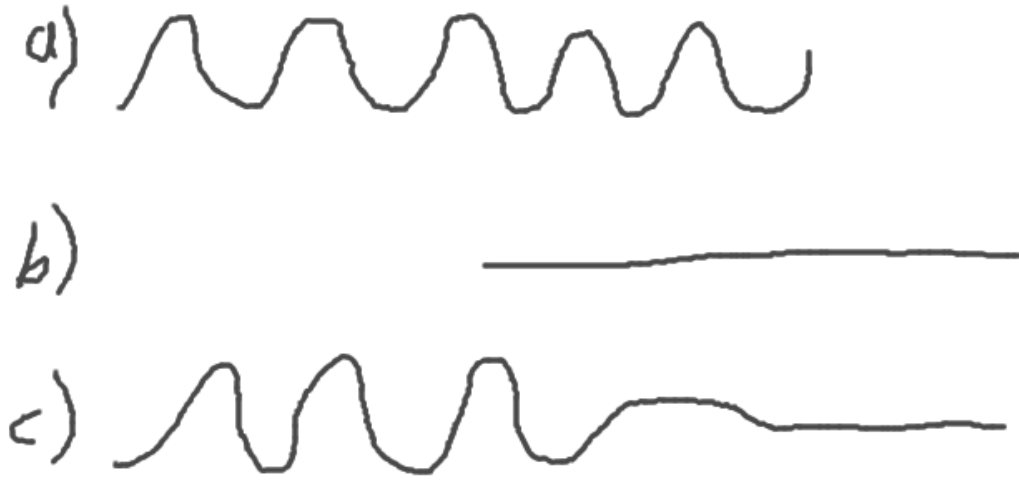


Figure 3.11: Convergence merge.

still interfere with each other somehow by inflicting unwanted forces and torques between the behaviors.

A compliance merge resolves this by selecting a group of joints between the two behavior's joint sets to be compliant or non-actuated. This has the result of absorbing any forces or torques transmitted by either behaviors and mechanically isolating one side of the snake from the other. An example is shown in Figure 3.12.

3.9 Compliant Motion

In the previous section, we mentioned compliance but not our implementation. Compliant motion is a much used technique in robotics and has been discussed widely (cite). The two approaches are either passive or active compliance. Our approach is to use passive compliance since we have no means to detect contact or sense obstacles.



Figure 3.12: Compliance merge.

Passive compliance is achieved by changing the settings on the max torque parameter of each joint's servo controller. We use a high setting for active motion, a low setting for compliant motion, and zero for keeping the joint unactuated.

Besides using a compliance merge to mechanically isolate two behaviors, we also use compliance as an exploration strategy. Since we have no exteroception, the only way to discover walls and obstacles is to collide with them. Compliant impacts with obstacles have a couple benefits. It prevents the force of the impact from transmitting to the body of the snake and possibly causing anchor slip. It also allows the joints of the snake to give out and take the shape of the environment around it.

This latter benefit is one of our primary means of sensing and exploring the environment. By passively letting the snake robot assume the shape of the environment, it guides our mapping and our locomotion. Until we have mapped out open space and boundaries, we have no way of directing our robot towards them beyond colliding with the unknown.

3.10 Stability Assurance

In a previous section on smooth motion, we discussed an interpolation technique to smoothly transition from one posture to another. The primary motive of this was to keep the parts of the snake body that are immobilized from being destabilized by transient forces and causing anchor slip. Static forces from prolonged pushing against an obstacle or wall are a separate matter.

For a pose transition that has a sufficiently large number of interpolation steps of sufficiently large duration, we can reasonably be assured that no transient forces from dynamics or collision will cause anchor slip because we are moving very very slowly. However, sufficiently long transition times for reliability may be impractical for applications, since times for a simple transition can be upwards of 1–2 minutes using a conservative approach. For a robot that performs hundreds of moves that require transitions, this is an unacceptable approach.

If we focus on being able to detect transient forces on the snake body instead, we can use this to control the speed of our movements instead of a one-size-fits-all approach of long transition times for all motion. We have developed a heuristic technique to do just this.

Our approach is to use our only source of information, joint angle sensors, as make-shift stability monitors of the entire snake. That is, if all the joints stop changing within a degree of variance, we can call the whole snake stable. Once we have established that the snake is stable, we can perform another step of motion.

For each, we compute a sliding window that computes the mean and variance of the set of values contained in. If at every constant time step, we sample the value of some joint i to be ϕ_{it} , then we compute:

$$\mu = \sum_{t=j-K}^j \frac{\phi_{it}}{K} \tag{3.7}$$

$$\sigma^2 = \sum_{t=j-K}^j \frac{(\phi_{it}\mu)^2}{K} \quad (3.8)$$

K is the width of the sliding window or the sample size used for computing the variance. This and the time step size δt , are used to determine the resolution and length of variance computation. In our implementation, with some exceptions, we use $\delta t = 1\text{ms}$ and $K = 20$. That is, for N joints, we compute the variance of each joint's angle for the last 20 readings once every 1ms. This may be changed and retuned depending on the available computing resources, the resolution of the sensors, and the sensor's sample rate.

Finally, we can determine if the snake is stable if all of the joint variances fall below a threshold S_v and stay that way for over time S_t . In our case, we set $S_v = 0.001$ and $S_t = 50\text{ms}$.

We are primarily interested in preventing anchor slip. Most often, it is not necessary to wait for the entire snake to hold still before moving. Instead, we can focus just on the joints in the neighborhood of the anchor points. By computing just the variances of the joints in the local neighborhood of the anchor points, we can determine local stability. Using local stability, we gain some confidence that our anchor points do not slip between motion steps.

In order to use this concept of local stability, we need to have some indication of which joints to monitor and which to ignore. Fortunately, the control vector c , output of the behaviors mentioned in a previous section, is just the kind of information we need to know where to direct our local stability attention. If the values of a control vector indicate '0', this means that these joints are not modified by the behavior and should remain stable before performing another move step. If the values are '1', these joints are actively modified by the behavior and we should not expect these joints to remain stable between move steps. The behavior prescriptively tells us how it should behave and the stability system processes it to accommodate.

3.11 Adaptive Step

Using these tools at our disposal, we can now build a suitable locomotion behavior for an unknown pipe with no exteroception. The entirety of our designed behavior is shown in Figure 3.13 and is called the adaptive concertina gait, a biologically-inspired gait based on the concertina gait but modified for the change in sensors. The behavior is divided into 6 states, and each level of Figure 3.13 shows one of those states. We describe the states as follows:

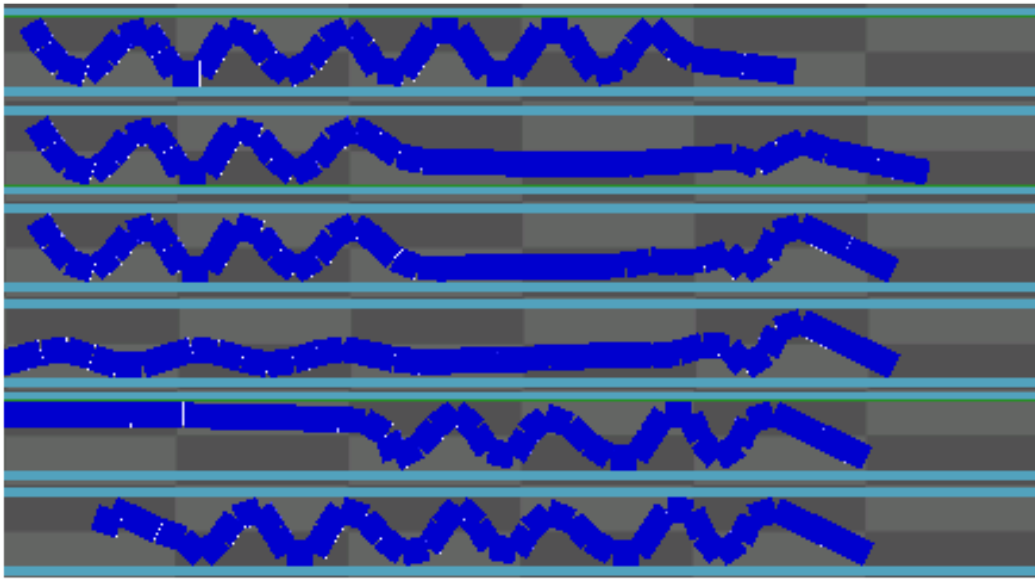


Figure 3.13: Adaptive Step Concertina Gait

1) Rest-State (Initial): Rest-State is the initial fully anchored posture of the snake robot. This is our initial pose and it acts as a stable platform from which exploratory or probing behaviors can be executed to sense the environment with little chance of slips or vibration due to the multiple anchor contact points. There is no other action here than to hold the posture that it was already in. The Rest-State is the initial state and the final state of the concertina gait.

2) Front-Extend: In the Front-Extend state, the forward segments are gradually transitioned from their initial position to a straight-forward position. The joints are compliant to the boundaries of the environment to accommodate turns in the pipe.

3) Front-Anchor: The Front-Anchor state takes the extended portion of the snake and attempts to establish an anchor to the pipe as far forward as possible. The locomotion distance is maximized the further forward the front anchor is.

4) Back-Extend: The Back-Extend state follows a successful Front-Anchor event. All anchors established in the back segments are gradually extended until they are straight. Again, the joints are compliant so that they can conform to the walls of the environment.

5) Back-Anchor: The Back-Anchor state involves establishing multiple anchors with the remainder of the body segments.

6) Rest-State (Final): Upon conclusion of the Back-Anchor state, a single step of the adaptive concertina gait is complete and the snake is now in the Rest-State. From here we can do probing of the environment or perform another step forward.

A successful transition through all the states results in a single step. Multiple steps are used to travel through the environment. We describe no steering mechanism for this locomotion gait because the robot has no means to sense the environment in front of it. However, the robot's compliant posture will adapt to any junctions or pipe curvature and follow it.

We now describe the implementation of each of these states and their composition of behaviors.

3.11.1 Front-Extend

From the fully anchored Rest-State stage, the goal of the Front-Extend stage is to release the front anchors and stretch the front half of the snake as far forward as possible without compromising the rear anchors. The further forward we can extend, the further the snake can travel in a single step.

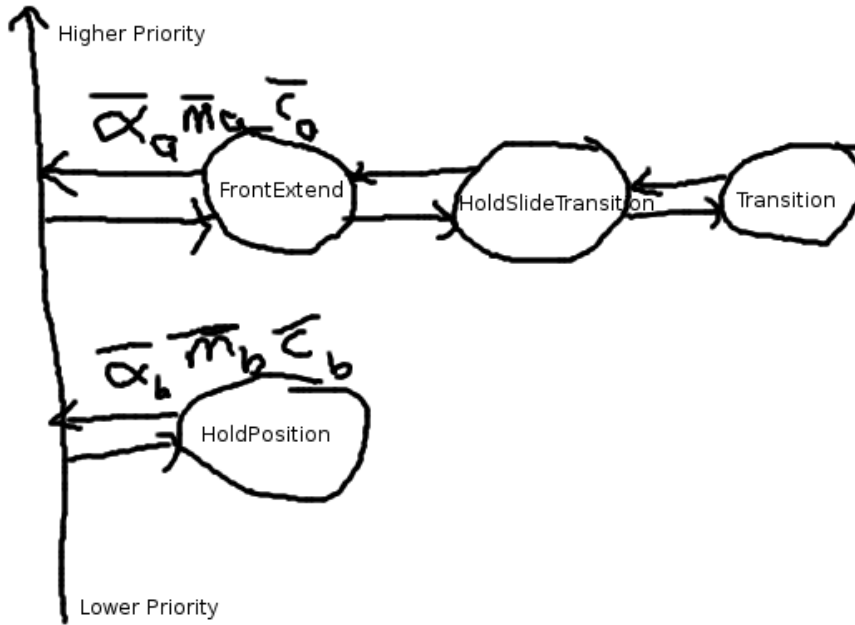


Figure 3.14: Front-Extend behavior assembly

If the extended snake arm makes a lateral impact, the walls will guide the movement of the snake but not otherwise hinder the behavior. In the event of an actual obstruction, the tip's movement will stop. We are able to track whether the position of the tip hasn't moved overtime and are able to set a flag to abort the behavior at the current posture.

Its implementation consists of 4 behaviors arranged as shown in Figure 3.14. We explain each behavior's functionality.

HoldPosition: The purpose of this behavior is to output the same joint commands indefinitely. It is instantiated with a vector of joint commands, and it continues to output these joint commands until termination. In this case, it is instantiated with the entire initial anchored posture of the snake from Rest-State and continues to output this posture. The behavior's output is gradually subsumed by the growth of the FrontExtend behavior in a precedence merge. HoldPosition is placed 2nd in the behavior ordering at the root level for this reason.

Transition: This behavior’s purpose is to take an initial and final pose and interpolate a transition between the two, outputting the intermediate postures incrementally. The number of interpolated steps used to transition between the poses is set by the parent behavior. It is often a function of how much difference there is in the initial and final poses. The clock-rate is dependent on the parent behaviors. Once it reaches the final pose, it returns a flag and continues to output the goal pose indefinitely until reset or deleted. Here it is instantiated by the HoldSlideTransition behavior and reset each time it needs to make a new move command.

HoldSlideTransition: This behavior was first mentioned in section 3.8 and implements the equation Equation 3.6. Its role is to use a convergence merge to transition from one posture to another. The convergence parameter c is incremented over time to slide the convergence from the front to the back of the snake, to smoothly transition from the fully-anchored posture to the back-anchored and front-extended posture.

For each change in c , the Transition behavior is set up to interpolate smooth motion between the two postures. Once the Transition behavior completes, c is incremented and Transition is reset to the new initial and final postures. c is changed from 8 to 20 while using the joint numbers as the indices in the convergence merge equation shown in X, assuming that the joint numbering starts at 0 at the front tip. An example of the HoldSlideTransition behavior in action is shown in Figure 3.11.

FrontExtend: Finally, the FrontExtend behavior creates HoldSlideTransition as a child behavior and gives it its initial and final posture. It passes through the output of HoldSlideTransition. It also monitors the pose of the snake tip to see if any obstructions are encountered. If the pose remains stationary for a period of time, an obstruction is declared and the behavior is halted. The behavior returns a collision flag.

3.11.2 Front-Anchor

Once the front-half of the snake has been extended by the Front-Extend stage, the next step is to place the first anchor using the already extended segments. The complete

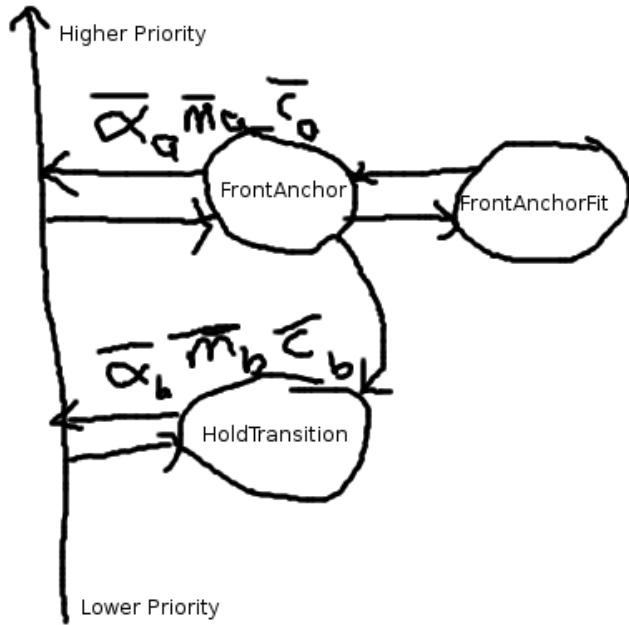


Figure 3.15: Front-Anchor behavior assembly

posture of the snake is submitted to a HoldTransition behavior while the front half of the posture is modified by the FrontAnchorFit behavior.

This stage attempts to create a 3-point anchor that is created with the previously extended segments. The anchor is rooted at an internal joint starting from the merge joint 7 giving 8 segments with which to create the anchor. In the event that not enough segments are available to create the full anchor, the anchoring process is restarted with +2 more segments by moving the root inward by 2 joints.

On successful completion of the 3-point anchor with the available segments, a test is performed to see if the anchor is secure, called a jerk-test. This is accomplished by a sudden rotation of four joints adjacent to the merge joint not on the side of the front anchor. While tracking the position of the anchor segments, if the anchored portion of the snake moves appreciably from the jerk-test, the anchor is deemed insecure, and the anchoring process is restarted with 2 more segments.

Whenever the merge joint is moved inwards, this also results in the contact positions of the anchor points moving inward as well. This can be useful for changing the anchor locations if no stable purchase is found, but also reduces the step distance of the gait by reducing the extension length.

The composition of the behaviors is shown in Figure 3.15 and described as follows:

HoldTransition: This behavior is originally initialized with the complete posture of the snake at the outcome of the Front-Extend stage. The front portion is laterally modified by the FrontAnchor behavior whenever new changes are required to the front anchor shape. The behavior is stepped and drives the robot joints for smooth transitions.

Though the FrontAnchor behavior has priority over the HoldTransition behavior, FrontAnchor almost never drives an output but instead laterally modifies the HoldTransition behavior. Therefore, the HoldTransition behavior is the primary driver of the snake robot.

FrontAnchor: This behavior has complete responsibility for the entire anchoring and testing process. It creates a 3-point anchor for static stability instead of the 2-point anchors previously described in section 2.1. This is because this will be the only anchor to the environment in the next stage. Complete secureness is required to avoid any slip conditions.

A 3-point anchor is created with a cosine curve of period 2.5π shown in Figure 3.16. The FrontAnchor behavior gradually increases the amplitude of this curve. As the amplitude increases, more and more segments are required to complete the fit. Should the curve be longer than the available number of segments, the anchoring process is restarted with the merge joint moved back 2 joints.

The anchoring process is halted after search algorithm 2 completes. The behavior then performs a jerk-test to determine if the anchor points are secure. If k 'th joint is the merge joint, then the joints $[k+1, k+4]$ are rapidly changed in the following sequence: $[(0,0,0,0), (-60,-60,-60,-60), (0,0,0,0), (60,60,60,60)]$. These joints are directly controlled

by the `FrontAnchor` behavior to create sudden motion and override the parallel `Hold-Transition` behavior that normally performs smooth motion.

A secure anchor will register little movement in the anchor segments while an insecure anchor will move a great deal. This movement is tracked through kinematics and assumes that the back anchors are secure and stable. Once the deviation in position of the anchor segments is below a certain threshold, then we determine that this is a secure anchor and return success.

FrontAnchorFit: This behavior is responsible for computing the curve-fitting process described at the beginning of section 2. It determines the correct joint orientations for a given curve. The curve is input by the `FrontAnchor` behavior and modified accordingly. The `FrontAnchorFit` behavior performs an efficient curve-fitting process assuming the curve starts rooted at the merge joint on the behavior boundary shown in Figure 3.16.

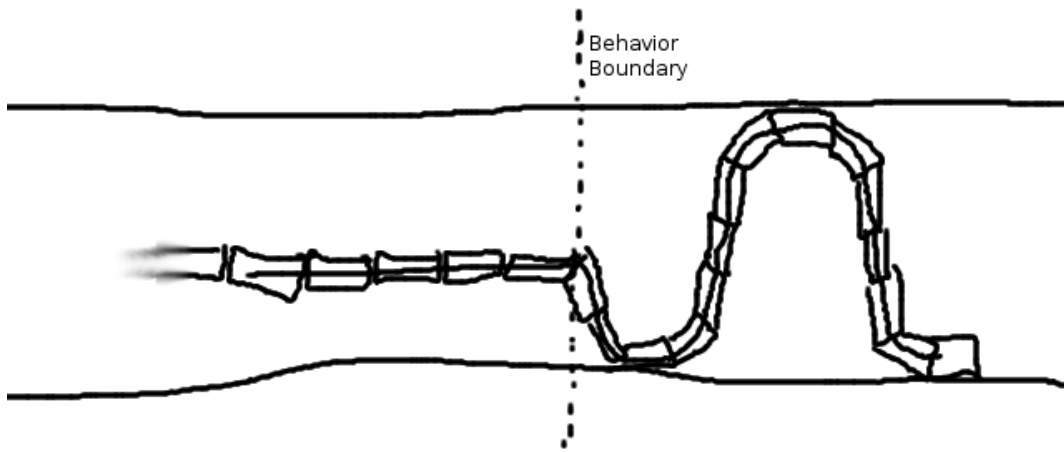


Figure 3.16: Posture that creates a 3-point anchor.

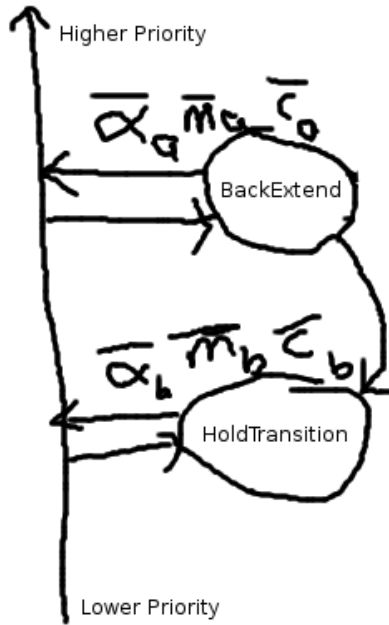


Figure 3.17: Back-Extend behavior assembly.

3.11.3 Back-Extend

After the front anchor has been securely established, the next stage's role is to remove the back anchors and extend the back half of the body straight. If the environment prevents the back half from being straight, the joints are compliant to the environment and will extend as far as they are allowed.

The behaviors are shown in Figure 3.17 and described as follows:

BackExtend: This behavior simply takes all the joints on one side of the merge joint behavior boundary and commands their values to be 0.0. It also sets all of these joints to have low torque to ensure compliant motion. These values are sent laterally to the HoldTransition behavior.

HoldTransition: This behavior is initialized to the posture from the outcome of the Front-Anchor stage. It receives as input from the FrontExtend behavior, the new straight 0.0 joint positions. It manages the smooth motion from the back anchored position to the back extended position.

3.11.4 Back-Anchor

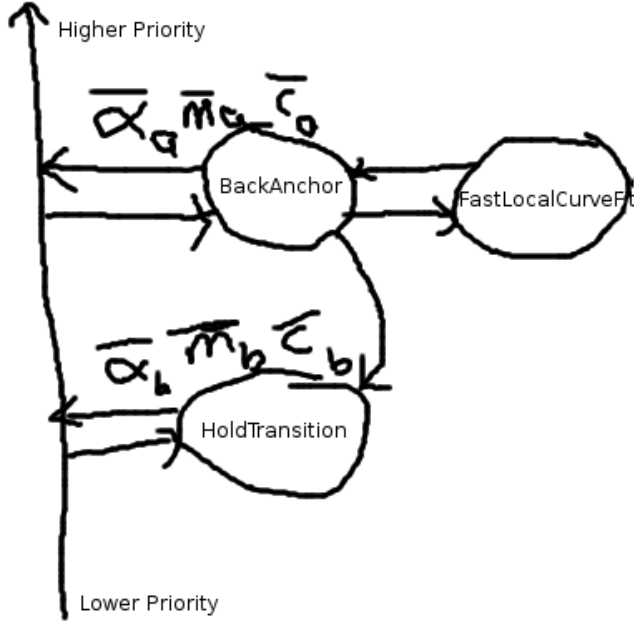


Figure 3.18: Back-Anchor behavior assembly

The purpose of this stage is form the 2-point anchors described in section 2.1 with the remaining extended segments of the back half of the snake. The sine curves are joined together with the front anchor cosine curve to make a continuous splice merge and produce a complete anchored posture of the whole snake.

New pairs of anchor points are created, using one period of a sine curve each, until all of the remaining back segments are used up. At each anchor pair, we use the adaptive anchoring algorithm 2 to detect contacts. However, we do not perform a jerk-test like in the Front-Anchor stage because we only have the front anchor as our reference point and no extra joints to perform the jerking motion. Furthermore, it is not as critical to determine if the back anchors are secure since there are more of them, and we have confidence in the security of our front anchor.

The behaviors are shown in Figure 3.18 and described as follows:

HoldTransition: This behavior fulfills the same role as all of the other instances. It takes the initial posture at the outcome of the previous stage and maintains that posture until modified by the primary behavior, BackAnchor. It manages the smooth transition between postures.

BackAnchor: This behavior performs the anchor contact algorithm 2, modifies the curve parameters, and continues to add anchor pairs until it runs out of segments. It creates the FastLocalCurveFit behavior as a child behavior.

FastLocalCurveFit: This behavior parameterizes the curves representing the series of back anchor curves of varying amplitudes. It is also responsible for efficiently computing the joint positions to fit the snake to the curves. Furthermore, it accepts compliance in the curve-fitting process between each anchor pair. That is, at each merge joint between two anchor pairs, compliance is to find the best anchor posture and the posture is saved for the remainder of the stage.

3.12 Analysis

Our theoretical contribution is a quantitative analysis of the trade-space between environmental characteristics, snake robot morphology, and locomotion control parameters. That is, given a snake robot morphology and control parameters, what types of environments can we successfully explore. Conversely, given a specific environment, what robot morphology and control parameters are required to successfully explore it.

First we will perform an analysis of the trade-space for forming a 3-point stable anchor in a smooth pipe. A 3-point anchor is shown in Figure 3.19 and is the minimum number of contact points required to form a stable anchor. This posture will hold the body of the snake rigid and prevent it from translating or rotating within a threshold of external force and torque.

We will define and quantify the parameters that describe this system: the environment, the robot, and the control.

Our particular environment of a smooth pipe can easily be described with one parameter, the pipe width W .

The complete snake robot morphology can be described by 3 parameters: segment width w , segment length l , and number of segments n .

Finally, control of the robot is achieved by fitting the body of the snake onto a curve described by a sinusoid. The parameters for control are the values of amplitude A and period P , where $y = A \cos(\frac{2\pi x}{P})$.

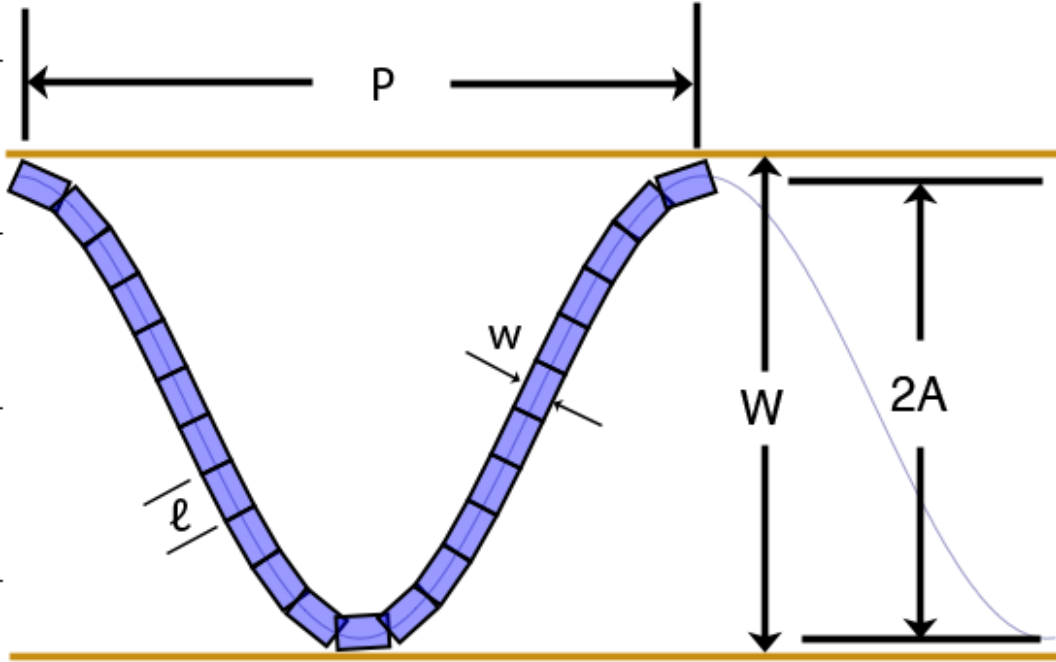


Figure 3.19: Parameterization of 3-point stable anchor in a smooth pipe.

3.12.1 Case: Snake as a Curve

We first consider the degenerate case where $l = 0$, $w = 0$, and $n = \infty$. This results in a snake that has no width and an infinite number of joints. Essentially, the snake body equals the curve equation. Since $w = 0$, this results in $2A = W$. This is shown Figure 3.20.

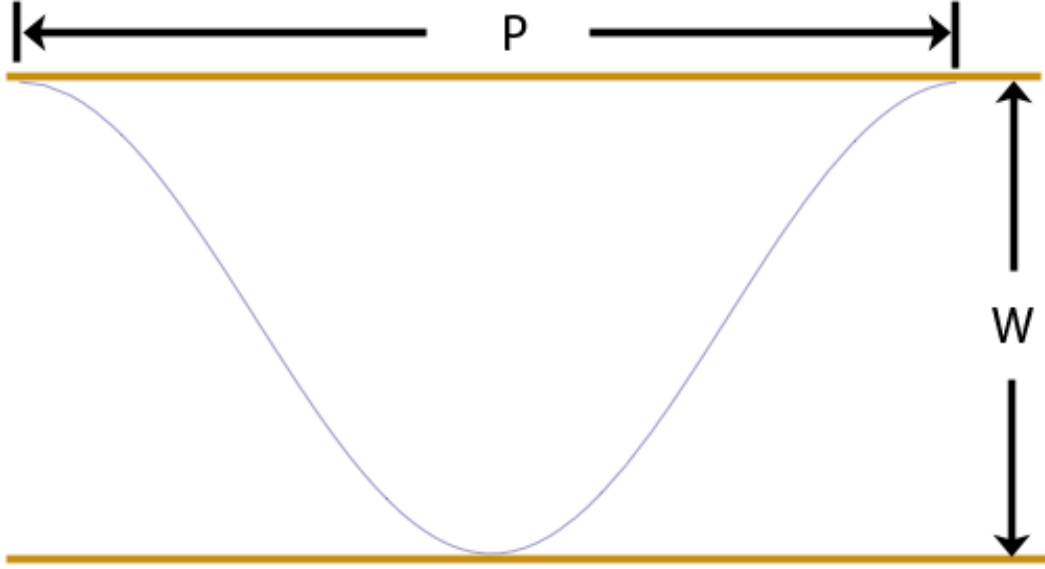


Figure 3.20: 3-point stable anchor with $w = 0$, $l = 0$, and $n = \infty$.

We define L to be the total length of the snake which can be computed from the equation of the curve.

$$f(x) = \frac{W}{2} \cos\left(\frac{2\pi x}{P}\right) \quad (3.9)$$

Equation 1 is the equation of the curve with P the period, W the width of the pipe. We can plug $f(x)$ into the equation for computing arc length shown in Equation 2 and 3:

$$L = \int_0^P \sqrt{f'(x)^2 + 1} \, dx \quad (3.10)$$

$$L = \int_0^P \sqrt{\left(\frac{-W\pi}{P} \sin\left(\frac{2\pi x}{P}\right)\right)^2 + 1} \, dx \quad (3.11)$$

This integration can not be solved analytical and must be solved by plugging in values for P and W and computing L numerically. In our control methodology, P is

usually held fixed and the width of the environment is always changing, so W is always varying. Here we show a plot holding P fixed for various values while changing the value of W in Figure 3.21.

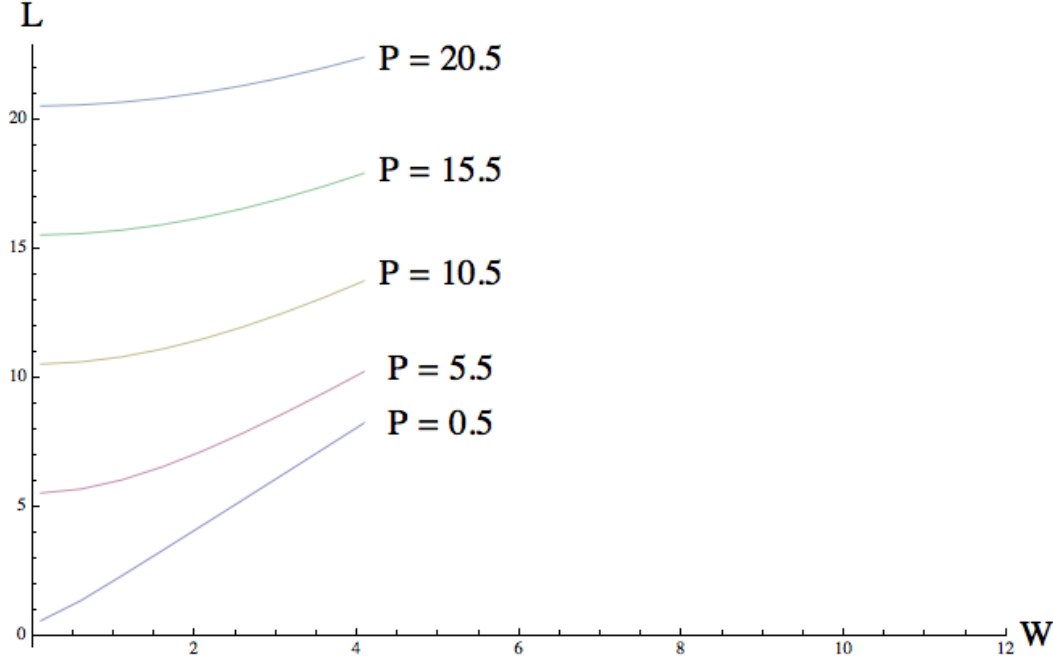


Figure 3.21: Plot of snake arc length L for various values of W and P .

This plot shows that when pipe width $W \rightarrow \infty$, the length L converges to a constant slope of $\frac{dL}{dW} = 2$ and $L = 2W, \forall P$ as $W \rightarrow \infty$. This can be seen by approximating the 3-point anchor and cosine curve as a triangle with a base of P and a height of W , and the vertices on the anchor points. Increasing W will achieve the above results.

The difference in L becomes large for different values of P when W is small. Once W becomes sufficiently large, W dominates and the period becomes less of a factor. Given that our application involves tight quarters, we are likely to find typical values of W to be small and P will vary depending on the context.

3.12.2 Case: Snake with Width

We now consider the case where $l = 0$, $n = \infty$, but $w > 0$. This in effect creates a continuous snake robot with infinite joints but has a thickness to it. To determine the total length of the snake given a pipe width W , a control period P , and a segment width of w , we first determine the equation of the curve:

$$f(x) = \frac{W - w}{2} \cos\left(\frac{2\pi x}{P}\right) \quad (3.12)$$

Since the snake centers its body on the curve, it has space of $\frac{w}{2}$ on either side of it. We start the cosine amplitude at $\frac{W}{2}$ and subtract $\frac{w}{2}$ as the width of the snake increases. This results in equation 4.

If we plug the $f(x)$ into the arc length equation, we get the snake length for given W , P , and w :

$$L = \int_0^P \sqrt{\left(\frac{-(W - w)\pi}{P} \sin\left(\frac{2\pi x}{P}\right)\right)^2 + 1} dx \quad (3.13)$$

Holding $P = 1$, and increasing the pipe width W for different values of w , we get the following plot shown in Figure 3.22. This plot captures the intuition that a snake robot is not able to explore a pipe that is thinner than the robot's body width. However, once you enter a pipe where $W > w$, the plot takes on the same curve as Figure 3.21. For large enough W , $L = 2(W - w)$ and $\frac{dL}{dW} = 2$.

3.12.3 Case: Snake with Segments

We now consider the case where the robot composed of discrete segments of a given length l . Up until now, we have represented the snake as a curve function. However, with segments, the robot needs to fit its body to be placed on the curve. Our current approach assumes a monotonic curve in the x-direction and the joint axes are placed directly on the curve. In this example, we assume that curve fitting is perfect and unique.

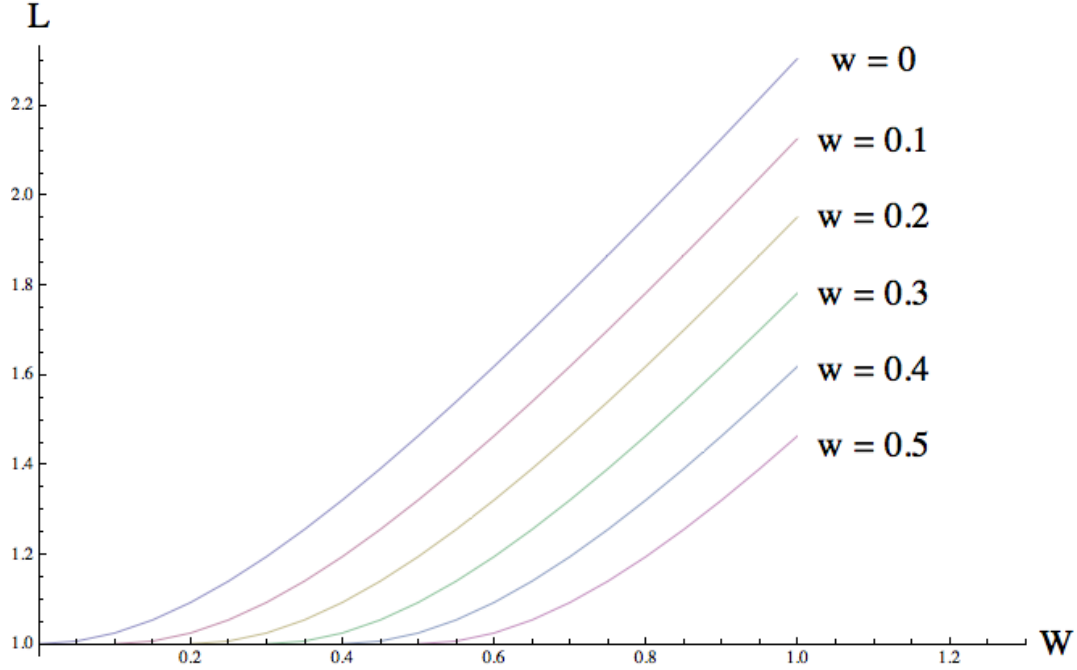


Figure 3.22: Plot of snake length L while $P = 1$, for various values of W and w .

Again we look at the 3-point anchor situation determine how the length of the snake changes with different parameters. Instead of length though, we are computing the number of required snake segments.

There are two approaches. The first is to examine the situation analytically, deriving an equation for the number of segments given period P , pipe width W , and segment length l . The second is to run an algorithm that performs the curve fitting given a curve and lets us determine the required number of segments. We do both.

Analytically, we can easily compute an upper bound for the number of segments. If we have already calculated L , we can determine that we will need at most n segments shown in equation 6.

$$n = \left\lceil \frac{L}{l} \right\rceil \quad (3.14)$$

At most n segments will be required in the worst case where the segments lay directly on the curve. However, in most cases, the segments will be cutting corners to put both

ends on top of the curve. This will result in the required number of segments being less than the worst case.

Algorithmically, we can determine the actual number of segments required for a given configuration. Given a monotonic curve γ , draw a circle c at the start of the curve with radius l and origin o . Take all the intersection points between c and γ . Take only the intersection points where $p_x > o_x$. Select p with the smallest x value. Place a segment going from o to p . Set $o = p$ and repeat until there is no more curve. This looks like the following in Figure 3.23.

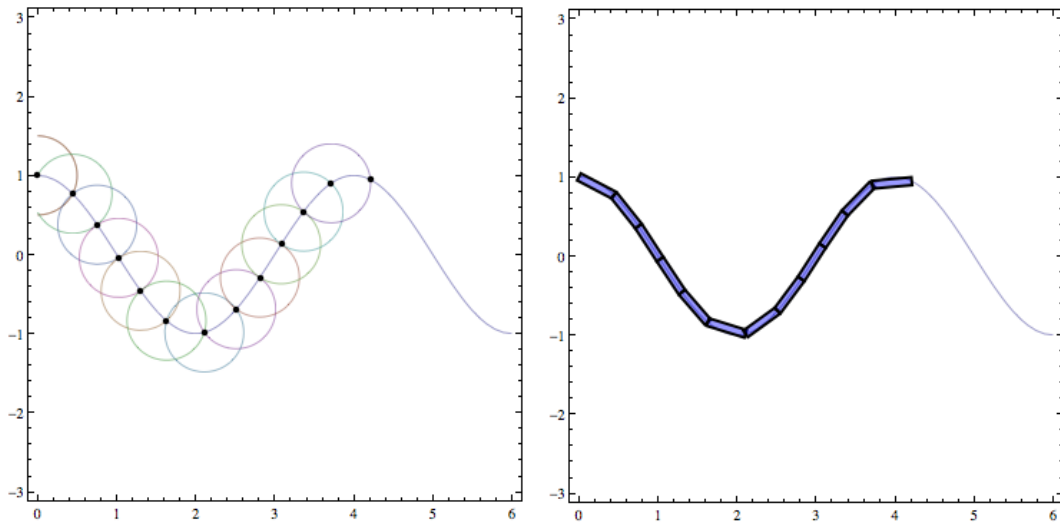


Figure 3.23: Intersecting circles along the line of the curve. Demonstration of curve fitting algorithm.

3.13 Experimental Results

We put our results here.

Chapter 4

Defining Position

4.1 Defining Pose and Direction

Articulated robot has no high-inertia center of mass to serve as its coordinate frame. Require method to establish forward direction of an articulated robot.

Establishes stability of robot frame under error of anchoring.

4.2 Motion Models

Naive motion model (fast time, low accuracy) Self-Posture motion model (cost of time, increase accuracy) *Step model with inter-pose overlap invariance (fast time, medium accuracy)

Examples of motion estimation results.

Naive + GPAC Frame Self-Posture + Body Frame *Pose Step + GPAC Frame (discussed later)* Shoot Step (discussed later)

4.3 Problem

Now that our snake robot is capable of moving through the environment with the adaptive concertina gait behavior, we need some way of estimating how far it is moving and in which direction.

As we established earlier, we have no external sensors because we assume their failure from environmental conditions. We cannot rely on GPS since it is not effective underground or in pipes. We do not have wheeled shaft encoders since we have no wheels and do not expect to always travel through flat terrain. Finally, although it may indeed

help, we cannot expect to make use of an inertial navigation system since they are bulky and expensive. Furthermore, we have not performed experiments to determine if they are capable of handling the high amount of rotation of each of the snake body segments during locomotion.

In absence of a global positioning or odometry, we need some form of alternative motion estimation. Knowing where the robot is located is the basic building block of creating a map. We focus on the problem of finding the relative geometric transform between the two poses at the beginning and end of one step of the adaptive concertina gait.

Our proprioceptive approach achieves motion estimation by anchoring multiple points of the body with the environment and kinematically tracking the change in distance between the immobilized parts as the snake contracts and extends. This gives us a motion estimation method that only depends on the joint sensors. We show the effectiveness in a series of experiments.

4.4 Immobilizing the Anchors

A fundamental property of the adaptive concertina gait is that it creates anchors to the surrounding environment. Our goal is to exploit this property to estimate our motion through the environment. In order to do this, we need to ensure that our anchors remain an accurate frame of reference to the global environment.

The primary goal of our previous work on maintaining smooth and stable motion of the snake in Chapter 2 was to prevent any sort of anchor slip that may harm our reference frame to the global environment. It is critical that our anchors remain firmly immobilized with respect to the environment to ensure accurate measurement of motion.

Though we are not able to localize the exact contact point of the anchor with the environment, we can assume that the segments comprising the anchoring curve are themselves immobilized and mechanically isolated by virtue of their static contacts with the

environment. We use these isolated bodies as immobilized references to the global environment.

Whether or not we consider the use of a body segment as a reference is determined by our work in Section 2.8. That is, if the joints in the local neighborhood of a segment are locally stable and the behavior’s control bit for the attached joint is 0, we assume this segment is immobilized. We can use immobilized segments as reference points to the global frame.

We call the monitoring of local joint variances as local stability and the output of the control masks as prescriptive stability. Though a body segment may be locally stable, it does not mean it is immobile. If we also include prescriptive stability, the behavior’s prediction of what joints should be moving and what should not, then we greatly decrease the chances that we will use a slipping anchor as a reference.

If any point the anchor should slip while, our assumption that a body segment is immobilized is violated and could lead to accumulated errors in our motion technique. Therefore, it is critical that we analyze and mitigate all the possible failure modes for anchoring.

We are generally able to classify the types of anchoring and reference errors we encounter during both static and locomotive anchoring. For each, we are forced to either avoid the condition from occurring or detect and correct it. We list the failure modes and explain our mitigation strategy for each.

The *floating reference* occurs when a locally stable segment is made a reference, but it is not part of an anchor. This was particularly troublesome in our early implementations, but we are able to largely avoid this failure mode by having the behaviors explicitly classifying which joints are part of an anchor. The other possibility for a floating anchor would be if an anchoring behavior erroneously reports success in establishing an anchor in free space. This was largely avoided by adding the more careful anchoring process in Section 2.2 that detects impacts to the walls and follows up by doing a jerk test to test whether the anchor is secure.

A *weak contact* occurs when the anchor the reference segment is on has an insecure anchor. This usually happens if an anchor is placed within a pipe junction or if one of the anchors of the Back-Anchor is insecure. The Back-Anchor case is more likely since they are not jerk-tested. Weak contacts usually do not display local instability since the physical contact stabilizes the local joints but does not immobilize them. If it is available, we can use negative prescriptive stability from the behavior to minimize this failure but often occurs in prescriptively stable areas. There is nothing we can do to prevent this error from being added to the pose estimation besides detecting it. Luckily, a weak contact does not move much. Its error is bounded.

Buckling occurs when the anchored joints are frozen in a non-optimal position and external stresses put excessive torque on one or more joints that forces the anchor into a reconfigured position. This is similar to mechanical buckling of structural members under compression. In this case, it is for an articulated system attempting to hold a rigid pose. Buckling is easily detectable by tripping our local stability conditions and will quickly remove the references and reuse them once the joints have settled down. We have also reduced this occurrence by having our anchoring behaviors search for non-deforming anchors as a natural by-product of algorithm 2.

Impulses occur when the snake robot experiences a sudden collision or a buckling has occurred somewhere else in the robot. Usually this is not a fatal error and the robot will quickly return to its stable pose. However it can trip up the variance calculations and deactivate all the references we have leaving us with none. Recovery is achieved by resurrecting the last best reference, and assuming it is in the same pose. We show how to do this in the next section.

Funnel anchoring occurs when a secure anchor is established between a pair of walls that are monotonically increasing in width. If the anchor receives a force that pushes it towards the direction of increasing width, its anchor can become permanently loose. This is especially problematic in cases of irregular environments where there are many

possibilities for this to occur in local conditions. We currently do not have a solution for this yet.

Finally there is a class of *whole body slip* that is completely undetectable with only joint positions. That is, the whole body could be slipping through an environment such as a straight and featureless pipe without causing any joint variance at all. This would only occur if the ground was exceptionally slippery and able to use the robot's momentum to move it large distances or if the robot was on a slope and gravity was exerting a global force. We avoid this error by limiting the environments we explore. Other environments may require extra sensor instrumentation such as accelerometers to detect this failure mode.

Rotational error is the dominant form of error we encounter because, unlike a traditional robot with a stable frame of reference on its chassis, every reference point in the snake robot's body is constantly in rotational motion. Any form of disturbance of a reference node will manifest itself with a rotational error that will propagate through kinematic computations of new reference nodes. Translational error occurs primarily by anchor slip. Rotational error is easier to correct in our later localization process in Chapter 5.

4.5 Tracking Motion

In order to track motion through the environment, we need to establish our mathematical framework for defining the relative position of things between the robot and the environment. We then define the concept of a *reference pose* to track the position of the environment while the snake is in motion.

4.5.1 Pose and Coordinate Frames

A pose P defines the position and orientation of a rigid body in a 2D plane. Each pose is defined with respect to a coordinate frame O using 3 values: (x, y, θ) . A coordinate

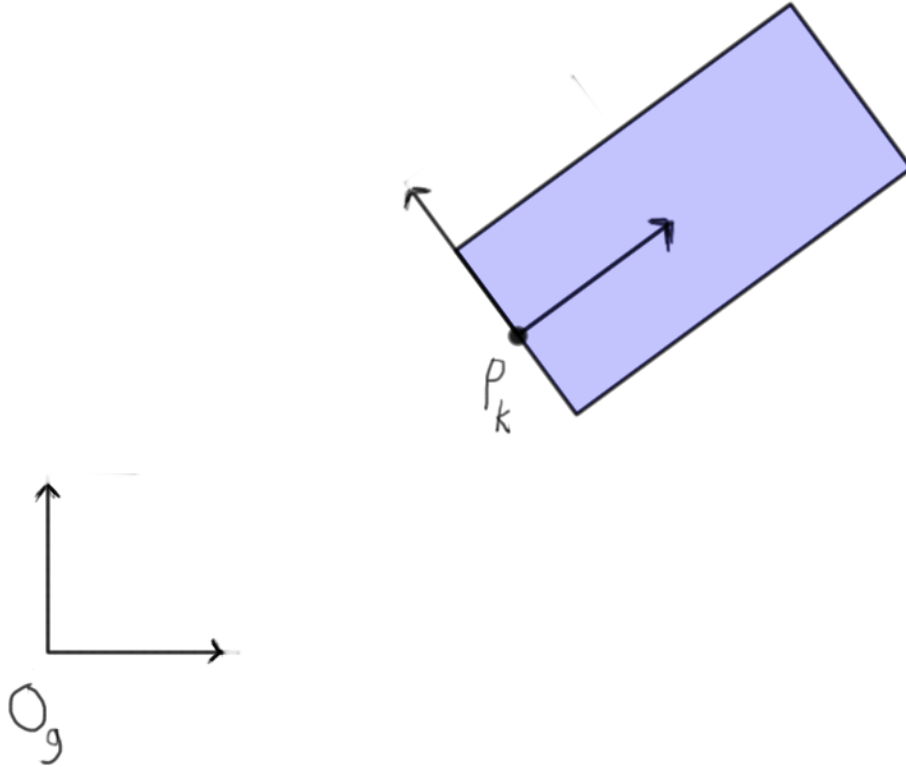


Figure 4.1: Pose of rigid body with respect to global frame.

frame is either affixed in the global environment or affixed to a rigid body on the snake. An example of the global frame O_g and a pose P_k are shown in Figure 4.1.

By convention, we will specify in the superscript which coordinate frame a pose k is defined with respect to. For the global frame, the pose is written as P_k^g . If the pose is with respect to some other coordinate frame O_a , the pose is written as P_k^a . If the superscript is omitted, we assume the global frame.

In a robot system with multiple rigid bodies, we will have a coordinate frame for each body. Often times, we wish to transform poses between coordinate frames. To do this, we first need to define the relationship between coordinate frames, specified by the pose of their origins. In the global frame O_g , the pose of the origin O_g is $P_g = (0, 0, 0)$. For two example coordinate frames attached to rigid bodies, we define the pose of origin

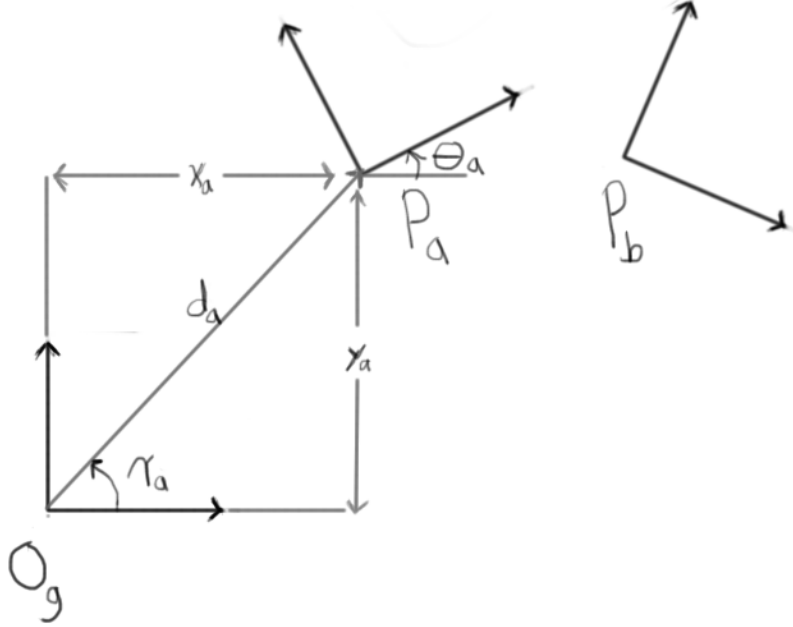


Figure 4.2: Pose of A and B with respect to global frame.

O_a to be $P_a = (x_a, y_a, \theta_a)$ and the pose of origin O_b to be $P_b = (x_b, y_b, \theta_b)$ as shown in Figure 4.2.

Suppose we wanted to compute pose b with respect to frame O_a . That is, we wish to find P_b^a and we are given P_a^g and P_b^g . First we focus on finding the Cartesian component of the pose, point $p_b^a = (x_b^a, y_b^a)$. We compute the angle portion θ_b^a separately. From Figure 4.2, we define the following:

$$R_a = \begin{bmatrix} \cos(\theta_a) & \sin(\theta_a) \\ -\sin(\theta_a) & \cos(\theta_a) \end{bmatrix} \quad (4.1)$$

This is the rotation matrix for the difference in orientation between the global frame O_g and local frame O_a .

$$d_a = \sqrt{(x_a)^2 + (y_a)^2} \quad (4.2)$$

This is the Cartesian distance from the global frame's origin to the local frame's origin.

$$\cos(\gamma_a) = \frac{(x_a, y_a) \cdot (1, 0)}{|(x_a, y_a)| |1|} = \frac{x_a}{d_a} \quad (4.3)$$

$$\gamma_a = s \cdot \arccos\left(\frac{x_a}{d_a}\right) \quad \begin{cases} s = 1 & \text{if } y_a \geq 0 \\ s = -1 & \text{if } y_a < 0 \end{cases} \quad (4.4)$$

γ_a is the angle of the vector from the global origin to the local frame origin. The sign of γ_a is determined to be negative if $y_a < 0$. Otherwise, γ_a is positive. This value corresponds to the angle shown in Figure 4.2.

$$G_a = \begin{bmatrix} \cos(\gamma_a) & \sin(\gamma_a) \\ -\sin(\gamma_a) & \cos(\gamma_a) \end{bmatrix} \quad (4.5)$$

G_a is the rotation matrix to rotate the local frame's origin onto the x-axis of the global frame.

To find p_b^a in frame O_a from p_b^g in O_g , we compute:

$$p_b^a = \begin{bmatrix} x_b^a \\ y_b^a \end{bmatrix} = R_a G_a^T \left(G_a p_b^g - \begin{bmatrix} d_a \\ 0 \end{bmatrix} \right) \quad (4.6)$$

To find the converse, p_b^g from p_b^a , we do the following:

$$p_b^g = \begin{bmatrix} x_b^g \\ y_b^g \end{bmatrix} = G_a^T \left(\begin{bmatrix} d_a \\ 0 \end{bmatrix} + G_a R_a^T p_b^a \right) \quad (4.7)$$

This approach performs a sequence of rotations to separate translation and rotation of the pose when converting between frames. To compute the angle portion of the pose,

we perform the rotation sequence by addition and subtraction of angles. Following the sequence, we get the following:

$$\theta_b^a = \theta_b^g + \gamma_a - \gamma_a - \theta_a$$

This reduces to:

$$\theta_b^a = \theta_b^g - \theta_a \quad (4.8)$$

The converse is achieved similarly using Equation Equation 4.7 and the following rotation sequence:

$$\begin{aligned} \theta_b^g &= \theta_b^a + \theta_a + \gamma_a - \gamma_a \\ \theta_b^g &= \theta_b^a + \theta_a \end{aligned} \quad (4.9)$$

The final result for the pose computation is to put the Cartesian and angular components together.

$$P_b^a = \begin{bmatrix} x_b^a \\ y_b^a \\ \theta_b^a \end{bmatrix} \quad \left\{ \begin{array}{ll} x_b^a, y_b^a & \text{from Equation 4.6} \\ \theta_b^a & \text{from Equation 4.8} \end{array} \right. \quad (4.10)$$

And the converse is:

$$P_b^g = \begin{bmatrix} x_b^g \\ y_b^g \\ \theta_b^g \end{bmatrix} \quad \left\{ \begin{array}{ll} x_b^g, y_b^g & \text{from Equation 4.7} \\ \theta_b^g & \text{from Equation 4.9} \end{array} \right. \quad (4.11)$$

Now that we have established the mathematical framework for relating the pose of the rigid bodies to the environment and each other, we describe our concept of reference poses to track motion in the environment.

4.5.2 Reference Poses

A reference pose is the position and orientation of a rigid body segment that has been immobilized with respect to the global frame. A reference pose is valuable because it gives a fixed reference point to the global environment and allows us to track the motion of the rest of the robot. Special care must be taken to ensure that when using a reference pose, the rigid body it's attached to is truly immobilized.

A reference pose is either active or inactive. A reference is active once it is created as a result of its rigid body becoming immobilized. We assess whether a reference pose is to be created by checking if it satisfies both our predictive stability and local stability conditions. We discussed predictive and local stability in section 3.10, where predictive stability is the output of the behavior's control masks and local stability is the result of monitoring local joint variances. Once the reference pose violates either of these conditions, it becomes inactive.

To deactivate a reference pose, if a reference violates either of the stability conditions and it was previously active, we flip a bit to signal it as inactive. Afterwards, we can create a new reference pose on this rigid body once it satisfies the stability conditions again.

To create a new reference pose, its associated rigid body must first have been inactive. Secondly, it must satisfy both prescriptive and local stability conditions. Once the following conditions have been met, the new pose is computed kinematically with respect to another currently active reference pose. If the pre-existing reference pose is correct, the kinematic computation of the new reference pose will be correct for its true position and orientation in the global environment.

Given the arrangement of rigid bodies and their attached coordinate frames shown in Figure 4.3, we need the kinematic equations for computing the pose of a rigid body given its neighbor's pose. That is, if we already have an active reference pose, we wish to compute the pose of neighboring reference in the global frame using only the joint angles from the robot's posture. To compute P_{k+1} if we are given P_k , we do the following:

$$\begin{aligned}
x_{k+1} &= x_k + l \cos(\theta_k) \\
y_{k+1} &= y_k + l \sin(\theta_k) \\
\theta_{k+1} &= \theta_k - \phi_{k+1}
\end{aligned} \tag{4.12}$$

For the opposite direction, to compute P_{k+1} given P_k , we do the following:

$$\begin{aligned}
\theta_k &= \theta_{k+1} + \phi_k \\
x_k &= x_{k+1} - l \cos(\theta_k) \\
y_k &= y_{k+1} - l \sin(\theta_k)
\end{aligned} \tag{4.13}$$

If we use the equations iteratively, we can compute the pose of a rigid body segment given the pose of any other segment.

The algorithmic process for creating and deactivating reference poses is shown in Algorithm 4, where N is the number of rigid body segments in the snake from which to create reference poses. The implementation of the function for the kinematic computation of new reference poses is shown in Algorithm 5.

Algorithm 4 Reference Pose Creation and Deactivation

```

 $N \leftarrow 40$ 
 $activeMask \leftarrow$  array of size  $N$  initialized to 0
 $activeRefPoses \leftarrow$  array of size  $N$  initialized to  $\emptyset$ 
 $preStabMask \leftarrow$  behaviorControlOutput()
 $locStabMask \leftarrow$  stabilityCompute()
for  $i = 0 \rightarrow N$  do
  if  $preStabMask[i]$  &  $locStabMask[i]$  then
    if  $\neg activeMask[i]$  then
       $activeRefPoses[i] \leftarrow$  computeRefPose( $i$ )
       $activeMask[i] \leftarrow 1$ 
    end if
  else if  $activeMask[i]$  then
     $activeRefPoses[i] \leftarrow \emptyset$ 
     $activeMask[i] \leftarrow 0$ 
  end if
end for

```

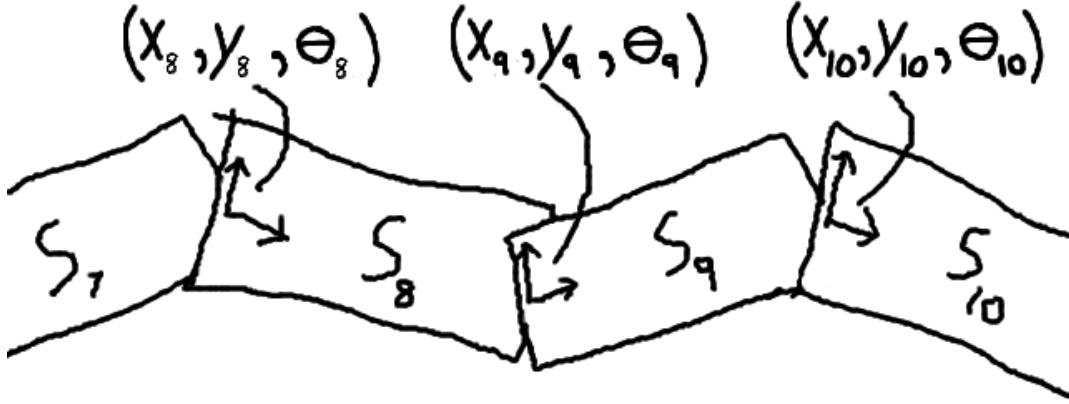


Figure 4.3: Local coordinate frames attached to segments and described by reference poses.

This algorithm assumes that an active reference pose always exists. There are two special cases when no reference poses are currently active. In the first case, the algorithm is initializing and no reference poses have been created yet. In the second case, all of the reference poses violate the stability condition and all have been deactivated. These special cases are not shown in the algorithms, but we explain our approach here.

For the first case, when we initialize, the first reference pose is set to $(0,0,0)$. This becomes the origin of the global frame centered at the robot's starting position in the environment. From this first initial reference pose, all new reference poses are derived.

In the second case, no active reference poses are available since no stability conditions have been satisfied. The robot has effectively lost track of its position in the environment. In the event that a new reference pose needs to be created, there is no parent pose from which to kinematically compute. Instead, from the last used inactive reference poses, we select the reference that was contiguously active the longest and use this as the parent pose to compute the new active reference pose. The reasoning behind this is that a

Algorithm 5 *computeRefPose(i)*: Kinematics for Computing Reference Pose

```
 $N \Leftarrow 40$ 
 $\bar{\phi} \Leftarrow$  array of current joint angles
 $i \Leftarrow$  target new reference pose index
 $j \Leftarrow$  index of nearest active reference pose to  $i$ 
 $k = j$ 
 $(x_k, y_k, \theta_k) \Leftarrow (x_j, y_j, \theta_j)$   $\triangleright$  pose of active reference  $j$ 
if  $i > j$  then
  while  $k < i$  do
     $x_{k+1} = x_k + l \cos(\theta_k)$ 
     $y_{k+1} = y_k + l \sin(\theta_k)$ 
     $\theta_{k+1} = \theta_k - \phi_{k+1}$ 
     $k = k + 1$ 
  end while
else if  $i < j$  then
  while  $k > i$  do
     $\theta_{k-1} = \theta_k + \phi_{k-1}$ 
     $x_{k-1} = x_k - l \cos(\theta_{k-1})$ 
     $y_{k-1} = y_k - l \sin(\theta_{k-1})$ 
     $k = k - 1$ 
  end while
end if
 $(x_i, y_i, \theta_i) \Leftarrow (x_k, y_k, \theta_k)$   $\triangleright$  new pose for active reference  $i$ 
```

long-lived reference pose is more likely to be correct than a short-lived reference pose due to the sometimes intermittent nature of reference poses. This last best reference pose approach is very effective in practice.

So long as the active reference poses satisfy the assumption of no-slip anchors and there always being at least one active reference, the tracking of the robot's trajectory through the environment is correct. Violations of these assumptions introduce error into the motion estimation.

4.6 Robot-Centered Coordinate Frame

Though we now have a local coordinate frame for each segment in the snake, we need a coordinate frame that represents the mobile robot body as a whole. In traditional mobile robots, we usually have a large rigid body chassis with high inertia that is suitable for

defining the position and orientation of the robot. In a snake robot, there are multiple rigid bodies, all of which are small in mass, small in inertia, and poor at defining the overall snake’s position and orientation. While the snake is executing its locomotion, the body segments are undulating and rapidly changing orientation, making dubious their use as an indication of heading.

In the wake of these phenomena, we found the need to create a dynamically generated coordinate frame that best represents the position and orientation of the snake robot’s posture as a whole. We cannot use the center of mass of the robot, because the centroid can be outside of the body if the snake’s posture is curved. Instead, we generate a curve called a Gross Posture Approximation Curve (GPAC) that we use to generate a local coordinate frame that is oriented in the direction of travel. This allows us to describe consecutive poses of the snake with local coordinate frames oriented in the same forward direction.

We describe in detail the GPAC and follow with the generation of the local coordinate frame.

4.6.1 Gross Posture Approximation Curve (GPAC)

The GPAC is a curve that approximates the posture of the robot in the environment without the articulation, as seen in Figure 4.4. The blue lines indicate the posture of the snake and the green line is the GPAC.

The GPAC is derived by taking the ordered points of the snake segment positions and fitting a smoothed B-spline curve to them. To generate the points, we first start from a body frame fixed to one of our body segments. In this case, we use segment 19 centered on joint 19 as our body frame O_{19} . With respect to frame O_{19} and using the current joint posture vector $\hat{\phi}_t$, we compute the segment posture vector $\hat{\rho}_t$ that specifies the N segment poses using the iterative kinematic equations Equation 4.12 and Equation 4.13. If we take only the cartesian components of the segment posture $\bar{\rho}_t$, we set this as a series of ordered points from which we compute a B-spline curve.

$$\mathbf{dist}(u_1, u_1 + K) \neq \mathbf{dist}(u_2, u_2 + K) \quad (4.15)$$

where the function $\mathbf{dist}()$ computes the arclength between two u values on the curve, and the constant K adds the same u offset at two different points on the curve specified by u_1 and u_2 . What this means in practical terms is, the u values cannot be relied upon to give us reproducible positions on the curve. In particular, if we retrieve the point $\beta_t(0.5)$, this will be close to the midpoint of the curve, but not the true midpoint and is subject to change between different curves.

We create a more accurate method that allows us to specify a point of true arclength on the curve. We present it in the form of a parameterized function:

$$O(\log n) : \quad \sigma_t(d) = (x_d, y_d, \theta_d), \quad 0 \leq d \leq d_{max} \quad (4.16)$$

Here d is the arclength starting from the $u = 0$ terminator of the curve. d_{max} is the maximum arclength of the curve.

Though this is defined in the form of a function, it is implemented with a search algorithm. If we pre-process the curve by uniformly pre-sampling n points with $\beta_t(u)$ in $O(n)$ time, we can achieve a binary search time of $O(\log n)$ for each invocation of the function. The n parameter here corresponds to the number of samples of the curve we use to search over. The more samples, the more accurate the function will be. Here we use a tractable size of $n = 100$.

To perform the inverse operation for curve functions, we use the same pre-processed n sample points from equation Equation 4.16 and define the following functions:

$$O(n) : \quad \beta_t^{-1}(x, y) = u \quad (4.17)$$

$$O(n) : \quad \sigma_t^{-1}(x, y) = d \quad (4.18)$$

These inverse operators find the closest sample point on the curve to (x, y) and returns the sample's associated u or d parameter. The correctness of these functions depend on the queried point being reasonably close to the curve, the curve not be self-intersecting, and the point not be equidistant to two disparate points on the curve. They are $O(n)$ because we must compute the distance to all n sample points. Notice that we omit the angle portion of the curve for inverse operations. We do not define closest point for orientations.

Since these inverse curve functions are very similar, we develop a unified algorithm that produces parallel results. We do this to prevent duplication of search operations when similar information is needed.

$$O(n) : \quad c_p(x, y) = (u, d, (x_p, y_p, \theta_p)) \quad (4.19)$$

This function returns the closest point on the curve to (x, y) , and its associated u and d parameters.

Finally, we have functions that convert between u and d .

$$O(\log n) : \quad \mathbf{d}(u) = d \quad (4.20)$$

$$O(\log n) : \quad \mathbf{u}(d) = u \quad (4.21)$$

These can be performed with a binary search on the pre-processed sample points.

4.6.2 Generation of GPAC Local Frame

For each generation of the GPAC, we can create a unique but predictable coordinate frame that represents the gross posture of the snake in the environment. Because the GPAC only follows the general posture of the snake, regardless of its articulation, the difference in curves between generations is small and within reason.

Once we have the new GPAC, to determine the location of our new coordinate frame origin \hat{O}_t with respect to O_{19} , we compute the following:

$$P_d = \sigma_t(d_{max}/2) \quad (4.22)$$

This specifies the halfway point along the curve in terms of arclength with respect to O_t . If we had used $\beta_t(0.5)$ instead, we would have had no guarantee how close to the middle it would be and no guarantees on repeatability. By using the arclength function $\sigma_k()$, we have more guarantee over the location at the expense of running time.

From our new local frame \hat{O}_t , the orientation of the x-axis is directed in the forward direction of the snake, regardless of the articulation of the joints. This approach now gives us the tools to make relations between snake poses where the orientations will have some correlation. If we had insisted on using a body frame O_{19} as a local coordinate frame, the orientations would have had very little correlation. We would have had no means to relate and correct orientations between snake poses.

In the future, we will drop the t subscript of a GPAC and local frame origin and only refer to them as $\beta_k(u)$, \hat{O}_k , and \hat{P}_k , where \hat{O}_k is the GPAC generated origin, \hat{P}_k is the origin's location in the global frame, and k is the particular pose number in the pose graph. We describe this in more detail in Section 5.

4.6.3 Geometric Transform between Poses

Now that we have defined a local coordinate system for the complete posture of a snake robot, we can compute a geometric transform T_{ij} between two poses of the robot \hat{P}_i and \hat{P}_j . We take the snake poses before and after one step of the adaptive concertina gait in the GPAC local frame for each. Each GPAC has a reference pose in the global frame, so it is only a matter of computing a transform between the two.

4.7 Results

Shown in Figure 4.5 is a plot of the snake robots poses as it travels through a variable width curved pipe. The boundaries of the pipe are drawn in green. The black poses represent the estimated positions and the pink poses indicate the ground truth positions. Notice that there is a discontinuity in the middle, which is likely because of the use of a reference node on an anchor with major slip. Also, notice the sudden rotation and translation at the end caused by the slip from hitting the termination wall. Here we do not show our collision detection and correction system, so the error introduced from the collision is shown in the plot.

Figure Figure 4.6 shows the trajectory plot of the snake robot through a fixed-width environment with junctions. This shows that the motion estimation has no problems estimating motion through junctions so long as the anchors are good.

In spite of the care taken in locomotion and motion estimation, the snake robot still accumulates positional errors. The primary cause of this is the failure of anchors. This can happen by the anchor originally failing to take hold, intermittent anchor motion or slip, or anchor slip caused by collision with a forward obstacle making a backward motion look like a forward motion.

The quality of motion estimation is a function of how slowly and carefully we perform our movements and maintain our anchors. Particularly, the parameters we tune for our local stability detection and the rate of linear interpolation for movement transitions.

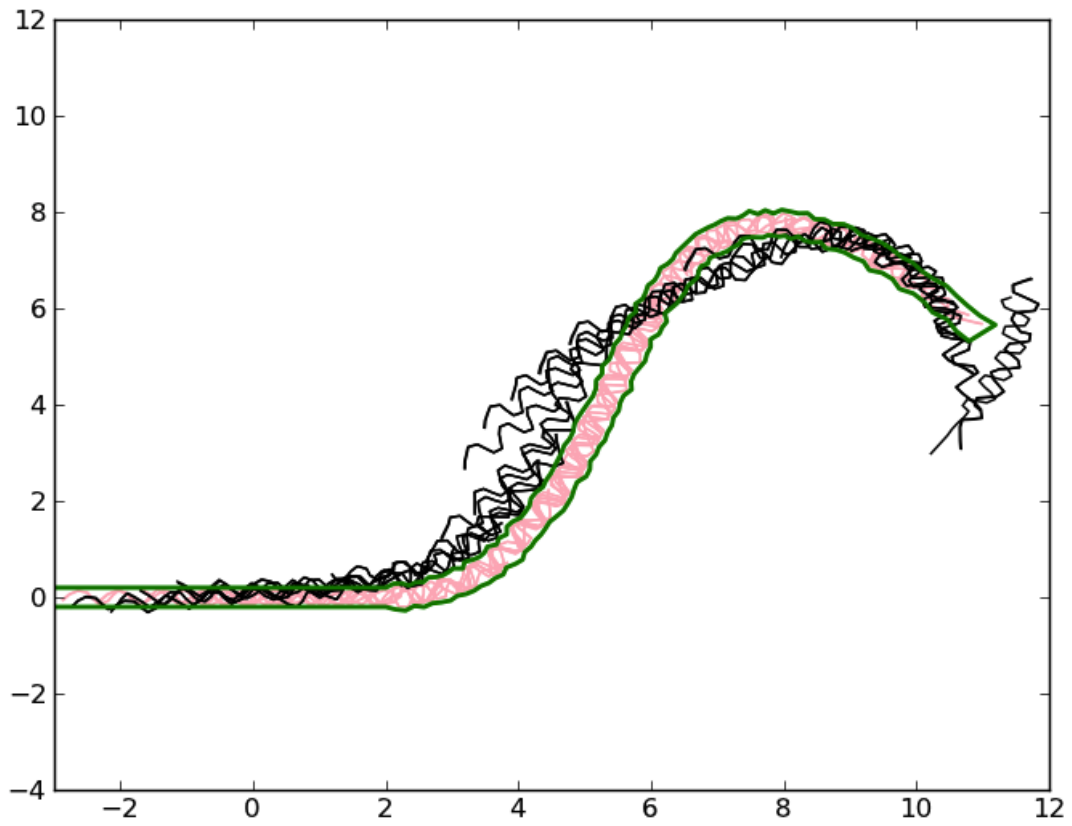


Figure 4.5: Estimated Trajectory of Robot through Variable-Width Pipe

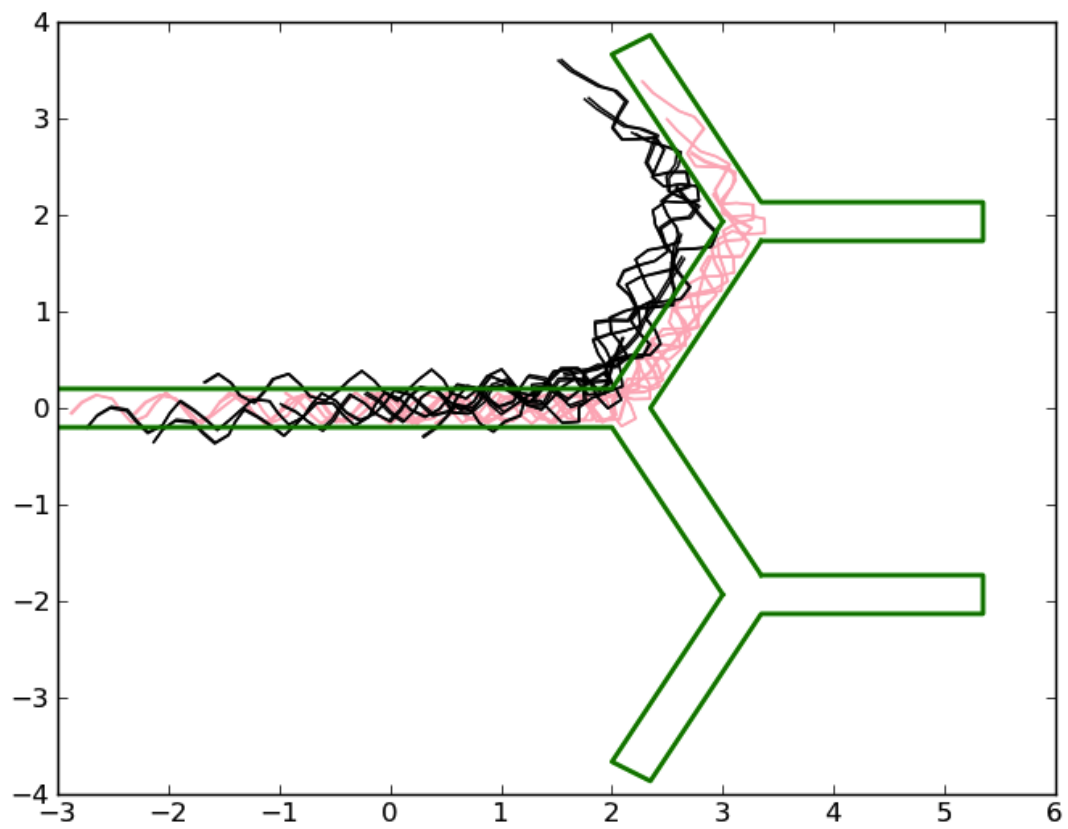


Figure 4.6: Estimated Trajectory of Robot through Fixed-Width Pipe with Junctions

Chapter 5

Environmental Landmarks

5.1 Finding Landmarks

Seeking landmark features for which we can correct the map and localize the robot. Most approaches use point features such as corners, environmental landmarks such as doors, visual features. Our options are very limited because we do not have sensing at a distance capability. All things that we can sense must be within touching distance. Any feature we choose is highly local.

One option is to find corner features by probing the walls. There are two approaches: 1) deliberate contact probing of the wall to produce corner features, 2) serendipitous corner features. Problem: 1 is feasible but slow, see [Mazzini]. 2) is also possible but the false positive rate is too high. Pull some data out of my archives.

Also try and find obstacles and openings . That is, non-obstacle openings. This presupposes that we can distinguish obstacles. Only contact probing methods can truly classify an obstacle boundary. Again, these methods suffer from time-consuming actions. Furthermore, this does not exactly give us a true positive for open space. So door openings cannot be a landmark since we cannot detect them directly.

What about the walls of the environment? The shape of the obstacles? This requires that we fully mark the boundaries of walls and obstacles. Either this is done through laborious contact detection or we make assumptions about what are obstacles based on the data we receive serendipitously. Given a posture image, we could make varying degrees of assumptions about where the boundaries of the environment lie. None of them are likely to be correct, but we can use this information as a feature. However,

this approach suffers when our probing actions are deficient for a particular pose. We receive a degenerate posture image that leaves out a lot of data.

Another approach we could take is a sort of approximation and averaging of boundaries of the posture images. This can be accomplished by the use of the alpha shape algorithm developed in [3]. It is a form of generalized convex hull algorithm that is capable of non convex polygons. This can give us our desired approximation effect for identifying the location of walls.

5.2 Corner Examples and Results

Corners are high false positive and too many false negatives.

Requires tuning of parameters, but does not guarantee correction selection.

Corners through serendipitous detection are not seen very often. Will not be seen through consecutive poses or even being in the same location. Not guaranteed to view.

Information too sparse to be useful. False correlation is very costly.

5.3 Wall Detection

Contact detection literature. Reference 2009 paper.

Time spent probing walls. Amount of information is broken up. Example information should walls from contact detection.

Punch probing. Hit the wall and measure the error incurred by the joints in the control loop. Avoids the need for torque sensor. Uses existing control algorithm parameter as error terms.

Broken information, time-consuming. Error prone and often will mark free space as wall. Not detailed enough for a landmark feature.

5.4 Pipe Shape, Macro Features

Use the contours and shape of the occupied space as our landmark feature.

Introduces strong lateral correlation, but weak forward-backward correlation. If the local environment is curved in any way, this provides stronger localization.

1st order curve is straight line. Only coaxial localization between poses 2nd order curve is a constant curve. Localization to any place with same curve constant. *3rd order curve is changing curvature. Localization to unique point with particular change profile.s

5.5 Macro Feature Extraction

1. curve of anchor points, represents walls. Does not include sensed data

Posture Image -> Alpha Shape -> Medial Axis -> Characteristic Curve

Medial axis is generated from an image and a tree is built. In most cases the tree has only two leafs and is a path graph, but sometimes the tree has more than two leafs and represents more complex space.

Represents local description of space.

Like scan-matching, we can use curves and ICP to find an alignment of the poses. The curves themselves become the landmarks.

5.6 Different Macro Features

The possibilities for curves representing the overall macro structure of the local environment are as follows:

1. Curves fitting through the anchor points of the articulated robot. Anchor points are the confirmed contacts and can approximate the walls. However, these are sparse data points, and cannot handle complex environments such as junctions or

gaps between the anchor points. Data is sparse and not well-representative of the environment.

2. Polygon created from alpha shape of posture image. Use the edges of the polygon and perform scan-matching of edges to edges. Problem, how to select the points pairs between two polygons. Use angle filter and match two sides together. Is sensitive to missing data. Unswept gap will distort the polygon. Performing matches on a distorted polygon will result in poor ICP fitting.
3. Given alpha shape, compute the medial axis of the interior. This is known to be a reduction and representation of the the space. This approach is resistant to noisy edges. Shown are some example of the results with simple single path pipes, and pipes with some junction features. Notice that the information on the width of the environment is lost using this approach.

Chapter 6

Pose-Based Mapping

6.1 Inter-Pose Correction

FIXME: apostrophe

Now that we have curve representations for each pose's posture image, we can apply an overlapping constraint. That is, assuming the invariant condition that two poses' posture images partially overlap each other, in what way(s) do the medial axis representations overlap each other. The best way to do this is with a generalized ICP algorithm, with an initial guess that is generated from the motion estimation method.

Although the two curves are guaranteed to overlap in some contiguous way, this does not mean they all overlap in the same way. The medial axis could be more than just a single curve segment, but a graph if there are some junction-like elements. Then the question is, how do you select which parts of the medial axis to match to the consecutive pose medial axis.

In a multi-curve medial axis, we can try all possible combinations. The result whose offset is the most consistent with the initial guess should be the proper result. In practice, a really great test for measuring the correctness of a particular ICP fit is to select the one with the lowest angle difference from the initial guess. This assumes that initial guess of the angle was reasonable. Getting good angle guesses is possible with the GPAC frame in Defining Pose and Direction section.

Technically, the relative offset between two poses is a 3 dimension problem (x, y, θ). However, this can be reduced to a 2 dimensional problem by defining an intersection point between the two curve segments. If the point on curve A remains fixed, if we vary the point on curve B and the angle of curve B, then the ICP problem is in a 2 dimensional

space. This intersection constraint enforces a particular type of solution that ensures the curve segments are overlapped.

So long as the initial guess from the motion estimation method is reasonable, performing an ICP fit of the two posture medial axes enforces a sanity check on their invariant overlapping.

Now that we have two medial axes, we show that the step motion model is defined by a constant arc length displacement between the GPAC origins of two consecutive poses. The step motion model combines the displacement estimate with the constraints of the locally perceived environment. Of course, the direction of that estimate may be erroneous if there are multiple splices of a multi-medial axis tree. Particularly, if we are in a junction that is sensed by a pose with two curves going to left or right, a displacement can choose to go left or right but the correct result is only determined after comparing macro-feature fit of the subsequent pose.

The step motion model is a combination of local tracking of macro-features of the environment and a model of the robot’s average displacement during locomotion. As shown in the figure, the results of the naive motion model, the self-posture motion model, and the step motion model show clearly the best answer for initial guess of the robot’s pose between consecutive poses. See our earlier discussion in Motion Models

6.2 Paired Pose Correction

For two poses that are theoretically at the same location but are split for the forward and backward sweep, we need some way for reconciling their relative offset. Taking the raw pose data and posture images, we see there are some discrepancies caused by the slip during the anchor transition. We can fix this by performing an overlap fit using the same method between consecutive steps in inter-pose correction.

The initial condition will be the poses located on top of each other and their medial axes intersecting near the origin points. After performing an ICP fit to change the angle

and the arc length displacement in the neighborhood, this creates a reasonable estimate transform between the two.

6.3 Constraint Mapping

Combining the motion model estimates and the inter-pose constraints, we can create an improved map that is better than just the simple motion estimation maps. The inter-pose constraints give a better trajectory for the environment. However, they are still deficient in a number of ways.

They do not provide any means of resolving the unique correlations of a junction, nor do they provide any consistency when backtracking through a local environment we have been before. That is, they do not have provide a solution for the loop-closing or data association problem.

A possible solution to this is to attempt to make additional hypothetical constraints between poses that are in the same neighborhood. Following [Olson], we can establish covariances between the constraints and generate consistency matrices to determine the most optimal constraint hypothesis set. This is the Graph SLAM [Probabilistic Robotics] approach that use a pose graph representation for generating the map.

The weakness of our problem domain is that we do not have available landmark features that fit into this framework. Landmark features are given their own positions and then observed from multiple robot poses which are then correlated. 1) Our data does not have point features with positions, we have macroscopic shapes of the environment. 2) Secondly, we are not guaranteed to observe the feature between consecutive poses or even poses that are in the same location.

The Graph SLAM approach becomes increasingly difficult because there is no clear way how to generate covariance matrices between poses. We could generate the covariance with a coaxial variance for greater variance in arc distance and low variance for lateral offset off the overlapping axes. This is clear for simple straight posture images.

However it is less clear for curved or multi-axis junction environments. Furthermore, using a graph optimizer can result in two hard constrained poses to be corrected to be off-center their medial axes to globally minimize the overall error. This is not the type of corrections we want to see since the local constraint is so certain in only one dimension. Any correction method should take advantage of that.

6.4 Aggregate Pose Constraint Mapping

Instead of creating geometric constraints between individual poses and struggling to search for which acceptable matches between poses, another approach we can take is to make a constraint between a new posture image and all of the other posture images in aggregate. In this way, we can avoid the difficulty of making individual pairwise constraints between poses.

The approach we take is to find the union of all past posture images together and compute the alpha shape from that. From the alpha shape we then compute the medial axis. This results in a much larger version of the medial axis curve representation.

To constrain the pose of the new posture image, simply perform ICP between the pose's medial axis curve and the past whole map medial axis. The result can be seen in the figure X. Like the inter-pose constraint, we have the invariant condition that the new pose's medial axis curve partially overlaps the global medial axis. Therefore, there exists a section of the global medial axis curve that the new pose at least partially overlaps. For poses that are backtracking through previously visited territory, the new pose will be completely overlapped by the global medial axis.

This is a maximum likelihood mapping approach. That is, the mapping method looks for the best possible result for the current pose. All past poses are fixed and unable to be changed. Should we ever make a significant mistake in the placement of the current pose, this will be permanently reflected in the map for the future.

Even using this simplistic approach, a significant translational error along the axis of travel in a straight section of the environment does not have severe consequences to the map. Along a straight section of the pipe, the current pose can be placed anywhere along that section with little consequence to the structural and topological properties of the map. The only thing that is affected is the current best estimate of the robot's pose.

The mapping system is able to localize the pose much better with respect to curved shape features in the environment. If there are sharp junctions or curved sections, the current pose can be localized with much better accuracy.

Once the current pose's posture image given it's most likely location, it is added to the existing set S and the union- \rightarrow alpha shape- \rightarrow global medial axis is recomputed. If the robot is pushing the frontier of the map, this will result in an extension of the medial axis. If the posture image pose is an incorrect position, the resultant global medial axis can be corrupted and result in kinks (distortions, discrepancies). These kinks can compound future errors and result in even further distorted maps.

To compute the raw medial axis of a path, we must take the union of the set of its constituent poses. For every pose, we take the set of points that constitute the polygon representing the pose's alpha shape in the local coordinate frame. For every point set B of every pose P , we transform the set B to B' in the global frame. The union of all sets B' is the resultant point set C .

We then compute the alpha shape of C with a radius of $[0.2]$. The resultant alpha shape is mapped onto an image of appropriate dimensions with a pixel size of $[0.05]$. All of the pixels contained within the grid framed alpha shape are set to 1 and all others are set to zero. The resultant image is input to the `computeMedialAxis` function.

The medial axis result will look similar to Figure [X] with overlap into the parent path and possibly multiple branches because the robot overlaps the junction in different ways for each pose. We cannot use the medial axis in this form because it does not logically correspond to the data representation we are looking for. Union path tree of all the paths overlap each other in multiple ways. Our goal is to extract the path fragment

that extrudes from its parent path at the designated branching point. Using only this section, this is our representation of the child path.

Identifying the junction requires some finesse. Given the divergence point on the branching pose, find the closest point on the union path tree to the local divergence point. This becomes our theoretical branching point. We create a branching leaf along the desired direction if the union path tree is too curvy or does not represent the sharp junction structure that we desire to represent. The comparison of the theoretical leaf and the generated path is shown in Figure [X].

We then call the `trimPath()` function which will prune the tree at the branching point, keep the section of the path tree that overlaps the our desired section of environment, and ensures that the result is a single path and not a tree, pruning off any extraneous leaves.

The first thing we do is find the longest path between a pair of leaf terminals on the path tree such that the longest path passes through the branch point at the target angle.

The topology of a path is computed from the union of all of the poses' alpha hulls classified into that particular path. The hull is populated with points in a grid and the medial axis is computed using the skeletonization (?) algorithm.

Given the set of points that are the skeletonization image, the pixels are converted into nodes of a graph, and edges are added between them if they are adjacent or diagonal neighbors. The pixel indices are converted back into global coordinates to give us a set of points that are nodes in a graph, edges connecting to their neighbors.

We reduce the graph first by finding its MST. Then we prune the tree by snipping off one node off of leaves. This removes any obvious MST noise artifacts but preserves real branches of the tree.

Paths are computed between each pair of leaves. We classify each node that has a degree > 2 as a junction and possible branch point for the target path we are trying to build. On each leaf-pairwise paths, we find the point on that path that passes through the junction.

In the case that there exists no junction or branching point close to the pre-existing branch point, we create a separate graph that includes a theoretical branch with the previously computed parameters. These parameters come from past computations of the path topologies. We know that a branch exists but it may have been erroneously smoothed out due to the addition of new poses in non-optimal locations.

The theoretical branch is computed by taking the orientation of the historic junction point, finding the closest node on the graph to the historical junction point, and extruding a new branch on the tree from this point. A series of uniform points are computed to represent this branch that terminates at the boundary of the alpha hull.

Each leaf-to-leaf path on the medial axis is extrapolated at the tips to intersect and terminate at the boundary of the alpha hull. This adds further usable information to the produced curve and in practice is a correct extrapolation of the environmental topology.

We select the longest leaf-to-leaf path that includes the branching arm of the junction from its parent path. The portion of the path that branches is the portion that we are interested for the current path. The portion that is not branching is overlapping its parent path. This information can be used to help localize the branching point with respect to the parent path.

We then compute the trimmed version of the computed topology path. At the junction point, the path is cut and only the remaining portion that forms the branching arms is kept. This portion is the final path portion and does not include any portion of its parent.

When using these path fragments, we splice them together in various hypothesized configurations to determine if our robot's posture fits into any previous paths and junctions. This splicing is helpful for localization and navigation when exploring the environment.

Chapter 7

Mapping with Junctions

7.1 Map Algorithm

1) Estimation motion of step

2) Collect posture image

3) Determine if there is a branch, if so, fork process (yes/no cases) (NEW)

4) Add pose to best fit shoot, generate new map (NEW)

5) Localize pose to most likely location in existing shoot map, fix map (NEW)

6) go to 1)

ESTIMATE MOTION - estimate position of pose based on motion estimation from the previous fore pose: {f, b}

SENSE ENVIRONMENT - capture environmental information through probing - perform forward sweep for front pose - generate local spline

ESTIMATE MOTION - estimate position of pose based on a zero move estimation from the paired fore pose: {0}

SENSE ENVIRONMENT - capture environmental information through probing - perform backward sweep for back pose - generate local spline

CLASSIFY POSES TO PATHS - Find each best fitting path splice for the front and back pose's local spline - If the pose's local spline does not diverge from the path splice, we add the pose to the splice's constituent leaf path(s) - Otherwise, if it diverges and branching parameters are sufficiently unique, create a new path from the branching point and add the new pose

PATH COMPARISONS FOR SIMILARITY - compare sibling paths to see if they are similar - queue them to be merged if they are similar

- compare parent-child paths to see if they are similar, - queue them to be merged if they are similar

MERGE PATHS THAT ARE SIMILAR - merge sibling pairs - merge parent-child pairs

- recheck for branching events from the constituent poses after merging

LOCALIZE POSE - Localize fore and back poses to their classified paths. - Maximum likelihood localization to classified path

7.2 Junctions

This approach works well for environments that are just a single continuous path. If we encounter an environment with a junction, we will need to modify this approach. One of the challenges of environments with junctions is that they are only partially observable. The robot may be passing through a junction without detecting it as such. Only by passing through all arms of the junction over time are we able to infer the location and properties of the junction.

Given that a junction is not visible on its first pass except for special circumstances, the best approach is to assume there is none and continue to add the pose's single posture image to the global union and compute the resultant global medial axis. Evidence for the existence of a junction is given by a posture image's medial axis curve partially overlapping a section of the global medial axis and then diverging from it at a sharp angle.

We must recognize that there are three possible ways for a new pose's medial axis to fit onto an existing global medial axis. It can either 1) completely overlap, finding a localized position in the map, 2) partially overlap by extension, pushing forward past the termination point of the global medial axis, or 3) partially overlap by divergence, curving off the global medial axis at a sharp angle signifying a junction-like feature.

One of the fundamental challenges of exploring environments with no ability to sense at a distance, there is no quick way to distinguish a wall from the limit of arm extension. That is, when the robot's body sweeps and reaches the limit of its motion, by either collision, slip, or complete extension, there is no way to immediately distinguish that the boundary of its swept space is an obstacle or just more free space. [complete extension is well-defined, therefore, it can be tagged when complete extension is made. Planned motion vs. actual motion.]

Though we can reason and safely map long tubes with hard turns or curved and undulating paths, if we add junctions to the mix such as Y and T junctions, recognizing the encounter and the parameters of the junction becomes especially challenging.

We define a junction to be the confluence of over two pipes at various angles. For instance, an L bend we do not consider a junction, but a T is a junction. To see how this is challenging, imagine the Figure [X] where the robot's body is within the L junction. Similarly, the robot's body is in the T-junction in the same configuration. Both position's give us the shape of the environment correctly. However, we can only partially view the junction at any given time.

In order to sense and completely characterize the T-junction, the robot would be need pass through or back up and make an effort to crawl down the neglected path. If we knew that the unexplored pipe existed, this would be an easy proposition. As it stands, it is very difficult to distinguish an opening from an obstacle.

There are deliberative ways to completely map and characterize the environment as we travel. The work of Mazzini and Dubowsky [cite] demonstrate a tactile probing approach to harsh and opaque environments. Though this option is available to us, this has it's own challenges and drawbacks.

For one, tactile probing is time consuming. A robot would be spending all of its time touching the walls of the environment in a small range and not enough time exploring the environment in the larger range. We decided very early on in our research [Everist2009] that although contact detection approaches have proven their effectiveness in producing

detailed environmental maps, they are not a practical solution to exploring complex environments that won't take multiple days to complete.

Similarly, the act of probing and sweeping the environment has the possibility of disrupting the position of the robot and adding defects to the contact data locations. Tactile probing is particularly vulnerable to this since it involves actual pushing against obstacles and possibly disrupting the robot's anchors.

For all of these reasons, it is desirable to find an approach for mapping environments with junctions when the junctions are only partially observable. That is, at best, we do not know if we are in a junction until we come through it a second time. Often times, junction discovery is serendipitous because openings look identical to obstacles in a free space map. Without deliberate tactile probing, junction discovery will always be serendipitous for rapid mapping.

Take for instance the 3-point T junction shown in Figure [X]. There are three possible occupancy states for the robot to fit into the junction. As we can see, states 0 and 1 together give us a complete representation of the junction. However, it is not clear from just the estimated poses and local spline curves of the data that they should be matched up together. There is ambiguity in their relationship since the poses can be arranged in a number of different configurations that represent completely plausible environments.

In order to reduce this ambiguity, we need additional observations of the junctions increase the likelihood that they fit together into a T junction. In particular, if the robot goes from state 0 to state 2 and back to state 1, this would give us a blueprint to fit all of the poses together to create a complete T junction.

Even though the data set we have gives us a very strong case for the detection of a T junction, there are still other possibilities in the event of poor motion estimation. Other plausible environments from the given data are shown in Figure X.

As we can see, the approach of mapping junctions using only free space data has its challenges. There is no full proof way to map a junction using only partial observations with ambiguous resultant data. However, we will see if a probabilistic approach will

give us to cut through the ambiguity and focus our efforts on the most likely cases. Furthermore, it could direct our efforts to make a costly targeted contact probing effort at the most likely junction location and resolve all confusion.

When making the hypothesis of a junction, we have some leeway on its location depending on the type of junction states of the composing local medial axes. As seen in Figure [X], if a junction has been hypothesized by the a local medial axis diverging from its parent path at location A with the shown junction state, there are a continuum of possible locations it could be at that are completely consistent. Though these possibilities are constrained by the estimated positions, these possibilities give us our search space for fixing the final product.

If we were to finally add in the local medial axis B in the depicted junction state, the freedom of movement gives us the option of resolving any conflicts and making the junction whole with the composed poses. The ambiguity places boundaries on the search space.

We call these unresolved junction arms to be phantom arms. We suspect that a junction arm exists, but we do not know until we actually explore them. Furthermore, we do not know the junction's location until we have an extra pose in the correct junction state, or we have gathered evidence that a junction does not exist and decreased its probability.

7.3 Shoot Map Representation

To represent and keep track of junctions and any instance of branching off from the main global medial axis, we introduce a new map representation called a shoot map. First we define the concept of a shoot to be a single path with an origin and termination point that represents a continuous representation of space with no junctions. In the previous section, our global medial axis of the entire environment represented a single shoot, since there were no instances of branching. Once a new junction is found, a new

shoot is created with origin starting at the branching off point from the original shoot and termination point ending at the extent the posture images map the branch's space.

Corresponding to the three cases of how a posture curve overlaps an existing global medial axis, 1) either the pose is contained within an existing shoot, 2) the pose extends the shoot, or 3) the pose is added to a new shoot that branches off. Given the nature of the shoot structure, there is a parent-child relationship between shoots, with the stem being the root shoot. All shoots except for the root, have an origin placed from another shoot.

The curve of a shoot is represented by an ordered series of points that are generated from the medial axis computation of the union of member posture images. We say a pose is a member of a shoot S_p if it has some overlap with S_p but does not overlap a child, S_c , of S_p . That is, if any portion of a pose overlaps a child S_c , the pose is a member of S_c and not S_p . A pose can be a member of more than one shoot if there are more than one child shoots. The member shoots can be siblings or any other combination where the shoots are not direct ancestors or descendants.

The complete representation for a shoot map is the following parameters:

- Poses: $X_{1:t}$
- Images: $I_{1:t}$
- Shoots: $S_{1:N}$
 - Shoot member pose sets, $c_1 = \{1, 2, \dots, k\}$, , $c_N = \{k+1, \dots, t\}$
 - Branch point: $b_{1:N} = (x, y, \theta)$

The first half are the same parameters used for the pose map. We add the additional parameters of shoots. A shoot is composed of a set of member poses and a branch point. For a non-root shoot, the branch point is a location on its parent shoot and an accompanied direction.

7.4 Generating Shoots

Compute the union of posture images for a shoot set. Cut and paste each medial axis at the designated branch points between the parent and child shoots.

For each shoot S_j , For each pose k that is member of S_j , Plot posture image I_k to pose X_k

Find alpha shape A_j of union of pixels

Find medial axis M_j of alpha shape.

For every pair of shoots S_j, S_k , If $S_j = \text{isParentOf}(S_k)$ Find closest point on M_k to b_k . Cut section from the extra portion of medial axis starting at b_k in the direction of b_k Add section to trimmed shoot map T_k

If $\text{isRoot}(S_k)$:

Add M_k to trimmed shoot map as T_k

Medial axis from union of set of posture images of particular shoot S where exists vertices degree > 2 . Trim the section closest point to the branch point in the direction oriented by the branch point b_k .

7.5 Adding Poses to Shoots

If first poses, add to root shoot.

Check for branching conditions

Best Overlap, get ordered overlapping path ids

Select child shoot IDs, add pose to the shoot.

MOVE ESTIMATION - estimate position of nodes based on motion estimation from the previous pose

MAP INTEGRATION - integrate the new pose into the map

ADD NEW POSES, CREATE NEW PATHS - Which path or set of paths does this pose currently overlap? `getOrderedOverlappingPaths()` - of all splices in local neighborhood, find the best fit based on highest contiguity with initial estimated pose - in order of best fits, pick the first that overlaps all constituent paths, that is, does not have paths in the splice beyond the range of the pose sensor data - for the constituent path IDs of the chosen splice, order them according to sequence they are overlapped by the pose curve - return the ordered list of path IDs that this pose curve overlaps

- Does this pose fit on the path splice or does it depart internally? `getDeparturePoint()` of `orderedPathIDs`
 - get departure state of the front pathID and back pathID with pose curve
 - if the pose curve does not depart internally, add this node to the leaf path(s)
- If it internally departs, given the departure state of the splice, are the pose departure parameters sufficient for a new branch?
 - is the proposed new branch sufficiently unique
 - * is the distance from the parent's branch point sufficiently far? (0.8)
 - * is a path sibling's sufficiently close (0.5) branch point not angled in the same direction ($\pi/6$ tolerance)?
 - * is the pose curve featured?
 - * if all true, then this new branch is sufficiently unique
- If the new branch is sufficiently unique, then create the new branch with the current pose
- Regenerate the paths with the new node data
- select parent and child path pairs
- select sibling path pairs

PATH COMPARISONS FOR SIMILARITY - if sibling pairs, - create a stitched path of parent with section between two child junction points excised and the relative orientations of the junction points are aligned - select common point between parent path and stitched parent path - perform ICP fit between stitched parent and original parent - return the resulting pose offsets for both sibling paths and their relative junction angle - if the angle of both offsets is < 0.5 and the junction angle difference is $< \pi/4$, then we queue the siblings to be merged

- if parent-child pairs,
 - create a set of splices for the parent path and the child path
 - * if grandparent exists,
 - generate gparent/parent splices and gparent/parent/child splices
 - * else
 - generate parent splices and parent/child splices
 - select common point between parent splice and child splice
 - perform ICP fit between parent splice and child splice `pathOverlapICP()`
 - return the resulting offset between the two
 - if the resulting offset angle < 0.5 radians
 - * compute the departure state of the two paths given their relative offset `getPathDeparture()`
 - * if one path does not internally depart from the other
 - and if the two paths with their relative offset partially overlap `getPathOverlapConditionn()`
 - then we queue the child and parent paths for merging

MERGE PATHS THAT ARE SIMILAR - merge sibling pairs - for the pair of sibling paths to be merged - transform the nodes in path1 by the offset from the previous ICP

fitting - transform the nodes in path2 by the offset from the previous ICP fitting - perform `consistentFit()` of each node from path2 into best possible splice (NOTE: should be onto a spliced parent-path1 curve) - for each merged node, perform the “ADD NEW POSES, CREATE NEW PATHS” procedure for checking for branching events and classifying nodes into leaf paths

- merge parent-child pairs
 - select child nodes
 - move them by earlier ICP-fitted offset
 - find the most consistent fit of all set of splices in the node’s new neighborhood using `consistentFit()`
 - change their membership from child path to parent path
- Finally, if the node hasn’t been made fitted already to its path, do so now using `consistentFit()`

FUNCTION `consistentFit()` - find the most consistent fit in all set of splices in the node’s new neighborhood `consistentFit()` - for each possible splice, find the common point between pose curve and splice path - perform 11 guesses of where the pose should be along the length of the splice path curve in the neighborhood of the its starting location - perform ICP between pose curve and path curve for each starting guess - compute the departure state, contiguity, and overlap sum for each final position - discard result if - internal departure exists - terminal departures on both ends of pose curve - contiguity is less than 0.5 - the resultant pose is > 3.0 from original estimated pose - difference between starting guess angle and corrected angle is > 0.7 radians - select the splice and fit location with the best utility given by following equation: - $utilVal = (0.5 - angDiff2)/0.5 + (contigFrac - 0.5)/0.5 + (3.0 - dist)/3.0 + 1 - isDeparture * 0.5$ - weighting angle difference from initial guess, contiguity %, distance from starting estimate, and if any internal or terminal departure exists

7.6 Detecting Branch

If a posture medial axis is detected that does not completely fit on the existing shoot, it is possible that we have discovered a branch. It is vital that we properly and detect branching events in order to fit them properly into the map. In the event that we add a posture image to a shoot that is not completely contained into the target shoot, this will distort the medial axis computation of the union of images and result in kinks the shoot curve.

Branching is detected on the individual pose level. For the medial axis of a single posture image, if the single medial axis curve diverges from a shoot, then it is said to be branching and a new child shoot should be formed.

Care must be taken in determining the parameters for when a curve is diverging. We define divergence distance to be the distance between the target curve endpoint and the diverging point on the parent curve. The diverging point is defined by the difference between the tangent angle of the point at which the curve last leaves the parent curve and the next point along the curve at which the minimum angle threshold has been made. The closest point on the parent curve to this minimum angle threshold point is the diverging point.

There are two constants that must be set that determine the threshold parameters for divergence detection. The first parameter is A, the angle difference between the departure point and the divergence point. The second parameter is D, the minimum distance threshold between the divergence point and the target curve endpoint.

The points are: departure point, divergence point, and end point.

7.7 Localizing On Shoot Map

Assuming that the decision of making a branch or not has been made by the branch detection method, and that all the current poses have been added to their respective shoots, we can assume that the current pose can be completely localized on some location

of the shoot map. There are two possibilities for the locations of the posture curve. Either it is 1) completely contained within a single shoot or it is 2) overlapping two or more shoots at once. In the latter case, to overlap more than one shoot, the posture curve must be inside of a map junction.

Initially, the only information we have is the initial guessed location of the new pose from the chosen motion estimation method and the categorization of the pose into a particular shoot.

One use of the maps is to be able to localize the pose of the robot. Given the current state of the shoot map, we need methods by which we can localize the robot's pose.

Why should we want to localize the robot? Though we have used motion estimation techniques and local constraints to iteratively construct the map and robot's trajectory to the best of our ability, for circumstances when the robot is backtracking or returning to a location we have visited before, a localization technique will give us a way to perform loop-closing or data association. If we are traveling down a pipe in only one direction, loop-closing is not necessary since there is no chance of visiting the same location twice.

In the event of visiting the same location, there are two questions that must be answered: 1) is the robot at a location that it has visited before and 2) if so, where is its best fit? Since we have already decided if this pose is branching and have added all the necessary branch points, and categorized this pose into individual shoots, it is already true that this pose is somewhere on the map. However, the location that we chose for the pose may be incorrect or may have broken the map.

1) Cases where the pose is in the wrong location: - Poorly overlapped poses add kinks to shoot - Many locally identical indistinguishable locations - Shoot map self-intersects

If the current pose is wrong, but all past poses are correct, then it is a simple matter of fixing the current pose. However, as is often the case, if a whole history of poses is incorrect, it becomes more challenging to fix an entire history of poses. We have an

approach to selecting different histories of poses in the next chapter on Probabilistic Mapping, but for this section we will only focus on fixing the current pose.

7.8 Finding the Best Fitted Location

Immediately after motion estimation, branch detection, and shoot categorization, our next task is to find the best likely location for the current pose. We measure the likelihood in terms of the best possible fit of the current posture curve to the current shoot map. To do this, we again utilize ICP between the posture curve and splice curves representing different permutations of spliced sections of the shoot map.

For instance, if we wanted to test whether the posture curve fits into a junction shown in Figure X, there are three different spliced curve permutations of this junction. By performing ICP of the posture curve onto each of these splice curves, we receive different candidate localized poses for the robot's current position. By performing several such ICP experiments with several splice curves, we can apply a selection criteria to be our best fit, use that as our maximum likelihood pose, and make any necessary changes to the shoot map.

We now describe the steps we take during the localization phase:

- 1) Choose the shoot splices that we wish to localize on
- 2) Select a set of initial poses for each splice to input to our ICP algorithm
- 3) Perform ICP on each initial pose on each splice
- 4) Collate, sort, and filter results
- 5) Choose most likely result and set as the current pose.

7.8.1 Choosing Shoot Splices

In step 1), if there is only one shoot in the shoot map then the resultant splice is simply the parent shoot itself. However, if there is more than one shoot, a number of possible splices are possible. We can take an exhaustive approach and select all possible splices, including splices with multiple junctions contained within them.

One approach we can take is to select all splices that terminate at every possible combination of terminal points in the shoot map. So for instance, for a map with N shoot and $N-1$ junctions, the number of possible splices is represented by $(2 + N - 1)$ choose 2. However this can be problematic if we consider junctions that are not in the neighborhood of the pose in question. In particular, if we have three junctions A, B, and C, there will be $(4 \text{ choose } 2) = 10$ possible splices between all possible terminals. However, if only A is in the neighborhood of our pose, many of the possible splices are locally identical so there is no value in using splices that include junctions B and C unless B and C are in the neighborhood of the pose.

We can discriminate the type of splices we will use by excluding some junctions from consideration if they are not in the neighborhood. If the pose of P is less than some distance D to the branch point J of the junction, then we can instead treat the junction J as a termination point. For instance, in figure X, if we turn junctions B and C into termination points for the number of splices and include A as a junction of interest, we result in $(3 \text{ choose } 2) = 3$ possible splices.

7.8.2 Selecting Initial Poses for ICP

Now that we have our set of shoot splices on which we will localize the current pose, we must determine the initial pose for each splice to input to our ICP algorithm. The ICP algorithm takes two sets of points and an initial transform between them and outputs another transform that represents the best possible fit. In our case, the two sets of points are uniform samples from the posture curve and the shoot splice curve respectively. The initial transform represents the initial pose of the posture curve and the output transform is the pose of the best locally optimal pose. Since the results are locally optimal, it makes sense to run the algorithm with multiple initial pose inputs to find a more globally optimal result.

Globally, there are multiple local minima that represent best fits of the posture curve. However, only one of these is the true location. We can bound the space of possibilities

by only selecting initial poses that are near the initial pose from the motion estimation step. That is, we can select sets of input poses that are within a diameter of the initial pose P .

For each shoot splice, select the closest point to the initial pose P . Given a spacing of S_d , select new points along the curve such that the arc distance between them is S_d and the cartesian distance of P_s to P is less than some neighborhood diameter D_n . These represent the inputs to the ICP algorithm for each run. If we assume that we have 10 initial poses for each shoot splice and 3 shoot splices, we have 10x3 executions of the ICP algorithm and 10x3 output result poses.

7.8.3 ICP Algorithm

- Orientation
- Closest pairs intersection point
- Closest pairs computation
 - Local angle variance
 - Closest point $A \rightarrow B$
 - Closest point $B \rightarrow A$
 - Select pair that has lowest angular variance
- Result serves as intersection point between two curves.
- 3DOF \rightarrow 2DOF conversion
- (x,y,o) transform \rightarrow (u,o) transform
- Covariance and mahalanobis distance?
- Point-to-line constraint

- Point-matching search
- Cost function
- Repeat N number of times or convergence $(c1-c2) < \text{minCostDiff}$

7.8.4 Collate, Sort, Filter

Given all of the results, we need to select just one as our final localized pose. We need some criteria to evaluate the fitness of each pose. There are a number of metrics that we can use in this evaluation. However, there is no straightforward method for choosing the best pose since there is ambiguity in the map, identically featured locations, and sometimes there is not enough discriminatory information to make a good localization fit. Therefore, the process by which we select a single pose to be our best fit is derived empirically and experimentally which we show here. The ambiguity and uncertainty of this problem is handled more explicitly in the next chapter on Probabilistic Mapping.

1. Curve extension
2. Curve divergence
3. Contiguity Fraction
4. Angle difference
5. Position displacement
6. Match count *
7. Overlap sum *
8. Utility function

$$\text{utilVal} = (0.5 - \text{angDiff}) / 0.5 + (\text{contigFrac} - 0.5) / 0.5 + (3.0 - \text{posDist}) / 3.0 + 1 - (\text{isExtension OR isDivergence}) * 0.5$$

Filter criteria:

- `isExtension ==> Reject`
- `isDiverge ==> Reject`
- `contigFrac <= 0.5 ==> Reject`
- `posDist >= 3.0 ==> Reject`
- `angDiff > 0.7 ==> Reject`

Sort by utility value Take result with highest utility

7.9 Curve Segment Algorithms

- `IsOverlapped()`
- `getOrientation()`
- `getContiguity()`
- `GetOrderedOverlappingPaths()`

The purpose of the divergence computation is to detect the concrete event of the target curve diverging from the host curve. This is used to classify whether or not a junction has been detected or whether the host path is simply being extended.

The difficulty associated with this task is that there is no discrete event to determine a divergence. It is measured by passing a threshold that must be calibrated to the task. The thresholds are both sensitive to cartesian distance and angular difference between the diverging curve and the divergence point on the host curve.

We first begin by computing the closest point distance between the target curve points and the host curve. At the point which the closest point distances begin monotonically increasing until the curve runs out, we start our search for the branch point. That is, we select the minimum distance inflection point before distance increases monotonically.

From this point, we walk.

Divergence between two curves is the point at which the overlapping curves separate. It is not a complete overlap but a partial overlap of two noisy curves. The challenge is defining under what conditions two curves are considered to be overlapping and under what conditions the curves are diverging. Finally, one must decide the location where the two curves transition from overlapping to diverging.

We may require the divergence point to have particular properties. That is, we may want the point to reflect an extrapolation of where the two curves would meet if they were not smoothed so much. We may also want the divergence point to have an angle that represents the approximate angle of divergence.

The divergence can be slow transition, but we would like to specify a fixed point at which it occurs. Satisfying the above conditions at the same time, determining the divergence point becomes a challenge.

We have defined 2 different types of divergence. The simple divergence and the angle-biased divergence.

The simple divergence is computed based on the closest point distance between the host curve and the target curve.

`getDeparturePoint():`

- receive as input the global path and the local spline of a pose

`getOrderedOverlappingPaths()`

The purpose of this function is to find the minimum fitting path splice for a given target local spline curve.

We define the minimum fitting splice as the shortest curve splice in which the target curve is completely contained.

For all possible combinations of path splices and for the target curve in its designated global pose, find the splice that has the highest contiguity and passes overlap condition for all of the splice's constituent path fragment.

The function returns an ordered list of path IDs that correspond to the overlapping order of the target curve on the selected path splice.

The purpose of the overlap condition computation is to determine if a proposed path splice curve is at all overlapping another curve such as a local spline or another path splice curve. The actual value of the overlap sum is not necessarily interesting, only that it is a tractable value instead of infinity.

It has two possible conditions: 1) is overlapping partially, and 2) does not overlap at all.

The computation is achieved by taking the target curve, which is usually the local spline, and for each point along the local spline, find its closest matched point on the secondary curve, usually the path.

The closest is also biased by the relative tangential angle between the two points. Two curves crossing each other's paths at 90 degrees will result in a non-overlapping condition since their are no points that have like tangential angles.

Also, closest points are limited by distance. Our upper value is 0.2 which is hand-calibrated constant. The value should be chosen based on the scale of the robot, the resolution of the sensor data, and the data noise and uncertainty. If a closest point less than 0.2 is not available, then no pair is created.

This particular computation is used as a quick and dirty filter for rejecting curve overlap hypotheses that do not overlap in any conceivable or workable way. It does not allow for any displacement or rotation of the two curves since this is the province of the ICP algorithms.

The purpose of this particular computation is to determine how much of two curves are contiguously overlapped. This is a complement to the overlap sum computation which computes scalar quantity which is an average of point-to-point closeness over the whole curve.

The contiguity calculation determines what percentage of the target curve is completely overlapped and assumes that the remained of the portions are diverging from the host curve.

Contiguity is computed by counting the number of points on the target curve have a matched point partner with distance less than 0.2 whose neighbor's are also of distance less than 0.2. The value of 0.2 is experimentally chosen to reflect the type of data that we receive. If there are more than one set of contiguous points that are less than 0.2 distance to their matched pair, the larger set is chosen. Only the target set is used in the percentage calculation.

The contiguity is computed by dividing the maximum total number of contiguous points with matched pair distance of less than 0.2 by the total number of points in the target curve. The value is from 0.0 to 1.0.

This particular metric is useful for validating divergence conditions. A non-diverging curve pair should have a contiguity of close to 1.0. Whereas, a target curve that internally diverges from the host curve or extends the host curve should have a contiguity of 0.7 or lower.

At what threshold to make decisions based on these unitless metrics is something that must be done experimentally, probabilistically, or in a machine-learning approach. The value itself is scale independent so it should not vary based on the size of the environment and robot, but on the relative data size of the compared curves.

The purpose of the overlap sum computation is to determine how well a proposed path splice curve overlaps another target curve such as a local spline or another path splice curve.

The computation is achieved by taking the target curve, which is usually the local spline, and for each point along the local spline, find its closest matched point on the secondary curve, usually the path. The sum of all the cartesian distances is added up and the result is the overlap sum divided by the number of points to give a normalized result.

If extraordinarily short curve overlaps well, it will have a comparable value to a very long curve overlapping well. It also introduces ambiguity for certain situations. If a curve overlaps at a medium constant displacement offset, its value will have the same result as a curve that half overlaps well and half overlaps poorly.

A fundamental primitive problem when mapping confined environments is determining when two partially overlapping curve segments diverge from each other. That is, at which point does curve A diverge from curve B. See the attached figure.

The definition of the divergence point is not obvious from the offset. Given that the two curves are not exactly overlapping and that the instance where curve A begins its divergence, it is not clear where the point should be defined. Generally, we want an extrapolation of where we think the intersection of two arms of a junction are intersecting. This requires the extrapolation of the incoming direction of the divergent curve and intersect to its parent curve.

We examine multiple approaches to this definition.

Chapter 8

Probabilistic Mapping

8.1 Space of Possibilities

Given our shoot map representation in the previous chapter, our mapping decisions were based on a maximum likelihood evaluation of the pose's fitness. The best possible fit at the given moment is made and the decision remains committed. There is no opportunity to resolve ambiguity or correct decisions made in error. For some applications, this is sufficient. However, incorrect decisions can lead to irrevocable consequences in the map. Such things can include multiple repeated instances of a junction, misidentification of a junction, distortion of the shoots, and self-intersecting shoots.

Some examples of maps where the decisions of whether or not to branch or fit into an existing junction, and the accumulation of pose error over time, are shown in Figure X. (Y junction, 3-pass new branches) (T-junction backtracking fail)

We wish to broaden the number of scenarios that our mapping can handle. We wish to explicitly represent different possible valid maps given the input data. We need some way to explicitly represent the variety of different mapping choices and weigh them in terms of likelihood. Following the Bayes' Rule formalization of the SLAM problem, we first identify the sensor percepts, the robot actions, and the state space representation of the environment.

In our formulation, there are three possible actions that can be taken. Either the robot moves forward, it moves backward, or it moves not at all. The total distance traveled is not subject to control in our formulation, so there are only 3 possible actions. The robot simply takes a step. The series of actions is denoted by:

$$U_{1:t} = \{\text{fore, back, 0}\}_{1:t} \quad (8.1)$$

The percepts are represented by the posture images we created from Chapter 2. The percepts are represented as:

$$I_{1:t} = \{f(i, j) \text{ for } 0 \leq i \leq N_g, 0 \leq j \leq N_g\}_{1:t} \text{ where } f(i, j) = 0, 1 \quad (8.2)$$

Starting from Chapter 6, we represented the map in terms of poses of each posture image in the environment. Representing and improving the map was approached in terms of finding better poses to make the map the most consistent. Different techniques were used to approximate motion and localize the pose based on previous poses. The poses are represented with the following notation:

$$X_{1:t} = x_t, y_t, \theta_t \quad (8.3)$$

With the introduction of the shoot map representation in Chapter 7, we have add the shoot structure composed of pose node membership set and a branch point pose.

$$S_{1:N} = \{b_i, c_i \text{ for } 0 \leq i \leq N\} \quad (8.4)$$

$$c_i = \{\exists k \text{ s.t. } 0 \leq k, k \leq t\}, |c_i| \geq 1, \text{ for } i = 1 \text{ to } N \quad (8.5)$$

$$b_i = (x_i, y_i, \theta_i), \text{ for } i = 2 \text{ to } N, b_1 \text{ is undefined} \quad (8.6)$$

We can begin to gradually introduce a probabilistic framework by defining the state space representation for each variable, representing it with a random variable, and approximating the Bayes' Rule.

8.2 Pose Particle Filter

Population of pose hypotheses, localized, evaluated, resampled.

We first begin by building and representing the state space of possible poses of the robot. The full and complete state space is the full space of possible (x, y, θ) combination values. Either a parameterization or discretization approach is required to computationally represent it. However, computing over the full range of values is computationally expensive and unnecessary. In our case, we make some assumptions and simplifications to make computation more tractable.

First, we take the maximum likelihood approach of all past poses to build our shoot map. However, the current pose is represented by a random variable and a belief distribution given the maximum likelihood map. We begin our probabilistic map by considering the multiple possible poses of the robot and increase the belief of poses that have the best possible fit.

Since the robot is in a confined space and all the sensed area is void space, it stands to reason that any possible location of the robot will be close to or on one of the shoot curves. With this observation, it is possible to reduce the dimensionality of the possible pose locations and make the localization problem much simpler.

The pose is originally represented by 3 values: (x, y, θ) . We can reduce the dimensionality of the pose by restricting the pose to be a point on a shoot splice. Specifically, given a curve, a pose on the curve can be represented by two variables, the angle θ and the arc distance u . Therefore, the current pose of the robot given the maximum likelihood map is represented by the vector (u, θ) and its designated shoot splice s curve.

The shoot splice s is a small number of possible values. The 2 dimensional pose vector dramatically reduces the state space of the pose. Therefore, our posterior distribution need only cover 2 dimensions for a finite number of shoot splices. This makes the computational problem much more tractable compared to the full 3 dimensional state space. **Image of 3d space vs shoot splice space**

This approach assumes that any possible pose will be located on a shoot splice curve. This approach can encounter difficulties if this is not the case. Any situation where the pose would not be on the shoot curve is either, the shoot is distorted by improperly localized previous poses, or the robot is not in the center of the pipe. The latter case is possible if the pipe is too wide for the robot to anchor to the edges. One of our original assumptions is that environment is not too wide for the robot to anchor.

The choice of Bayes' Rule approximation method must consider a number of factors. These include the computational cost of evaluating a pose's fitness for a particular location, the computational representation of the prior and posterior, and the computation of the update for the Bayes' Rule equation.

$$P(X_{t+1}|X_{t:1}, U_{t:1}, I_{t:1}) = P(X_{t+1}) \times P(X_t|X_{t+1})/P(X_t) \quad (8.7)$$

8.2.1 Particle Filter Implementation

Particles represent a hypothesis of u, θ, s .

Update step.

1. Move step. Displace by arc distance + random(), align angle only (costly)
2. ICP fit, localize to all local splices. (costly)
3. For each particle, evaluate every splice localization (costly)
4. For each particle, select best fit
5. Create probability distribution over particles
6. Resample particles according to probability distribution

However, for the current pose, we represent the posterior of possible poses with a particle filter \cite{particle filter}.

8.3 Pose + Branch Location Particles

Pose + Small grid of branch locations. Evaluated by overlapCost of full medial axis of child on parent.

The next parameter of the shoot map that we wish to represent as a belief distribution is the branches and their branch locations. Specifically, we assume that whether a branch exists is a given and is taken as completely true for a particular map. The only question that remains is at what point does a new shoot branch from a parent shoot.

Given a parent shoot A and a child shoot B, what point on the shoot curve A does the shoot B branch from. A related question is, at what angle does shoot B branch at from the branch point on shoot A? The branch point can be uniquely described as a 3-tuple: (x, y, θ) . Similar to section 8.2, we can reduce the problem state space by only considering points on the curve of shoot A. Therefore, a branch point can be uniquely described with the 2-tuple: (u, θ) .

Our approach is to discretize the u -space over the parent shoot curve, making a finite number of possible branch locations. Choosing the correct granularity is critical. If the discretization is too sparse, it is possible that the correct branch location is missing from the possible locations. If the discretization is too dense, it will be too computationally costly to evaluate all possible locations.

An example of the discretized space over branch locations is shown in Figure X. Here the entire child shoot medial axis graph is shown with a weighted rendering corresponding to the location's fitness. Locations that overlap with the parent shoot are more likely. Locations where the child and parent don't overlap are evaluated as unlikely.

It is also clear from Figure X that there are a large swath of possible locations that are not worth considering. For instance, the entire range of branch locations where the overlap is zero have virtually zero chance of being correct. It would be helpful if we could disregard these locations so that we need not continue to evaluate them during our computation. This can save on computational costs.

However, the question still remains, what set of possible branch locations *should* we keep track of? It helps to consider where information about branch locations come from in the first place.

Once a branching condition has been detected by a particular posture image and pose, a new branch point is created with respect to the pose. Therefore, branch points are conditionally dependent on poses. For a particular pose hypothesis, we must create a range of possible branch point hypotheses. That is, from pose X , the branch point detected at X' is located on the curve at u' . Therefore, we track a range of discrete branch point values around u' . In our implementation, we keep track of 11 possible values for a given pose hypothesis. We keep track of 40 pose hypotheses in the particle filter. This creates 11×40 possible branch points. Many of these branch points are identical.

To save on computational costs, we identify identical branch point hypotheses and only evaluate them once. This provides an upper bound to the number of possible branch point evaluations to the total number of bins on the discretized u -space of the shoot curve.

You may notice that this discretization over u -space does not provide any considerations to the angle of the branch point. There are two types of angular considerations for branch points. The first is the child shoot's angle of divergence from the parent shoot. This is generated from the medial axis computation of the union of posture images. It is a byproduct of the shoot generation process and is not directly controllable. Therefore it is not considered as part of the branch space.

The second angular consideration is that the set of posture images that constitute the child shoot may misalign with the parent shoot by some rotational transformation. While this is possible, it is our experience that the relative angular relationship of fitted posture curves and shoot curves remains fairly stable on a local level. Should there be some angular discrepancy, this is usually symptomatic of degenerate map state and should be pruned from consideration.

Evaluation of *shoot skeleton* and parent shoot curve. Evaluation cost = matchCount * overlapSum .

Secondary complementary observation of junction. Branch belief distribution should have site on consistent location. Figure X shows the possible locations and Figure Y shows the final location and only possible consistent location. Any poses that do not have the consistent location in branch space are given low probability score and are rejected by particle filter.

Maximum likelihood for non-branching map state tries to find the most consistent, non-branching fit. Given that the new diverging posture curve is not going to create a new branch, of all the pose particles, what is the best fit location on the existing map. Could resolve into two different child shoots, but we do not yet consider that. Assume that each pose can only be assigned to one child shoot.

Drawback to this approach: if there are insufficient number of particles to approximate the belief distribution over poses and branch points, correct branch point location may be unavailable in sample set when complementary junction observation occurs for a successful resolution to occur.

Another challenge is that branch points are considered independent between shoots. Therefore, if a posture image is taken overlapping two sibling shoots, there is no mechanism to explicitly correlate this possibility. Two branch space belief distributions are maintained independently and if there is significant representation over the sample space, it would be extraordinarily fortunate to identify the two pairs of branch point hypotheses that align to fit the single posture curve.

Splices over branch hypotheses.

8.4 Branch Decision

Shoot map for each go/nogo branch decision. Eliminate options based on degenerate conditions.